



MAX-PLANCK-INSTITUT
FÜR POLYMERFORSCHUNG

Optimization of polymeric light emitting diodes by organic/organic or organic/inorganic blending

Kumulative Dissertation

zur Erlangung des Grades “Doktor der Naturwissenschaften”

am Fachbereich Chemie, Pharmazie, Geographie und Geowissenschaften

der Johannes Gutenberg-Universität in Mainz

Elham Khodabakhshishalamzari

geboren in Shahrekord, Iran

Mainz, November 2019

The thesis was carried out from March 2016 until July 2019 in the group of Molecular electronics, under supervision of Prof. Dr. Paul W. M. Blom and Dr. Jasper Michels at the Max-Planck Institute for Polymer Research, Mainz.

Dekan: Univ.-Prof. Dr. Dirk Schneider

Prodekan: Univ.-Prof. Dr. Katja Heinze

1. Berichterstatter: Prof. Dr. Paul W. M. Blom

2. Berichterstatter: Prof. Dr. Rudolf Zentel

Date of oral examination: 27.11.2019

Acknowledgment

None of the work presented in this thesis would have been possible without the generous support of my supervisors, all my friends, family and colleagues. First of all, I would like to express my deepest gratitude to my doctorate supervisor Prof. Dr. Paul Blom for his guidance, motivation, endless patience and his immense support. I really appreciate your help, for giving me the opportunity to work first of all in such an inspiring and impressing environment of the Max-Planck Institute in Mainz, and on the other hand on this exciting and at the same time challenging project, which made me outgrow myself. I want to thank you for your remarkable guidance and support during those years of supervision and your precise time you always found for discussions and assistance.

Very special gratitude goes to my supervisor Dr. Jasper Michels. You gave me the trust and the freedom to work on my research, but offered me guidance and directions anytime I needed. In discussions you not only met me with respect, but you pushed me beyond my limits by giving me confidence. Your expertise and your exceptional commitment as a supervisor helped me to develop further and to achieve this work. Thank you so much!

My sincere thanks to Prof. Dr. Zentel (Johannes Gutenberg University Mainz) for his support, guidance and appraising my work. I am grateful for the fruitful discussions and collaboration that we had.

Very special thanks goes to Dr. Gert-Jan Wezler and Dr. Charusheela Ramanan. I am profoundly grateful to them for their everlasting support, guidance and sharing their immense wisdom.

Many special thanks to our lovely Petra Pausch who was always warm-hearted and helpful with all kind of issues. Besides administrative work, you gave us advice and support on things beyond work and shared your valuable experiences in every aspect of life. I always receive a wonderful positive energy from you which can make my day. Thank you for always being there for us.

My appreciation also goes to my colleagues and friends at AK-Blom at MPIP. You have each provided me with endless joyful moments and encouragement both inside and outside of the laboratory. My great time during the PhD is most of all enriched by the people, who became more than just colleagues to me. I want to thank Leona Lingstedt, the time we spent together was one of the highlights of my time at MPIP. Many thanks to my wonderful office roomies Anielen Halda Ribeiro and Alexander Kunz for creating a place at work not just for helpful scientific discussions, but also for laughter and joy. Special thanks go to my brilliant friends Kai Philips, Morteza Hassanpour, Irina Rörich and Bas van der Zee. A very special thanks to Mohammad Sajedi and Katharina Lieberth who have been always there for me. I would like to thank also the rest of my colleagues from the AK Blom for their great support and the nice atmosphere.

In addition, I want to express my appreciations to all the technicians in the AK-Blom group at MPIP for their considerable technical support. Especial thanks go to Michelle Beuchel, Christian Bauer, Verona Maus, and Frank Keller. Thanks to Gunnar Glasser who helped me with the SEM. I also would like to thank my committee members for their valuable time.

Finally, I would like to thank my dearest family. In particular, thanks to my father Said, mother Parvin and brother Alireza. Thank you to for enduring difficulties of long distances through my PhD and providing me with unwavering support even from thousands of miles away. Regardless of your own well-being, you were always there for me and comforted me in any possible way. You shaped me to the person I'm today and without you I would have never had the courage and confidence to come so far. Last, but certainly not least, my heartfelt gratitude is extended to my beloved husband for his love, patience, sacrifice, support and encouragement in all of these years. His continued support provided light in even the darkest of nights and gave this journey meaning. After all we went through, you became not only my closest friend and partner but also you played the role of every missing part of my life and family here in Germany. You're the best. My achievements are your achievements and they could not be possible without all your sacrifices and support throughout the years. I strive to make you all proud.

Abstract

Recently organic light emitting diodes (OLEDs) have been widely used in display industry and are believed to be the most promising candidate for the next generation planer and flexible display. However, there are still some issues with organic-semiconductors (especially polymeric ones) that have to be solved to compete with commercialized technology. To make that happen, one of the ideal solutions would be focusing on eliminating the negative effect of loss processes in polymeric light emitting diodes (PLEDs) to improve the device performance. One of the main loss processes is the charge trapping occurs in the active layer of the PLEDs which adversely affect the device performance. Mostly when a charge trapped in the trap centers, it would decay non-radiative process. However, there are some radiative trap-assisted recombination originating either from the defects or extra components like chromophores into the system.

This thesis is divided into two main parts. In one part we focused mostly on the systems with radiative trap-assisted recombination and eliminating their negative effect on the device performance. Polyfluorene (PFO)-based PLEDs are an excellent model system to visualize this trap elimination effect. The blue emission from PFO is accompanied by a broad, featureless green emission band originating from ketone defects that act as an electron trap. In the first part of this work, we demonstrate that the visible green trap-assisted recombination is nearly eliminated upon blending with an insulator polymer. As a result, not only the blue emission from PFO can be fully restored, but also the efficiency of the devices enhances drastically. To proof the generality of the concept, we apply the same method to also improve the color purity of PLEDs based on a ladder-type polymer, methyl-substituted poly(p-phenylene) ladder polymer (Me-LPPP).

In the second part of this thesis we put the focus on another main issues in PLED field which is realizing full-color displays with high color purity. In displays it is important to have small linewidths to make saturated colors. This is why nowadays quantum dots (QDs) are attractive candidate for display technology. However, QD LEDs are suffering from unbalanced charge transport and also complexity of their device structure. The way out to a robust and simple structure would be to use system in which the QDs are simply blended with an organic host. All attempts in this direction failed due to the problem of electron trapping in QDs. In the second part of this thesis we demonstrate that electron trapping by CdSe/Cd_xZn_{1-x}S core/shell red QDs in a blue-emitting PFO host can be strongly suppressed by functionalizing them with a thin insulating shell. Our results open a new route towards emissive devices with narrow linewidth, where due to the preservation of charge transport there are no limits to the active layer thickness.

Abstrakt

In letzter Zeit sind organische Leuchtdioden (OLEDs) in der Displayindustrie weit verbreitet und gelten als vielversprechendster Kandidat für die nächste Generation von Planern und flexiblen Displays. Es gibt jedoch noch einige Probleme mit organischen Halbleitern (insbesondere polymeren), die gelöst werden müssen, um mit der kommerziellen Technologie mithalten zu können. Um dies zu erreichen, besteht eine der idealen Lösungen darin, die negativen Auswirkungen von Verlustprozessen in polymeren Leuchtdioden (PLEDs) zu eliminieren, um die Leistung des Bauelements zu verbessern. Einer der Hauptverlustprozesse besteht darin, dass in der aktiven Schicht der PLEDs ein Ladungsfallen auftritt, das die Geräteleistung nachteilig beeinflusst. Meistens würde eine Ladung, die in den Zentren der Falle gefangen ist, den strahlungsfreien Prozess abbauen. Es gibt jedoch einige strahlenfallenunterstützte Rekombinationen, die entweder von den Defekten oder von zusätzlichen Komponenten wie Chromophoren im System herrühren.

Diese Arbeit gliedert sich in zwei Hauptteile. In einem Teil haben wir uns hauptsächlich auf die Systeme mit strahlungsgefangener Rekombination konzentriert und deren negativen Einfluss auf die Geräteleistung beseitigt. Auf Polyfluoren (PFO) basierende PLEDs sind ein hervorragendes Modellsystem zur Visualisierung dieses Effekts der Fallenbeseitigung. Die blaue Emission von PFO wird von einer breiten, nichtssagenden grünen Emissionsbande begleitet, die von Ketonddefekten herrührt, die als Elektronenfälle wirken. Im ersten Teil dieser Arbeit zeigen wir, dass die durch sichtbare grüne Fallen unterstützte Rekombination beim Mischen mit einem Isolatorpolymer nahezu eliminiert wird. Infolgedessen kann nicht nur die blaue Emission von PFO vollständig wiederhergestellt werden, sondern auch die Effizienz der Geräte wird drastisch verbessert. Um die Allgemeingültigkeit des Konzepts zu belegen, wenden wir dieselbe Methode an, um auch die Farbreinheit von PLEDs zu verbessern, die auf einem Polymer vom Leitertyp, einem methylsubstituierten Poly (p-phenylen) -Leiterpolymer (Me-LPPP), basieren.

Im zweiten Teil dieser Arbeit haben wir uns auf ein weiteres Hauptthema im PLED-Bereich konzentriert, nämlich die Realisierung von Vollfarbdisplays mit hoher Farbreinheit. Bei Displays ist es wichtig, kleine Linienbreiten zu haben, um gesättigte Farben zu erzielen. Aus diesem Grund sind heutzutage Quantenpunkte (QDs) ein attraktiver Kandidat für die Display-Technologie. QD-LEDs leiden jedoch unter einem unausgebalancierten Ladungstransport und auch unter einer Komplexität ihrer Vorrichtungsstruktur. Der Weg zu einer robusten und einfachen Struktur wäre die Verwendung eines Systems, bei dem die QDs einfach mit einem organischen Wirt gemischt werden. Alle Versuche in diese Richtung schlugen aufgrund des Problems des Einfangens von Elektronen in QDs fehl. Im zweiten Teil dieser Arbeit zeigen wir, dass das Einfangen von Elektronen durch rote CdSe / $\text{Cd}_x\text{Zn}_{1-x}\text{S}$ -Kern / Schale-QDs in einem blau

emittierenden PFO-Wirt durch Funktionalisierung mit einer dünnen isolierenden Schale stark unterdrückt werden kann. Unsere Ergebnisse eröffnen einen neuen Weg in Richtung emittierender Bauelemente mit schmaler Linienbreite, bei denen der aktiven Schichtdicke aufgrund der Aufrechterhaltung des Ladungstransports keine Grenzen gesetzt sind.

Table of Contents

Chapter 1: History and introduction.....	1
1. 1 History of lighting.....	2
1. 2 Application of OLEDs	4
1. 3 Evolution of OLEDs	5
1. 4 Basic principles of OLEDs	8
1. 4. 1 Introduction of organic semiconductors.....	8
1. 4. 2 Small molecules vs polymers.....	9
1. 4. 3 OLED working principle	11
1. 5 Electrical properties of organic semiconductor.....	12
1. 6 Photo-physics of an organic semiconductor	25
1. 7 OLED challenges	28
1. 8 Scope of this thesis.....	30
References.....	33
Chapter 2: Visualization of trap dilution in polyfluorene based light-emitting diodes.....	40
2.1 Introduction.....	41
2.2 Results and discussion	42
2.3 Conclusion	52
References.....	53
Chapter 3: Efficiency enhancement of polyfluorene:polystyrene blend light-emitting diodes by simultaneous trap dilution and β -phase formation.....	55
3.1 Introduction.....	56
3.2 Experimental section.....	56
3.3 Results and discussion	57
3.4 Conclusion	66

References.....	67
Chapter 4: Suppression of electron trapping by quantum dot emitters using a grafted polystyrene shell ..	71
4.1 Introduction.....	72
4.2 Experimental section.....	76
4.3 Results and discussion	79
4.4 Conclusion	97
References.....	98
Chapter 5: Trap-Assisted Triplet Emission in Ladder Polymer-based Light Emitting Diodes.....	102
5.1 Introduction.....	103
5.2 Results and discussion	104
5.3 Conclusion	115
References.....	116
Chapter 6: Summary and conclusion	120
Appendix.....	124
Declaration.....	124
List of publications	125
List of conferences.....	126
Curriculum Vitae	127

List of figures

Figure 1. 1 Lighting evolution from fire to LED bulb (adapted from Ref 12).....	3
Figure 1. 2 Products with OLED display a) Samsung galaxy X b) LG G flex c) Apple watch d) LG EC9300 curved TV.	4
Figure 1. 3 Next generation of OLED lighting a) Siemens b) Acuity.....	5
Figure 1. 4 The simple structure of an OLED including anode, cathode and emissive layer.	6
Figure 1. 5 Generation process of OLED materials. a) Conventional fluorescent OLED in which only 25% of excitons (Singlet) are radiative, b) phosphorescent materials which in theory can reach to 100% internal efficiency by using heavy metals c) TADF materials, the S1 and T1 levels are close to each other and reverse energy transfer occurs with a high efficiency, enabling 100% radiative excitons in theory.	7
Figure 1. 6 Alternation of single and double bonds between carbon atoms in polyacetylene.	8
Figure 1. 7 The chemical structures of-(a) poly(p-phenylene vinylene) (PPV), (b) polyfluorene and (c) ladder-type poly(paraphenylene)	10
Figure 1. 8 Schematic overview of a) the three dominant processes during PLED operation: 1) injection, 2) transport and 3) recombination b) Electron-only device with two low work function electrodes c) Hole-only device with two high work function electrodes	12
Figure 1. 9 schematical picture of a disordered conjugated polymer. Distribution of long conjugation length which corresponds to a narrow band gap and short conjugation length which results in a wider bandgap.	14
Figure 1. 10 a) Plot of the current density versus voltage for a MEH-PPV based hole-only device (black squares), electron-only device (blue diamonds), and PLED (dual carrier) device (red circles). Obtained from ref ⁶⁵⁻⁶⁶ . b) Schematic image of trap-free hole transport and strongly trap-limited electron transport because of a trap level in the band gap. Two types of recombination processes are possible: Radiative Langevin recombination between free carriers and non-radiative Shockley-Read-Hall recombination between trapped-electrons and free holes.	20
Figure 1. 11 Slope of log J-log V of the hole or electron current versus HOMO or LUMO level shown for different organic semiconductors which define an energy window for trap-free charge transport. Obtained from Ref. 70.	21

Figure 1. 12 Simulation of contribution of loss effects to the PLED efficiency for a 75 nm MEH-PPV diode as a function of voltage. Obtained from Ref. 75	24
Figure 1. 13 a) Hole and electron transport in hole-only and electron-only devices of 10:90% MEHPPV:PVK. b) luminous efficiency versus applied voltage for reference MEH-PPV and 10%MEH-PPV:90% PVK PLED Obtained from Ref. 79, 78, 68.....	25
Figure 1. 14 The summary of photophysical processes in an isolated organic molecule in Jablonski diagram. The vibrational levels for a given electronic energy level lie above each other, shown as vertical lines. The ground vibrational state is highlighted in bold. VR: vibrational relaxation; IC: internal conversion; ISC: intersystem crossing.....	26
Figure 1. 15 Schematic illustration of a) the Förster energy transfer and b) the Dexter energy transfer mechanism between Donor and Acceptor molecules.	28
Figure 2. 1 Hole and electron current density versus voltage for unblended PFO-F (a) and PFO-F:PS blend (1:9) (b). The thickness for the hole-only and electron-only devices amounts to 100 and 160 nm, respectively. The dashed lines are the calculated hole currents for the layer thickness that corresponds to the electron-only devices (160 nm).....	44
Figure 2. 2 Electroluminescence spectra of a PLED based on a 100 nm active layer of unblended PFO-F, recorded at different voltages. The spectra have been normalized relative to the peak at 438 nm, corresponding to the 0-0 transition (color on-line)..	46
Figure 2. 1 Electroluminescence spectra of PLEDs based on ~100 nm active layers of unblended PFO-F and PFO-F:PS blends with various blend ratios. All spectra have been recorded at 6V.....	47
Figure 2. 4 Electroluminescence spectrum of a PLED containing a 100nm active layer based on the 1:3 PFO-F:PS blend, recorded at different voltages. The spectra have been normalized relative to band corresponding to the 0-0 transition (438 nm).....	48
Figure 2. 5 <i>J-V</i> characteristic of hole-only devices based on a 100 nm film of a) unblended PFO-F and b) PFO-F:PS (1:9) blend for temperatures ranging from 295K to 215K.	49
Figure 2. 6 Ratio of bimolecular Langevin recombination and trap-assisted SRH recombination as a function of voltage for different blend ratios... ..	50
Figure 2. 7 Deconvolution of Normalized electroluminescence intensity For a) Unblended PFO-F b) PFO-F:PS(1:1) c) PFO-F:PS(1:3) d) PFO-F:PS(1:9)..	51
Figure 2. 8 Comparison between calculated and experimentally determined ratios of green to blue emission, respectively stemming from trap-assisted and Langevin recombination in PFO-F:PS blends. The	

recombination ratio is plotted as a function of polystyrene weight fraction. The experimental and calculated data have respectively been obtained from EL-spectrum deconvolution and numerical drift-diffusion modeling and correspond to an operating voltage of 6V... 52

Figure 3. 1 Hole and electron current density versus voltage for unblended PFO (dash black) and PFO:PS blend (1:3 w/w , solid red). The thickness for the hole-only (HO) and electron-only (EO) devices amounts to 100nm.. 58

Figure 3. 2 (a) Current density- and photocurrent density-voltage characteristics of PLEDs: unblended PFO (dash black) and blend with PS (1:3 w/w, solid red) (b) Luminous efficiency of the devices in part a... 59

Figure 3. 2 (a) Electroluminescence (EL) spectra of PLEDs based on unblended PFO (dash black) and PFO:PS (1:3 w/w, solid red) as emissive layer. The EL spectra have been normalized relative to band corresponding to the 0-1 transition (448 nm, unblended PFO) and 0-0 transition (PFO:PS blend) at 436 nm. (b) Photoluminescence (PL) spectra (in absolute counts) of PFO and PFO:PS (1:3) films ($d = 100$ nm) cast from chlorobenzene.....61

Figure 3. 4 Peak-normalized absorption spectra of unblended PFO (dash black) and PFO:PS (1:3 w/w, solid red) films casted from chlorobenzene. 63

Figure 3.5 AFM surface topography a) Unblended PFO with scale bar 4 μm , b) PFO with low molecular weight PS with scale bar 2 μm and c) PFO with high molecular weight PS with scale bar 5 μm65

Figure 4. 1 Schematic energy diagram and electroluminescence spectrum of a) Blend of large band gap organic host and an organic dye resulting in severe electron trapping. b) Blend of large band gap organic host and an inorganic QD, leading to electron trapping and charging effects that enhance hole capture... 74

Figure 4. 2 a) Synthesis of diblock copolymer poly(styrene-block-cysteaminemethyldisulfide) (P(S-b-SSMe), b) The ligand exchange procedure and c) Energy-band diagram of PFO:QD system..... 80

Figure 4. 3 Solubility change from pure QDs to QD/PS-hybrids, normal (left) and UV light (right). Pure QDs, coated by oleic acid, are soluble in hexanes. QD/PS-hybrids, coated by polymer, are insoluble in hexanes, resulting in precipitation. In a biphasic system of hexanes (upper phase) and *ortho*-dichlorobenzene (lower phase), pure QDs are soluble in upper hexanes phase, QD/PS-hybrids are soluble in lower *ortho*-dichlorobenzene phase. 81

Figure 4. 4 T IR spectra of QD/PS-hybrids and polymer and TGA spectra of pure QDs and QD/PS-hybrids. (left) IR spectra of QD/PS-hybrids and polymer, signals at 3000 cm^{-1} attributed to -CH-vibrations and signals at 1650 cm^{-1} and 1520 cm^{-1} attributed to the disulfide anchor group are observed in the IR spectra of QD/PS-hybrid, (right) TGA spectra of QD/PS-hybrids, coated with polymer, weight loss 25 wt%. ... 81

- Figure 4. 5** IR spectra of P(S-*b*-PFPA) and after post-polymerization modification of P(S-*b*-SSMe). IR spectra of P(S-*b*-PFPA) shows characteristic signal at 1786 cm⁻¹ attributed to reactive ester block before post-polymerization modification and IR spectra of P(S-*b*-SSMe) shows characteristic signal at 1654 cm⁻¹ attributed to the amide group of the disulfide anchor block, the signal at 1786 cm⁻¹ vanished after post-polymerization modification..... 82
- Figure 4. 6** 19F-NMR spectra of P(S-*b*-PFPA) (top) and after post-polymerization modification of P(S-*b*-SSMe) (bottom). 19F-NMR spectra of P(S-*b*-PFPA) shows characteristic signal of reactive ester block... 82
- Figure 4. 7** SEC curves of all reaction steps. Measured in THF, polystyrene standards (UV-vis detector). 83
- Figure 4. 8** DOSY 2 D NMR spectrum of P(S-*b*-SSMe). Only one diffusing species demonstrates the successful post-polymerization modification step. 83
- Figure 4. 9** Voltage dependence of normalized EL spectra for PLED with 100 nm PFO:3% oa-QD/PS blend active layer a) first up-scan and b) consecutive down-scan. Voltage dependence of normalized EL spectra for PLED with 100 nm PFO:3% QD/PS-hybrid blend active layer c) first up-scan) and d) consecutive down-scan, e) fifth up-scan and f) corresponding down-scan..... 86
- Figure 4. 10** EL spectrum of a device based on PFO with 3% QD-Hybrid versus energy. the FWHM linewidth of the red QD emission is significantly smaller as compared to the blue PFO emission..... 87
- Figure 4. 11** Voltage dependence of normalized EL spectra for PLED with 100 nm PFO:5% QD/PS-hybrid blend active layer a) second up-scan), b) consecutive down-scan, c) third up-scan and d) corresponding down-scan, e) fourth up-scan and f) corresponding down-scan. 88
- Figure 4. 12** Photoluminescence spectra of PFO: oa-QD blend and QD/PS-hybrid blend for 5% QD concentrations. An excitation wavelength of 390 nm was used. 89
- Figure 4. 13** Normalized electroluminescence spectra of PFO with 5% QD/PS hybrids with shell thickness of a) 3nm b) 6nm. The relative contribution of red QD emission to blue PFO emission strongly decreases with increasing PS shell thickness.. 90
- Figure 4. 14** SEM image of PLED active layer with PFO:5% oa-QDs. b) SEM image of PLED active layer with PFO:5% QD/PS-hybrids.. 91
- Figure 4. 15** Cross-sectional SEM image of PLED active layer with PFO:5% QD/PS-hybrids..... 91
- Figure 4. 16** Voltage dependence of normalized EL spectra and SEM images for PLED with 100 nm. a) PFO:3% QD/PS-hybrid b) PFO:5% QD/PS-hybrid c) PFO:7% QD/PS-hybrid blend active layer. 92

Figure 4. 17 Normalized electroluminescence spectra of PFO with 5% QD/PS hybrids with shell thickness of a) 3nm b) 6nm. The relative contribution of red QD emission to blue PFO emission strongly decreases with increasing PS shell thickness.. 93

Figure 4. 18 a) Current density and photocurrent density vs voltage after initial charging, b) Photocurrent efficiency vs current density of PLED..... 95

Figure 4. 19 a) Chemical structure of the PSF-TAD polymer. The composition copolymers are $m = 50\%$ and $n = 37.5\%$ (PSF) and $o = 12.5\%$ (TAD) b) schematic energy diagram of blend of PSF-TAD with QD with high injection barrier for holes from host to guest. c) Electroluminescence spectra of PSF-TAD with 5% QD/PS-Hybrid d) electron current density of devices with 110nm active layer for unblended PSF-TAD and blend of PSF-TAD with 5% and 10% QD/PS-hybrid and 10% of oa-QD..... 96

Figure 4. 20 Lifetimes of devices with 110nm active layer for unblended PFO and blend of PFO with 5% QD/PS-hybrid under constant-current over time.. 97

Figure 5. 1 Hole and electron current density versus voltage for Me-LPPP hole- and electron-only devices. Symbols are experimental results, the solid lines are fits using EGDM (free electrons and holes) and electron traps consisting of universal electron traps (dashed line) and an additional single-level trap (solid line)..... 106

Figure 5. 2 J - V characteristic of a) hole-only devices based on a 115 nm film of Me-LPPP for temperatures ranging from 295 K to 215 K. b) electron-only devices based on a 115 nm film of Me-LPPP for temperatures ranging from 295 K to 275 K. (symbols: experimental results, solid lines: modeling results)..... 107

Figure 5. 3 a) Current and photocurrent density of PLED based on a 120nm active layer of Me-LPPP, b) Electroluminescence spectrum (solid line) and Photoluminescence spectrum (dash line) of the same device..... 108

Figure 5. 4 Voltage sweep of normalized electroluminescence spectra for PLED with Me-LPPP as emissive layer. 110

Figure 5. 5 Figure 5. 5 Deconvolution of EL Spectra recorded at different voltage a) 5V b) 6V c) 7V d) 8V 111

Figure 5. 6 The light output of the singlet and triplet peaks as function of PLED current density..... 112

Figure 5. 7 a) Differential capacitance C versus frequency at various bias voltages. The symbols represent the experimental data, while the solid lines are a fit to Eq. (3) using τ_r 20 ms and b) C - V characteristics of a Me-LPPP PLED at different frequencies c) $\alpha(V)$ values obtained from Eq. (3) as a function of voltage.. 114

Figure 5. 8 Electroluminescence spectra of PLEDs based on ~120 nm active layers of unblended Me-LPPP and Me-LPPP:PS blends with various blend ratios. All spectra have been recorded at 8V. 115

Chapter 1

History and introduction

In this chapter, a brief history of lighting technology and the evolution of organic light emitting diodes (OLEDs) have been provided. To understand the operation of polymer based light emitting diodes (PLEDs), the device characteristics, including charge transport, recombination and charge trapping processes, are introduced. Finally, a general overview of the OLED challenges and the scope of this thesis is presented.

1.1 History of lighting

The discovery of primal light sources based on fire, like oil lamps, candle and gas lamps was one of the biggest steps along the humankind progress path. The availability of these lighting sources gave mankind extended freedom from natural light limitation; sunrise and sunset. In the 19th century, carbon arc light as the first form of electric lighting was developed. The arc light works based on creating bright plasma due to the ionization of air between two carbon electrodes. Later Thomas Edison was awarded for introducing light bulb with improved design as a more proper light source which revolutionized the modern life. The light bulb is working based on incandescence. In a light bulb a thin tungsten filament is heating up when an electric current is applied. The emission from filament results from its elevated temperature. Although, the light bulb has been used for more than a century, they are highly inefficient since they convert almost 95% of the consumed energy into heat rather than light. ¹⁻⁵

For the past few decades power crisis is one of the most concerning problems due to increasing population and rapid industrial growth. In the last decades almost majority of the power generation techniques are based on fossil fuel, gas and coal, which is not only limited but is also a treat for air and water pollution and therefor global warming. So, to solve the power crisis, alternative means are needed to be taken account. ⁶ In last few decades lots of attempts have been done to generate power in coherence with the demand of consumers with reduced power consumption. Newer technologies alternative to the light bulb are the fluorescent and the compact fluorescent lamp with higher efficiency. However, still the production of heat as loss process is a major problem. Recently in the past decades, a new field of study called solid-state lighting (SSL) has been developed. SSL offers many benefits such as long life, energy saving and better quality light. In

SSL light emitting diodes (LEDs) based on semiconductors are used to generate light via electroluminescence process. LEDs have an efficiency of around 100 lm/W which is significantly higher than the incandescence bulb (15 lm/W) and compact fluorescent lamp (60 lm/W).⁵ One of the special classes of LEDs is organic light-emitting diodes (OLEDs) in which the active layer consists of an organic semiconducting material instead of typical inorganic semiconductor like silicone and gallium arsenide.⁷⁻¹¹ The evolution of lighting sources can be seen in **Figure 1. 1**.



Figure 1. 1 Lighting evolution from fire to LED bulb (adapted from Ref 12)

OLEDs have thin film device structure, typically only a few hundred nanometers which show several advantages over other lighting sources even inorganic LEDs. Usually the temperature during operation of an OLEDs is around 30°C whereas it reached to 90°C for incandescent bulbs and 60°C for fluorescent tubes.¹³ Moreover compared to inorganic LEDs, they have the potential to be produced in large flexible area with lower cost, less power consumption, color tuning flexibility with very good color rendering index (CRI) and so on. More importantly, the OLED's advantages enable new design concepts such as transparent lighting panels and luminescent

wallpapers. However, the OLED research field is relatively new and improvement with respect to lifetime and efficiency is still required before they can make their inroad into the market.

1.2 Application of OLEDs

The enormous growth of the electronics industry over recent years has led OLED technology transfer from research concepts in laboratory into a commercialized technology. Nowadays OLEDs can be found as the emissive element in many modern consumer electronic devices, like television, smart phones, tablets, smart watches and digital cameras. The large well-known electronic companies such as LG, Samsung, Sony and Apple are driving the technological movement in state-of-the-art OLEDs applications (**Figure 1. 2**). This growth is expected to come from large screen televisions, to the automotive, aerospace industry, and wearable electronics.



Figure 1. 2 Products with OLED display a) Samsung galaxy X b) LG G flex c) Apple watch d) LG EC9300 curved TV.

Compared to OLED displays, OLED lighting still hasn't reached a full-level of commercialization. However, it is expected that in the near future, OLED lighting systems can

become cost and performance competitive with conventional technologies, since the industry is becoming more sophisticated and mature. For example companies like Siemens¹⁴ and Acuity¹⁵ have released their next generation OLED lighting prototypes as promising environmentally friendly lighting source in new design media (**Figure 1. 3**)

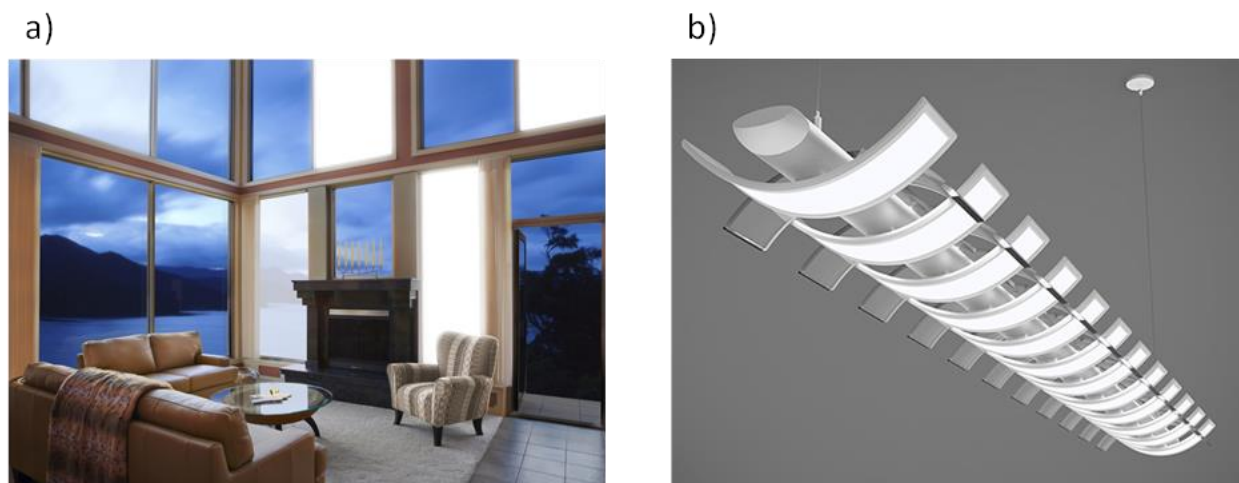


Figure 1. 3 Next generation of OLED lighting a) Siemens b) Acuity.

1. 3 Evolution of OLEDs

The simplest OLEDs as electroluminescent devices consists of multiple organic layers sandwiched between two electrodes: an anode and a cathode.^{16,17} **Figure 1. 4** shows a simplified cross section of a single active layer OLED. Tang and Van Slyke reported for the first time a simple and efficient OLED structure in 1987.¹⁶ Their device structure consisted of a two-layer organic stack between indium tin oxide (ITO) and silver as anode and cathode respectively. Electroluminescence from organic materials had been reported before,¹⁷ but this structure was the first one achieving an external quantum efficiency above 1% with high luminance values. However, due to the limitation of emission from singlet excitons and losing 75% of exciton due to

their triplet origin, the initial fluorescent LEDs can reach up to a maximum of 25% internal quantum efficiency (IQE).

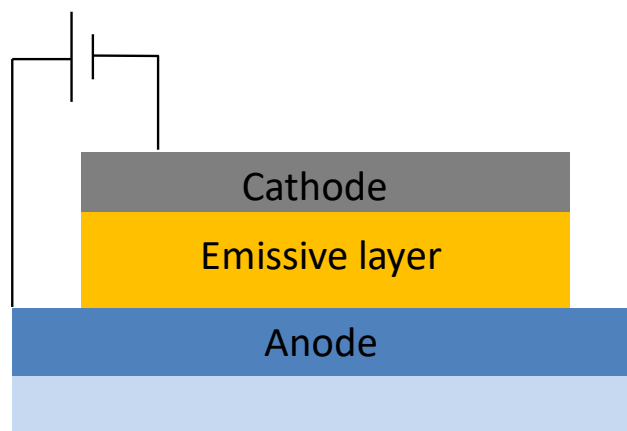


Figure 1. 4 The simple structure of an OLED including anode, cathode and emissive layer.

OLED based on fluorescent emitters remained the state-of-the-art active materials for almost a decade. In 1998, Forrest and Thompson reported the first phosphorescence emitters by incorporating iridium and platinum complexes to harvest triplet state excitons. This strategy would allow reaching 100% IQE and therefore could pave the way for further development of highly efficient OLEDs.¹⁸ After this first report, a wide variety of iridium and platinum based emitters have been developed which reach the EQE's more than 25% for blue-, green- and red-emitting doped structures, with both vacuum and solution processed techniques.^{19,20,21} Phosphorescent emitters are usually doped in a host material to be used as a blend representing the emissive layer (EML) of the OLED. In order to design higher efficiency OLED devices with low voltage operation, a multi-layer device structure is needed.²² In general, these layers consist of hole and electron injection and transport layers (HIL and EIL, respectively). Each of these layers is selected to reduce the energetic barrier between the electrodes and the EML. In addition, the multi-layer structure would lead to charge balance in the system.

Although, phosphorescent OLEDs can reach a very high efficiency, these materials have several problems, such as their structure being limited to organic metal compounds containing rare metals. A promising solution to this problem is to move away from phosphorescent emitters towards fluorescent emitters that exhibit a phenomenon known as thermally activated delayed fluorescence (TADF). In a TADF emitter which is the latest generation of OLEDs, the singlet (S_1) and triplet (T_1) levels are strongly coupled which allows for reverse intersystem crossing (ISC) between the two levels.²³ In addition the molecule is designed so that the energy difference between the S_1 and T_1 (ΔE_{ST}) is much smaller than in typical organic molecules which enables reverse intersystem crossing (RISC) to occur: triplet excitons are converted back into singlets in a thermally activated process (**Figure 1. 5**). Consequently, in the singlet state the excitons can decay back to the ground state via delayed fluorescence. The TADF mechanism can pave the way for achieving internal quantum efficiency of 100% without using heavy metal complexes.²³

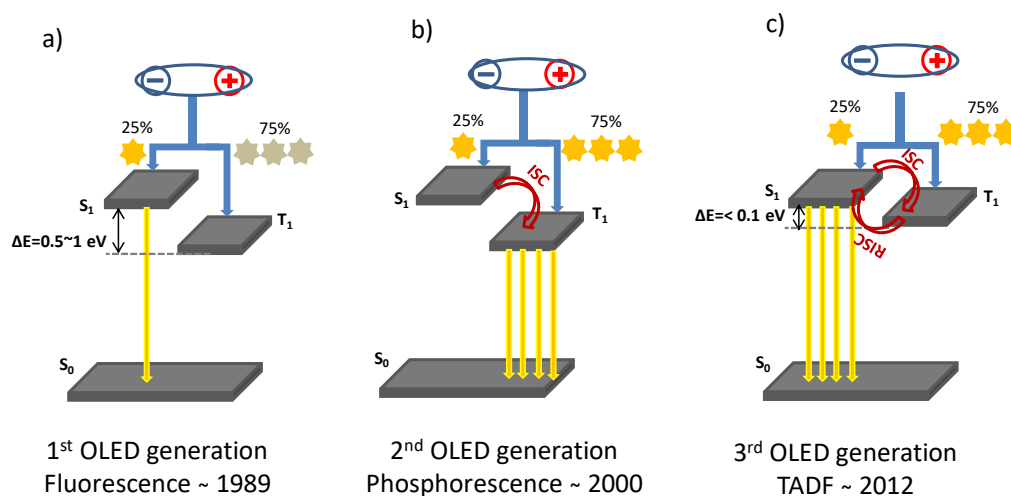


Figure 1. 5 Generation process of OLED materials. a) Conventional fluorescent OLED in which only 25% of excitons (Singlet) are radiative, b) phosphorescent materials which in theory can reach to 100% internal efficiency by using heavy metals c) TADF materials, the S_1 and T_1 levels are close to each other and reverse energy transfer occurs with a high efficiency, enabling 100% radiative excitons in theory.

1.4.1 Introduction of organic semiconductors

6) This discovery was honored with the nobel prize in chemistry in the year 2000.³⁵

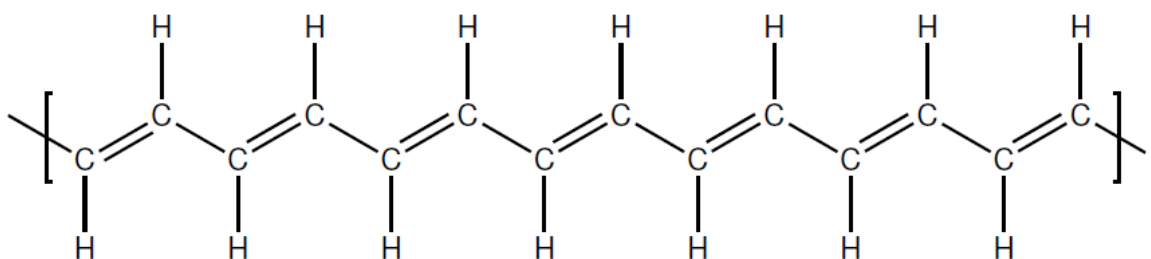


Figure 1. 6 Alternation of single and double bonds between carbon atoms in polyacetylene.

The special feature which leads to this unique property in organic semiconductors is the alternation of single and double bonds between carbon atoms, called conjugation. Conjugation results from the overlap of one p orbital with another across an involved σ bond. In organic semiconductors, carbon atoms bind to each other by an in-plane σ bond as a result of SP^2 orbital hybridization. There would be also a second bond which is a π bond. This bond results from overlapping between the remaining electron in p_z orbital of one carbon atom (which is perpendicular to the σ bond) with that of the neighboring carbon atom. This overlap leads to delocalization of electrons over the polymer backbone to some extent (which is known as effective conjugation length) and therefore conducting properties. The π bond can be excited to a π^* anti-bond. The energy of the π bond, which is occupied in the ground state, is named the highest occupied molecular orbital (HOMO) whereas the excited π^* bond is called the lowest unoccupied molecular orbital (LUMO). The HOMO and LUMO levels are equivalent to the valence and conduction band of inorganic semiconductors. In organic semiconductors the band gap corresponds to the π - π^* energy difference (HOMO-LUMO energy difference) which is typically between 1 to 4 eV. This makes organic semiconductors proper candidate for optoelectronics applications.

1. 4. 2 Small molecules vs polymers

Organic semiconductors are categorized into two classes based on the molecular weight, namely semiconducting polymers and small molecules. Based on that there are two main classes of organic light-emitting diodes: OLEDs (small-molecule based light emitting diodes) and PLEDs (polymer light emitting diodes). PLED materials do not perform as well as OLEDs in terms of lifetime and efficiency, but are easily soluble and so can be easily adapted for printing and other

solution-based processes. The variability in design possibilities in semiconducting polymers allows for tailoring of the material properties such as emission color, solubility, and charge transport properties. Some examples of conjugated polymers are shown in Figure 1. 7.

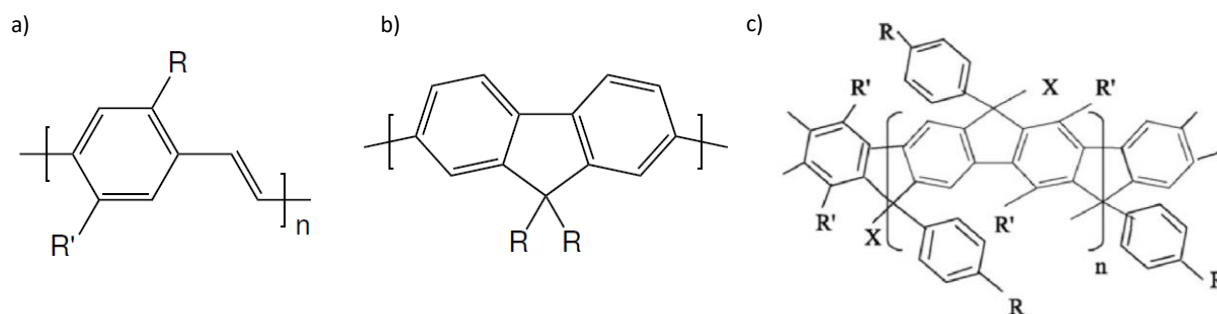


Figure 1. 7 The chemical structures of-(a) poly(p-phenylene vinylene) (PPV), (b) polyfluorene and (c) ladder-type poly(paraphenylene)

One of the well-studied conjugated polymer is poly (p-phenylene vinylene) (PPV). In Figure 1. 7a the general structure of a PPV polymer can be seen. Since PPV has a poor solubility in organic solvents, it should be functionalized with proper side chains. By differing the side chains different PPV derivatives can be synthesized, for example poly[2-methoxy-5-(2-octyldioxy)-p-phenylene vinylene] (MEH-PPV) is one of the well-studied PPV derivatives which emits red.

Blue emitting materials are essential to have the full color spectrum. Poly(9,9-dialkylfluorene) (PFO) (Figure 1. 7b), is one of the well-known blue emitting conjugated polymers which has been used in this thesis as the main EML material in PLEDs in chapters 2, 3 and 4.

In a typical one-dimensional polymer, the monomers form two bonds, giving a chain. Ladder polymer are a class of conjugated polymers in which the monomers are interconnected by four bonds and therefore they have a rigid structure with reduced disorder. Methyl-substituted Poly(p-

phenylene) (Me-LPPP), shown in figure 1.7c, is one of the ladder type polymers which has been studied in the past few decades. In chapter 5 of this thesis, the device operation of LPPP-based PLED will be addressed.

1. 4. 3 OLED working principle

As it has been shown in **Figure 1. 4**, in their simplest form OLEDs consists of a thin layer of an organic semiconductor sandwiched between two metallic electrodes, one of which is transparent to allow the light to transmit. The dominant processes that control the operation of the OLED are: charge injection, charge transport and recombination (**Figure 1. 8**).³⁶⁻³⁷ When a voltage is applied, holes and electrons are injected by the anode and cathode, respectively. The charge carriers move through the polymer film till they meet, recombine into an exciton, which emits a photon upon relaxation to the ground state. The energy released upon recombination depends on the bandgap of the material in the EML and determines the emission light color. The charges injected by the electrodes must overcome or tunnel through a barrier between the HOMO/LUMO of the EML and the electrode work-function. Therefore an efficient charge injection can be obtained when the work function of the anode and cathode match the HOMO and LUMO of the active layer, respectively, to achieve ohmic hole and electron contacts.³⁸⁻³⁹

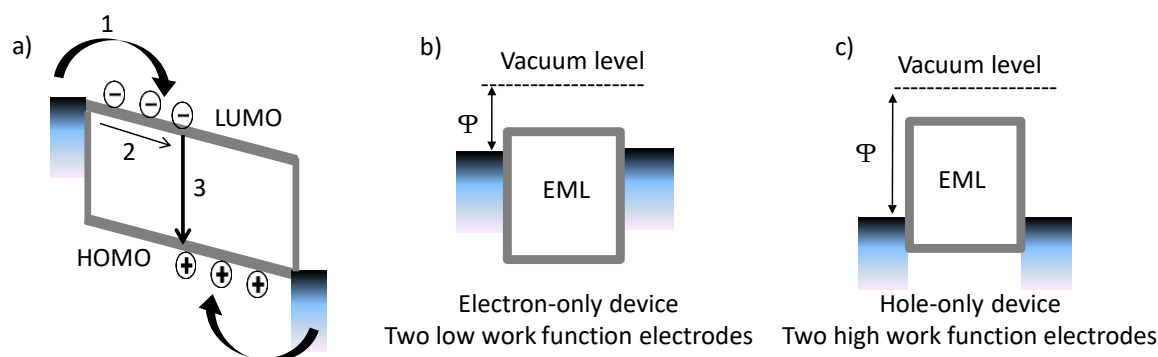


Figure 1. 8 Schematic overview of a) the three dominant processes during PLED operation: 1) injection, 2) transport and 3) recombination b) Electron-only device with two low work function electrodes c) Hole-only device with two high work function electrodes

1. 5 Electrical properties of organic semiconductor

1. 6. 1 Charge transport

The device current could be either limited by charge injection or by the bulk transport, depending on the height of the injection barrier.

Bulk limited transport occurs when the injection barriers are sufficiently small (< 0.3 eV).⁴⁰⁻⁴¹ An effective way to investigate the injection barrier and charge transport in organic semiconductors is to check them in single-carrier device structure. Hole- and electron-only devices can be fabricated by sandwiching the active material in between two high work function and two low work function electrodes, respectively (Figure 1.8b and c). Therefore, hole and electron injection and transport properties of the material can be investigated in hole- and electron-only devices. It has been shown that for PPV derivatives ohmic injection can be obtained by using typical injection materials such as barium and PEDOT:PSS for electron and hole injection respectively. However for materials with a deep HOMO level, such as PFO, PEDOT:PSS is not an ohmic contact anymore.

Very recently, a simple and robust way of forming an ohmic hole contact on organic semiconductors with a high ionization energy (IE) has been proposed.⁴² The injected hole current from high-work-function metal-oxide electrodes is improved by more than an order of magnitude by using an interlayer for which the sole requirement is that it has a higher IE than the organic semiconductor. Insertion of the interlayer results in electrostatic decoupling of the electrode from the semiconductor and realignment of the Fermi level with the IE of the organic semiconductor. The ohmic-contact formation is illustrated for a number of material combinations and solves the problem of hole injection into organic semiconductors with a high IE of up to 6 eV.⁴²

When the contacts are ohmic, the device current is limited by the bulk transport which is called space-charge limited current (SCLC).⁴³ In this type of transport, the amount of injected charges into the device per unit time is limited by an electrostatic field as a result of space charges. Mott and Gurney described the SCL transport as a function of voltage (V) and active layer thickness (L) by considering a constant mobility (μ):

$$J_{SCL} = \frac{9}{8} \epsilon_0 \epsilon_r \mu \frac{V^2}{L^3} \quad (1)$$

, where ϵ_0 and ϵ_r are the vacuum permittivity and dielectric constant of the semiconductor, respectively.

Mobility is one of the most important semiconductor material parameters. It is a measure for the conductivity. The mobility is defined by the quotient of the average drift velocity (v) of the carriers and the electric field (E): $\mu = \frac{v}{E}$.

To further understand how charges are transported through a semiconductor, energetic disorder has to be considered. Inorganic semiconductors are highly ordered materials with a periodic lattice

which results in delocalization of charge carriers. The charge transport in inorganic semiconductors is limited by scattering of carriers with phonons. Therefore, the charge carrier mobility is lower at higher temperature.⁴⁴ In contrast, in organic semiconductors due to the hopping nature of the transport, by increasing temperature the mobility decreases.⁴⁵ However, in general the mobility in organic semiconductors is much lower than in inorganic semiconductors. The reason is that organic semiconductors and specifically polymers are highly disorder and mostly with amorphous structure.⁴⁶ In addition, there are several physical defects in a polymer chain which leads to break in conjugation. Therefore, polymer chains consist of several segments with different conjugation length and consequently different energy states. This energy distribution leads to spreading in site energies, so-called energetic disorder, of about 0.1-0.2 eV.⁴⁷ As it shown in **Figure 1. 9**, the longer the conjugation length, the smaller the energy gap is.

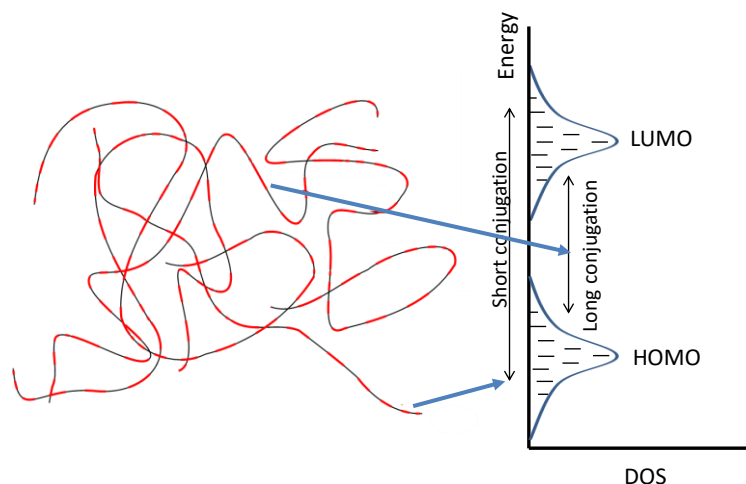


Figure 1. 9 schematical picture of a disordered conjugated polymer. Distribution of long conjugation length which corresponds to a narrow band gap and short conjugation length which results in a wider bandgap.

It has been shown that the trap-free hole transport at room temperature in most of the conjugated polymers can be described by SCLC model but only in low electric field. At higher voltage the current increases faster than SCLC model prediction. This observation means mobility

is field dependent as already has been shown in time-of-flight studies as well.⁴⁸ In addition, it was found that the mobility is also temperature dependent and obeys Arrhenius' law.^{47, 49} To explain this deviation caused by field and temperature dependence, Poole and Frenkel⁵⁰ proposed an empirical field-and temperature-dependent mobility by:

$$\mu_{\text{PF}}(T, E) = \mu_0^* \exp\left(\frac{-\Delta U}{kT}\right) \exp(\gamma\sqrt{E}) \quad (2)$$

where μ_0^* is the mobility when the temperature is infinite and electric field is zero, ΔU is the activation energy, k the Boltzmann constant, T the absolute temperature, E the electric field, and γ is a field activation parameter. In 1972 Gill applied equation (2) successfully for describing the transport properties in PVK for the first time.³⁰⁻³¹ However, the equation was purely based on empirical observation and a theoretical justification was still missing.

Later, a simulation-based model was introduced by Bässler which explains both the temperature and field dependency of the mobility. In this model, the charge transport mechanism is assumed to be hopping of carriers in a Gaussian distribution of states with a width σ . Hence, the mobility dependence that was proposed based on these calculations is known as the Gaussian disorder model (GDM).⁵¹ To calculate the mobility, a Monte Carlo simulation approach was used and an analytical description was obtained in the form of:

$$\mu = \mu_{\infty} \exp\left[-\left(\frac{2\sigma}{3kT}\right)^2\right] \cdot \begin{cases} \exp\left[C\left(\left(\frac{\sigma}{kT}\right)^2 - \Sigma^2\right)F^{1/2}\right], \Sigma \geq 1.5 \\ \exp\left[C\left(\left(\frac{\sigma}{kT}\right)^2 - 2.25\right)F^{(1/2)}\right], \Sigma < 1.5 \end{cases} \quad (3)$$

, with μ_{∞} as the mobility at infinite temperature, C is a constant that depends on the site spacing and Σ the degree of positional disorder. In this model $\ln(\mu)$ scales inversely on the square root of

the temperature and in contrast to Equation (2) is non-Arrhenius type. However, in high electric field the field dependency of GDM is in agreement with Equation (2).

To improve the agreement at low electric fields spatial energetic correlation between neighboring sites was taken into account by Gartstein and Conwell. This model is called correlated distribution model (CDM) in which the stretched exponential field dependence is extended to wider range of electric fields.⁵²⁻⁵⁴

$$\mu_{GDM}(T, E) = \mu_0 \exp \left[- \left(\frac{3\hat{\sigma}}{5} \right)^2 + 0.78(\hat{\sigma}^{3/2} - 2) \sqrt{\frac{qaE}{\sigma}} \right] \quad (4)$$

, where $\hat{\sigma} = \sigma/kT$, q is the elementary charge and a is the intersite spacing.

The field- and temperature-dependence of the mobility has been known since the mid-90's. However later it was found out that charge carrier density is another interfering factor which can influence the mobility as well. In measurements on diodes it is not straightforward to distinguish between the effect of the charge carrier density and the electric field on the mobility. In 2003 Tanase et al. combined diode measurements with field-effect transistor (FET) measurements.⁵⁵ In this study, they reported very different mobilities from FET and diode measurements. The measured mobility in FET was orders of magnitudes higher than the one from diode measurements. In a FET, the charge carrier density in the conductive channel of a FET is much larger than a the typical charge density in diodes, even though the electric field between source and drain is considerably smaller than the electric field in diodes.⁵⁶ Therefore, it can be concluded that the higher mobility in a FET is due to the higher charge carrier density in the conductive channel, which can be controlled by the gate voltage. This also explains the gate-voltage dependency of the mobility in a FET.⁵⁷⁻⁵⁹ The density dependent mobility can be explained by the depth of filling

states. In diodes, hopping mostly occurs via the sites in the tail of the DOS in which only few transport sites are available. In contrast, in a FET, due to the enhanced charge carrier density, the fermi-level will move toward the center of the DOS in which more hopping sites are available. Therefore, in a FET a higher mobility can be obtained than in a diode. It had been already shown that the mobility depends stronger on the charge carrier density than on the electric field.⁶⁰ Therefore, it was found out that the mobility cannot be reported as a single value for a material since it is highly dependent on measurement conditions and device structure.

In 1998, Vissenberg and Matters⁶¹ introduced an analytical definition for the density (p) dependence of the mobility in organic FETs, based on variable-range hopping in an exponential DOS:

$$\mu_{VM}(p) = \frac{\sigma_0}{q} \left[\frac{(T_0/T)^4 \sin(\pi T/T_0)}{(2\alpha)^3 B_c} \right]^{T_0/T} p^{T_0/T-1} \quad (5)$$

, in which σ_0 is a prefactor for the conductivity, B_c is the critical number for the onset of percolation, α^{-1} describes the effective overlap parameter between states and T_0 is the characteristic temperature describing the decay of the exponential DOS distribution.

More recently Pasveer et al⁶² introduced a model which fully describes the temperature-, field- and density-dependence of the mobility using the extended Gaussian disorder model (EGDM).⁶² In this model at higher temperature the density dependence becomes more important whereas at low temperature the field-dependence is more dominant. This model separates the density relation from the field dependence:

$$\mu_{EGDM}(T, n, E) = \mu_n(T, n) \mu_E(T, E) \quad (6)$$

The individual charge carrier density then is obtained by:

$$\mu(T, n) \approx \mu_0(T, n) \exp[-C\hat{\sigma}^2] \exp\left[\frac{1}{2}(\hat{\sigma}^2 - \hat{\sigma})(2na^3)^\delta\right], \delta = 2 \frac{\ln(\hat{\sigma}^2 - \hat{\sigma}) - \ln(\ln(4))}{\hat{\sigma}^2} \quad (7)$$

with a the intersite distance which is related to the transport site density as $a = \frac{1}{\sqrt[3]{N}}$ and $C = 0.42$.

The parametrized field dependency reads as:

$$\mu_E(T, E) = \exp\left\{0.44(\hat{\sigma}^{3/2} - 2.2) \left(\sqrt{1 + 0.8\left(\frac{eaF}{\sigma}\right)^2} - 1\right)\right\} \quad (8)$$

μ_0 is the mobility in zero field, zero charge carrier density and infinite temperature. In the limit of zero carrier density this model reduces to that of Bäessler in Equation 3.

1. 6. 2 Langevin recombination

Charge recombination is another important process in light emitting diodes. When holes and electrons are injected and transported into the active layer of organic semiconductor, charge recombination takes place. After electrons and holes recombine, the electron-hole pair forms an excited state, which is called an exciton.⁶³ These excitons play an important role in the photo-physical properties of the organic semiconductor. Generally, in pristine organic semiconductors recombination is considered as bimolecular recombination which is a radiative Langevin type process (**Figure 1. 10a**). In this process the limiting step is the diffusion of electrons and holes toward each other under the influence of their mutual Coulombic interaction.⁶⁴ The Langevin recombination rate is proportional to the density of holes and electrons with a prefactor that corresponds to the sum of the carrier mobilities:⁶⁴

$$R = \frac{e(\mu_n + \mu_p)}{\epsilon_0 \epsilon_r} np = k_L np \quad (9)$$

Where e is elementary charge, $\mu_{n,p}$ are the electron and hole mobility and k_L is the Langevin recombination coefficient.

1. 6. 3 Charge trapping in organic semiconductors

Based on the working principal of the OLED, it is obvious that the charge balance plays a critical role in the recombination rate and device performance. As mentioned, one way to investigate the hole and electron transport properties individually, is via single-carrier devices. Initial studies on PPV derivatives showed that the hole transport is quite high and well described by the space-charge-limited current, whereas the electron current is orders of magnitude lower and exhibits a much steeper voltage dependence (see **Figure 1. 10a**).⁶⁵⁻⁶⁶ This observation can be generalized for many of conjugated polymers. Although the hole and electron mobilities are usually equal in organic semiconductors, the electron current is orders of magnitude lower than the hole current in single-carrier devices. This observation is characteristic for trap-limited electron transport which indicates that electrons are severely trapped in the band gap of the organic semiconductor. Therefore, bimolecular Langevin recombination which has been discussed in last section is not the only recombination type in organic semiconductor. There is also a second pathway according to which free holes recombine with trapped-electrons non-radiatively, *i.e.* the so called Shockley-Read-Hall-recombination (SRH recombination), also known as trap-assisted recombination (**Figure 1. 10b**).

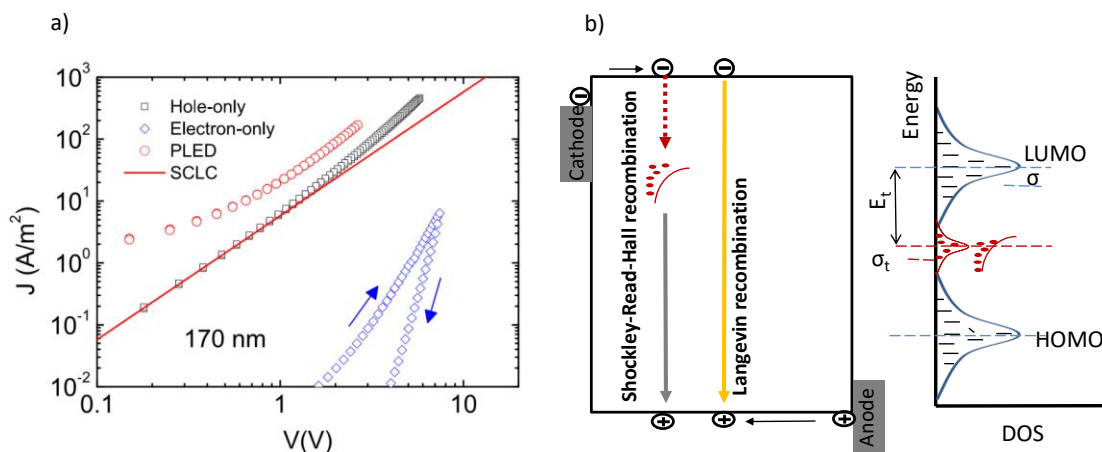


Figure 1. 10 a) Plot of the current density versus voltage for a MEH-PPV based hole-only device (black squares), electron-only device (blue diamonds), and PLED (dual carrier) device (red circles). Obtained from ref 65-66. b) Schematic image of trap-free hole transport and strongly trap-limited electron transport because of a trap level in the band gap. Two types of recombination processes are possible: Radiative Langevin recombination between free carriers and non-radiative Shockley-Read-Hall recombination between trapped-electrons and free holes.

Trap centers were initially attributed to physical defects in the polymer backbone, contamination from the environment or impurities which may remain from the synthesis.⁶⁷⁻⁶⁸ More recently Nicolai et al.⁶⁹ studied a range of conjugated polymers and plotted the double logarithmic slope of the electron JV characteristic as a function of the LUMO of the material in active layer (see **Figure 1. 11**). They observed that by increasing the LUMO of the material, the slope of the electron current decreases. For the polymers with a LUMO deeper than 3.8 eV, the slope of 2 was obtained which is a characteristic for a trap-free SCL current. By modeling electron current obtained from electron-only devices, they showed that electron traps are energetically centered around 3.6 ± 0.1 eV at a density of $N_t \approx 3 - 5 \cdot 10^{23} \text{ m}^{-3}$. Very recently the same investigation has been done for the hole transport in organic semiconductors.⁷⁰ Their study made it possible to identify an energy window inside which organic semiconductors do not experience

charge trapping for device-relevant thicknesses in the range of 100 to 300 nm, leading to trap-free charge transport of both carriers (**Figure 1. 11**). When the ionization energy of a material surpasses 6 eV, hole trapping will limit the hole transport, whereas an electron affinity lower than 3.6 eV will give rise to trap-limited electron transport. When both energy levels are within this window, trap-free bipolar charge transport occurs.⁷⁰ Organic semiconductors with energy levels situated within this energy window may lead to optoelectronic devices with enhanced performance. However, for blue-emitting light-emitting diodes, which require an energy gap of 3 eV, removing or disabling charge traps will remain a challenge. The fact that the electron and hole trap centers possess a specific energy level led to the assumption of a common extrinsic origin. Based on quantum-chemical calculations, it has been shown that water and oxygen complexes could be the origin of electron trapping.^{69, 71}

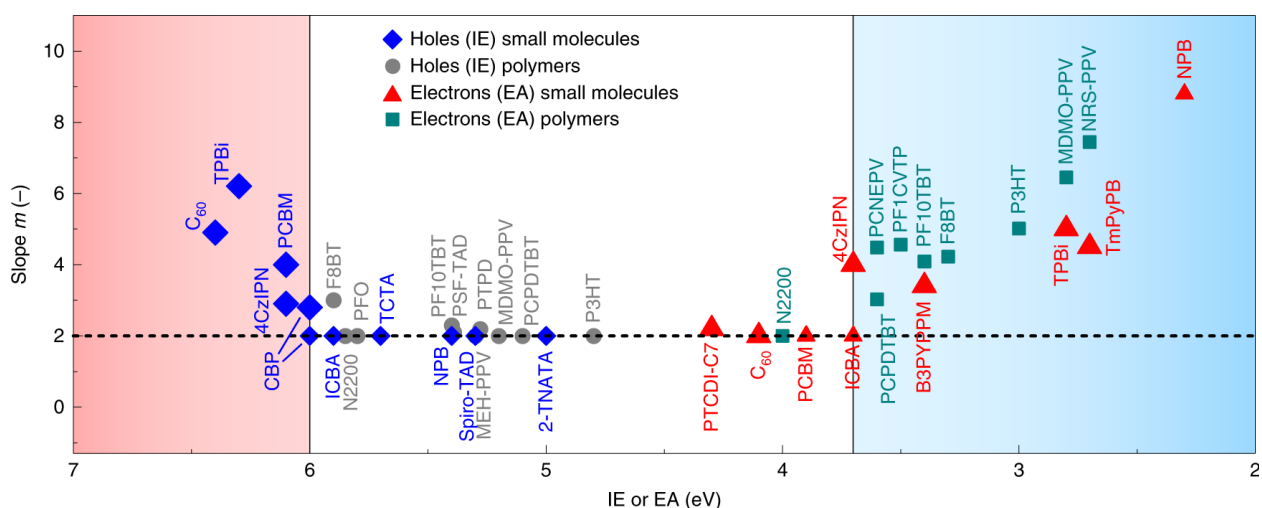


Figure 1. 11 Slope of log J-log V of the hole or electron current versus HOMO or LUMO level shown for different organic semiconductors which define an energy window for trap-free charge transport. Obtained from Ref. 70.

Lampert et al introduced an analytical expression for the trap-limited current when trap levels are discrete.⁷² In this definition the current density behaves space-charge limited (compare with Equation (1)) but requires a prefactor, in the equation below denoted θ :

$$J = \frac{9}{8} \theta \epsilon_0 \epsilon_r \mu \frac{V^2}{L^3} \quad (10)$$

$$\theta = \frac{N}{N_t} \exp\left(\frac{-E_t}{kT}\right) \quad (11)$$

, where N and N_t are the density of transport and trap sites, respectively and E_t defines the depth of the traps. This formula is valid only in a regime in which the trap states are not still completely filled. In this system the current is lower than SCLC by a factor of θ due to presence of traps. When it reaches a state where all trap states are filled, the current increases drastically and it finally approaches the trap-free SCLC. However, the assumption of a discrete energy level for traps is not valid for most organic semiconductors since the traps are mostly distributed in the band gap.

In 1962, Mark & Helfrich considered a distributed trap states for organic semiconductors.⁷³ In their model, the trap states are assumed to follow an exponential description:

$$D_{exp,t} = \frac{N_t}{kT_t} \exp\left(\frac{|E - (E_c - E_{tc})|}{kT_t}\right) \quad (12)$$

, where T_t is the characteristic trap temperature which determines the width of the exponential function. E_{tc} and E_c are the energy of traps measured from the top of the valance- (hole traps) or conduction (electron traps) band, respectively. Solving the Poisson equation considering this distribution results in the following expression for the a trap limited current:⁷³

$$J_{TLC} = N_c q \mu_n \left(\frac{\epsilon_0 \epsilon_r}{q N_t \exp\left(\frac{E_{tc}}{kT_t}\right)} \right)^r \left[\left(\frac{2r+1}{r+1} \right)^{r+1} \left(\frac{r}{r+1} \right)^r \right] \frac{V^{r+1}}{L^{2r+1}} \quad (13)$$

With q the elementary charge, μ_n is the free electron mobility and $r = \frac{T_t}{T}$. Based on the equation (13) the slope of double logarithmic JV plot directly scales with r and r is usually 4 for polymers.

As mentioned above, charge transport in organic semiconductors is described by a hopping mechanism through a Gaussian DOS. Therefore it would be more logical to consider also a Gaussian distribution for trap states centered at a depth E_t below the LUMO, according to:⁷⁴

$$D_t(E) = \frac{N_t}{\sqrt{2\pi}\sigma_t} \exp\left(-\frac{(E-(E_c-E_t))^2}{2\sigma_t^2}\right) \quad (14)$$

where σ_t is the width of the distribution and $E_c - E_t$ is the trap energy. Hwang and Kao,⁷⁵ modified the trap-limited current in equation (13) given by Mark and Helfrich by considering a Gaussian trap distribution in which r is related to the Gaussian distribution width, σ_t :

$$r = \sqrt{1 + 2\pi \left(\frac{\sigma_t}{4K_B T}\right)^2} \quad (15)$$

Nicolai et al,⁷⁶ implemented a Gaussian trap distribution in a numerical drift-diffusion model for device simulation and compared the results to previously reported discrete and exponential trap distributions. They showed that the temperature dependent electron transport in some PPV derivatives which had previously been modeled using an exponential trap distribution can be also described by a Gaussian trap model.⁷⁶

The SRH trap-assisted recombination is not the only loss process in a PLED. There is also a second loss process. This process is so-called electrode quenching which occurs when excitons are formed at a short distance from a metallic electrode (about 10 nm). The energy of these excitons can be transferred to the metallic electrode via long range dipole-dipole interactions. As a result of this process, a strong gradient in exciton concentration occurs close the electrode which leads to

even stronger diffusion of excitons towards the metallic electrode and therefore enhanced quenching. The presence of these two processes (SRH, electrode quenching) leads to a huge reduction in PLED efficiency (**Figure 1. 12**).⁷⁷⁻⁷⁸

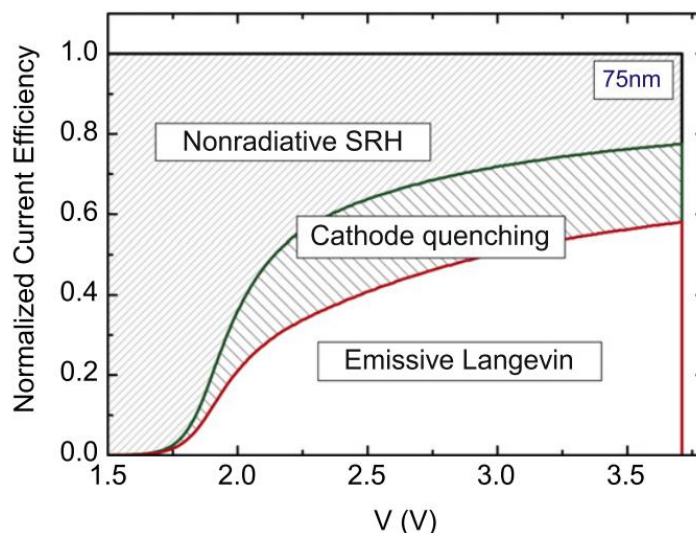


Figure 1. 12 Simulation of contribution of loss effects to the PLED efficiency for a 75 nm MEH-PPV diode as a function of voltage. Obtained from Ref. 75.

So far the loss processes in a PLED have been described. However, it is more important to address a practical solution to reduce the negative effect of these loss processes in the system. Recently Abbaszadeh et al^{66, 79} demonstrate an interesting method how the negative effects of electron trapping states can be strongly reduced and even nearly eliminated. For this they simultaneously diluted the trapping and transporting sites by mixing the active polymer in an electronically inert or large band gap host. The effect of dilution on trapping directly follows from the statistics between free and trapped carriers, as derived by Mark and Helfrich in 1962 (Equation (13)). Abbaszadeh et al showed that in conjugated polymer blends with 10% active semiconductor and 90% large band gap host the effect of electron trapping can be effectively eliminated. As a

result they were able to fabricate polymer light-emitting diodes with balanced electron and hole transport and reduced SRH recombination and cathode quenching, leading to a doubling of the efficiency at nearly ten times lower material costs (**Figure 1.13**).^{66, 79}

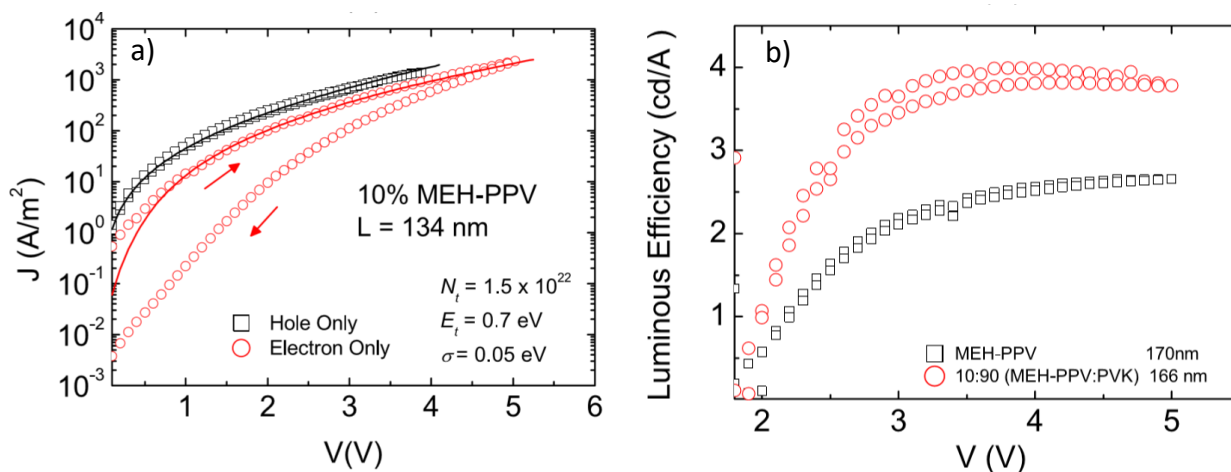


Figure 1. 13 a) Hole and electron transport in hole-only and electron-only devices of 10:90% MEHPPV:PVK. b) luminous efficiency versus applied voltage for reference MEH-PPV and 10%MEH-PPV:90% PVK PLED Obtained from Ref. 66, 79.

1. 6 Photo-physics of an organic semiconductor

In organic semiconductors, the formation of an exciton can also occur upon light absorption and its radiative decay occurs via emission of a photon. Here the most probable photo-physical processes in an isolated organic molecule are summarized in the Jablonski diagram shown in **Figure 1. 14**.

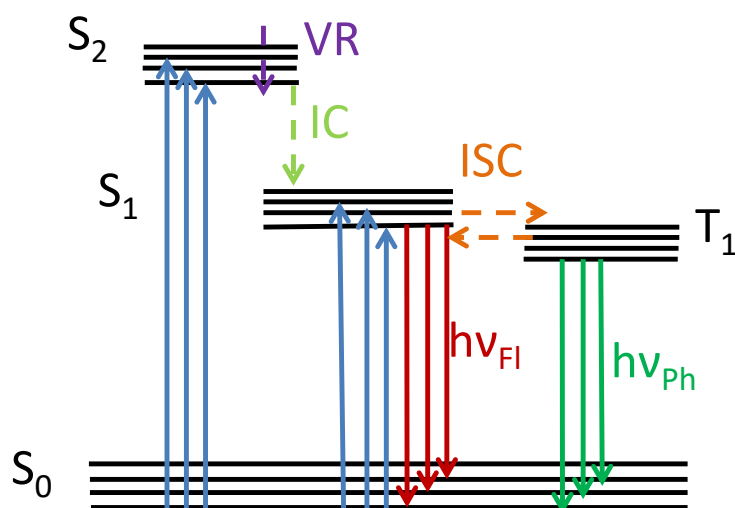


Figure 1. 14 The summary of photophysical processes in an isolated organic molecule in Jablonski diagram. The vibrational levels for a given electronic energy level lie above each other, shown as vertical lines. The ground vibrational state is highlighted in bold. VR: vibrational relaxation; IC: internal conversion; ISC: intersystem crossing.

The lowest vibrational state in an organic molecule (S_0) which is the ground state has net spin zero. An electron in the ground state is excited to a higher excited singlet state (S_n) upon photon absorption. There are several pathways for the excited electron to decay to the ground state. The excited electron can dissipate its energy to the environment via vibrational relaxation (VR) to a lower vibrational level within the electronic manifold. This decay is a non-radiative process. Higher excited states (S_n , $n \geq 2$) can also decay to the lowest excited state (S_1) via internal conversion (IC).⁸⁰

When transitions occur between different multiplicity (Singlet and triplet states), the process is called intersystem crossing (ISC). Since ISC includes spin-conversion, is slower than IC. Eventually, based on Kasha's rule,⁸¹ the excited molecule decays from the lowest vibrational state

of the lowest electronic state of the singlet or triplet to the ground state by emitting a radiative photon. The energy of the emitted photon corresponds to the remained excess energy of the excited molecule. This process can be either fluorescence or phosphorescence depending on the initial excited state.⁸⁰

1. 6. 1 Excitation energy and charge transfer processes

Excitation energy transfer (EET) requires two species: the molecule which transfers its energy is referred to as the donor (D) and the other molecule which accepts the energy is the acceptor (A). In this process the donor molecule which is in an excited state transfers its energy to the acceptor which is initially in the ground state. This is a non-radiative process which can be categorized to two different mechanisms, Förster and Dexter energy transfer as shown in **Figure 1. 15**. In the Förster process energy transfer occurs via dipole-dipole interaction and requires overlap between the emission spectrum of the donor and the absorption spectrum of the acceptor. Förster energy transfer occurs up to relatively long separation distances (<10 nm) between donor and acceptor molecules. However, the efficiency of the energy transfer scales with r^{-6} in which r is the distance between donor and acceptor molecules.^{80, 82}

In contrast, Dexter energy transfer which is referred to as an ‘electron-exchange’ process, is a short-range process ($r < 1$ nm), as this process requires overlap of the wave functions of the donor and acceptor molecule. The efficiency of Dexter EET decreases exponentially with r .⁸³

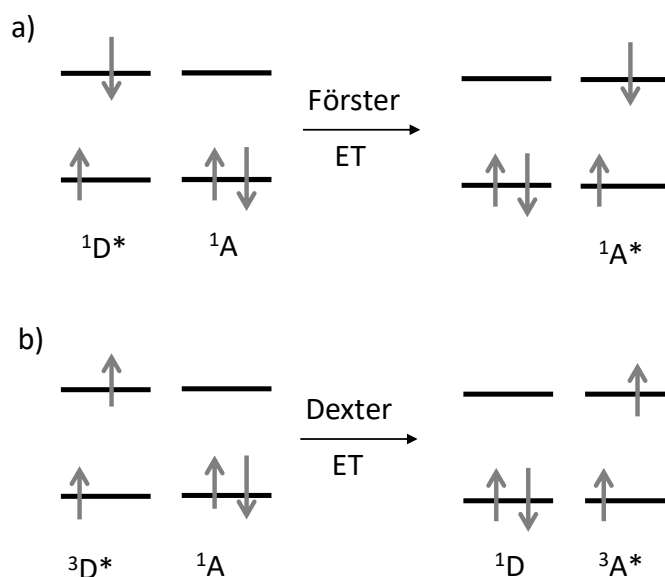


Figure 1. 15 Schematic illustration of a) the Förster energy transfer and b) the Dexter energy transfer mechanism between Donor and Acceptor molecules.

1. 7 OLED challenges

Despite the fact that OLEDs offer many advantages over competing technologies, there are still several challenges that must overcome before they can further increase their market share in the display and solid-state lighting industries. Significant progress needs to be achieved in device efficiency, operation life time, large scale manufacturing and device encapsulation. One interesting but undesired feature of OLEDs is that their efficiency decreases as the applied current increases. This is often referred to as ‘efficiency roll-off’. Although inorganic LEDs experience similar roll-offs, their on-set current density for roll-off is much higher ($> 10 \text{ A/cm}^2$) than for OLEDs ($\sim 0.1 \text{ A/cm}^2$).⁸⁴ This deficiency can be compensated by a large area emissive region, which is difficult to fabricate with inorganic LEDs, and optimized device structures/cost-effective out-coupling techniques.⁸⁵ The lifetime of red and green organic emitters are quite high but the main challenge

is organic blue emitters with a high lifetime. The newest generation blue TADF emitters has made huge improvement in terms of efficiency, however they still need to be improved with respect to life time to be able to compete in the market.

Manufacturing yield is correlated to invested resources and infrastructure. Currently, OLED manufacturing techniques are in their infancy and very expensive. This is especially true for large-area displays, where large glass substrates are required for back-plane patterning and OLED deposition.⁸⁶ In the future, improvements are needed in the manufacturing process especially for solution process techniques to allow scalability to large generation substrates. Most importantly, the industry needs to focus its resources and collectively work together if they want OLED technology to become the industry standard for display and solid-state lighting. The best way for technological standardization is industry wide collaboration.⁸⁵

In order to ensure OLEDs work as designed, encapsulation layers are needed to prevent small quantities of atmospheric moisture and oxygen from oxidizing the materials in the OLED.⁸⁷ Without a proper encapsulation layer, water will permeate through a thin-film barrier by four modes: micro-cracks, contaminant particles, along interfaces and through the bulk of the material. These mechanisms have been shown to reduce the operational lifetime quite fast. To prevent this quick degradation, a encapsulation (barrier) coating with a maximum water vapor transmission rate (WVTR) of $10^{-6} \text{ g m}^{-2} \text{ day}^{-1}$ is necessary.⁸⁷ The barrier coating for rigid applications has traditionally been a layer of glass sealed with epoxy,⁸⁸ but this issue becomes more complex with flexible substrates. To accommodate these new form factors, active research has focused on the development of thin film encapsulation (TFE) methods for OLEDs. However, this introduces a new set of challenges because the techniques used to deposit these materials require high temperature process steps, which could potentially damage or destroy the underlying OLED.⁸⁵

1.8 Scope of this thesis

The work presented in this thesis demonstrates new strategies to design high performance PLEDs. The work presented in this thesis aims to address some of the major concerns with PLED technology including: enhancement of color purity of the blue emitting conjugated polymer using trap dilution strategy, eliminating the negative effect of adding chromophores into the active layer of LEDs by designing a new polymer/quantum dot (QD) hybrid system and simplifying device structures for high performance QD-LEDs for flexible electronics.

The blue emitting polymers are very important for realizing full-color displays with high color purity. In Chapter 2, we test the dilution method on a blue light-emitting polymer which next to the non-radiative universal electron traps, suffers also from radiative trap centers due to on chain ketone defects. These ketone defect result in green emission contamination as a result of charge trapping. Polyfluorene (PFO)-based PLEDs are an excellent model system to visualize the trap dilution effect. The blue emission from PFO is accompanied by a broad, featureless green emission band originating from ketone defects that act as electron trap. In this chapter, it is shown that the effects of electron trapping and resulting trap-assisted recombination can be strongly suppressed by diluting the semiconducting polymer with a large band gap polymer as polystyrene (PS). In this chapter, we show that by blending PFO with low molecular weight PS, not only the negative effect of non-radiative trapping can be eliminated, but also the green trap-assisted fluorenone emission can be completely suppressed and the emission is tuned from green to blue with increasing the degree of dilution. Quantitative analysis of the voltage-dependent electroluminescence spectra reveals that the ratio between blue Langevin emission and green trap-assisted recombination is in

agreement with predictions obtained from a PLED device model based on drift-diffusion charge carrier dynamics.

In Chapter 3, we investigate more precisely the device characteristics based on the morphology change in the active layer of PLEDs based on PFO:PS blends. In the devices having a PFO:PS active blend layer a doubling of the efficiency is expected purely based on trap dilution. However, we show that a much larger efficiency increase of nearly an order of magnitude is observed. The electroluminescence and photoluminescence spectra of the PFO:PS blend show a sharpening of the vibrational peaks with regard to pristine PFO with the emission maximum at 436 nm. This spectral feature is characteristic for the formation of the β -phase in PFO upon polystyrene addition. From analysis of the absorption spectra the fraction of β -phase induced by blending typically amounts to 13%. The strong PLED efficiency enhancement therefore arises from the combined effect of β -phase formation (~ 4 times) and trap dilution (~ 2 times).

Another important issue which has to be addressed in displays technology, is having a small emission linewidth for each color to make saturated colors. This is why nowadays quantum dots (QDs) are being used as phosphor, meaning that they convert light generated by a blue/white LED backlight. An even more attractive option would be to incorporate the QDs directly in an electroluminescent device such that no backlight is needed, the QD LED. However, until now this approach only works when a very thin emissive layer containing only a few monolayers of QDs is used, surrounded by a number of organic transport and confinement layers, of which the thickness is very critical. A major problem is that in the QD emissive layer the charge transport needs to be exactly balanced, otherwise the layer becomes charged with one type of carrier, which blocks the current. Another issue in QD-LEDs is self-quenching problem which can be addressed by decreasing the tendency of the QDs to aggregate. The way out to a robust and simple structure

would be to use a thicker layer where the QDs are simply blended with an organic host. All attempts in this direction failed due to the problem that due to their high electron affinity QDs are deep electron traps, leading to strongly unbalanced transport. In Chapter 4, we demonstrate that electron trapping by CdSe/Cd_xZn_{1-x}S core/shell red QDs in PFO as a host can be strongly suppressed by functionalizing them with a thin insulating shell of polystyrene. The strong reduction of trapping is confirmed by charge transport measurements and a voltage independent electroluminescence spectrum of hybrid polymer:QD blend LEDs. Our results open a new route towards emissive devices with narrow linewidth, where due to the preservation of charge transport there are no limits to the active layer thickness.

In Chapter 5, the charge transport and recombination in PLEDs based on Me-LPPP are investigated. The transport is characterized by a room temperature hole mobility of $2 \times 10^{-8} \text{ m}^2/\text{Vs}$, combined with anomalously strong electron trapping. The electroluminescence (EL) spectrum is characterized by blue singlet emission, a broad green featureless peak and yellow-orange triplet emission. The voltage dependence of the EL spectrum and negative contribution to the capacitance indicate that the triplet-emission is of trap-assisted nature, consistent with the strong electron trapping. Consequently, the color purity of the blue emitting Me-LPPP polymer LEDs can be strongly improved using trap dilution.

References

1. Swan, J. W., Edison's New Lamp. *Nature* **1880**, 21 (531), 202.
2. Luckiesh, M., *Artificial light, its influence upon civilization*. University of London Press: 1920.
3. Luckiesh, M., A half-century of artificial lighting. *Industrial & Engineering Chemistry* **1926**, 18 (9), 920-922.
4. Anders, A., Tracking down the origin of arc plasma science-II. early continuous discharges. *IEEE transactions on plasma science* **2003**, 31 (5), 1060-1069.
5. Humphreys, C. J., Solid-state lighting. *MRS bulletin* **2008**, 33 (4), 459-470.
6. Rhaman, M. M.; Matin, M.; Toshon, T. A. In *Solid State Lighting can resolve the present power crisis in Bangladesh*, 2015 3rd International Conference on Green Energy and Technology (ICGET), IEEE: 2015; pp 1-5.
7. Sheats, J. R.; Antoniadis, H.; Hueschen, M.; Leonard, W.; Miller, J.; Moon, R.; Roitman, D.; Stocking, A., Organic electroluminescent devices. *Science* **1996**, 273 (5277), 884-888.
8. D'Andrade, B. W.; Forrest, S. R., White organic light-emitting devices for solid-state lighting. *Advanced Materials* **2004**, 16 (18), 1585-1595.
9. Misra, A.; Kumar, P.; Kamalasanan, M.; Chandra, S., White organic LEDs and their recent advancements. *Semiconductor science and Technology* **2006**, 21 (7), R35.
10. Kamtekar, K. T.; Monkman, A. P.; Bryce, M. R., Recent advances in white organic light-emitting materials and devices (WOLEDs). *Advanced Materials* **2010**, 22 (5), 572-582.
11. Gather, M. C.; Köhnen, A.; Meerholz, K., White organic light-emitting diodes. *Advanced Materials* **2011**, 23 (2), 233-248.
12. <https://www.hyperikon.com/pages/blog/lighting-evolution-and-the-falling-costs-of-led-lights/>.
13. Sasabe, H.; Kido, J., Development of high performance OLEDs for general lighting. *Journal of Materials Chemistry C* **2013**, 1 (9), 1699-1707.
14. Goushi, K.; Kwong, R.; Brown, J. J.; Sasabe, H.; Adachi, C., Triplet exciton confinement and unconfinement by adjacent hole-transport layers. *Journal of Applied Physics* **2004**, 95 (12), 7798-7802.

15. Okutsu, S.; Onikubo, T.; Tamano, M.; Enokida, T., Molecular design of hole transport material with various ionization potential for organic light-emitting diode applications. *IEEE Transactions on Electron Devices* **1997**, *44* (8), 1302-1306.
16. Tang, C. W.; VanSlyke, S. A., Organic electroluminescent diodes. *Applied physics letters* **1987**, *51* (12), 913-915.
17. Pope, M.; Kallmann, H.; Magnante, P., Electroluminescence in organic crystals. *The Journal of Chemical Physics* **1963**, *38* (8), 2042-2043.
18. Baldo, M. A.; O'brien, D.; You, Y.; Shoustikov, A.; Sibley, S.; Thompson, M.; Forrest, S. R., Highly efficient phosphorescent emission from organic electroluminescent devices. *Nature* **1998**, *395* (6698), 151.
19. Wang, Z.; Helander, M.; Qiu, J.; Puzzo, D.; Greiner, M.; Hudson, Z.; Wang, S.; Liu, Z.; Lu, Z., Unlocking the full potential of organic light-emitting diodes on flexible plastic. *Nature Photonics* **2011**, *5* (12), 753.
20. Bin, J. K.; Cho, N. S.; Hong, J. I., New Host Material for High-Performance Blue Phosphorescent Organic Electroluminescent Devices. *Advanced Materials* **2012**, *24* (21), 2911-2915.
21. Li, G.; Zhu, D.; Peng, T.; Liu, Y.; Wang, Y.; Bryce, M. R., Very High Efficiency Orange-Red Light-Emitting Devices with Low Roll-Off at High Luminance Based on an Ideal Host-Guest System Consisting of Two Novel Phosphorescent Iridium Complexes with Bipolar Transport. *Advanced Functional Materials* **2014**, *24* (47), 7420-7426.
22. Hung, L.; Chen, C., Recent progress of molecular organic electroluminescent materials and devices. *Materials Science and Engineering: R: Reports* **2002**, *39* (5-6), 143-222.
23. Adachi, C., Third-generation organic electroluminescence materials. *Japanese Journal of Applied Physics* **2014**, *53* (6), 060101.
24. Kittel, C.; McEuen, P.; McEuen, P., *Introduction to solid state physics*. Wiley New York: 1996; Vol. 8.
25. Mette, H.; Pick, H., Electric conductivity of anthracene monocrystals. *Z. Physik* **1953**, *134*, 566.
26. Helfrich, W.; Schneider, W., Recombination radiation in anthracene crystals. *Physical Review Letters* **1965**, *14* (7), 229.

27. Akamatu, H.; Inokuchi, H.; Matsunaga, Y., Electrical conductivity of the perylene–bromine complex. *Nature* **1954**, 173 (4395), 168.
28. Bolto, B. A.; McNeill, R.; Weiss, D., Electronic conduction in polymers. III. Electronic properties of polypyrrole. *Australian Journal of Chemistry* **1963**, 16 (6), 1090-1103.
29. Hoegl, H., On photoelectric effects in polymers and their sensitization by dopants¹. *The Journal of Physical Chemistry* **1965**, 69 (3), 755-766.
30. Pai, D. M., Transient Photoconductivity in Poly (N-vinylcarbazole). *The Journal of Chemical Physics* **1970**, 52 (5), 2285-2291.
31. Gill, W., Drift mobilities in amorphous charge-transfer complexes of trinitrofluorenone and poly-n-vinylcarbazole. *Journal of Applied Physics* **1972**, 43 (12), 5033-5040.
32. Shirakawa, H.; Louis, E. J.; MacDiarmid, A. G.; Chiang, C. K.; Heeger, A. J., Synthesis of electrically conducting organic polymers: halogen derivatives of polyacetylene,(CH) x . *Journal of the Chemical Society, Chemical Communications* **1977**, (16), 578-580.
33. Chiang, C.; Druy, M.; Gau, S.; Heeger, A.; Louis, E.; MacDiarmid, A. G.; Park, Y.; Shirakawa, H., Synthesis of highly conducting films of derivatives of polyacetylene,(CH) x . *Journal of the American Chemical Society* **1978**, 100 (3), 1013-1015.
34. Chiang, C. K.; Fincher Jr, C.; Park, Y. W.; Heeger, A. J.; Shirakawa, H.; Louis, E. J.; Gau, S. C.; MacDiarmid, A. G., Electrical conductivity in doped polyacetylene. *Physical review letters* **1977**, 39 (17), 1098.
35. Brütting, W., Introduction to the physics of organic semiconductors. *Physics of organic semiconductors* **2005**, 1-14.
36. Bäessler, H., Injection, transport and recombination of charge carriers in organic light-emitting diodes. *Polymers for Advanced Technologies* **1998**, 9 (7), 402-418.
37. Blom, P. W.; Vissenberg, M., Charge transport in poly (p-phenylene vinylene) light-emitting diodes. *Materials Science and Engineering: R: Reports* **2000**, 27 (3-4), 53-94.
38. Campbell, I.; Davids, P.; Smith, D.; Barashkov, N.; Ferraris, J., The Schottky energy barrier dependence of charge injection in organic light-emitting diodes. *Applied Physics Letters* **1998**, 72 (15), 1863-1865.
39. Shen, Y.; Hosseini, A. R.; Wong, M. H.; Malliaras, G. G., How to make ohmic contacts to organic semiconductors. *ChemPhysChem* **2004**, 5 (1), 16-25.

-
40. Crone, B.; Davids, P.; Campbell, I.; Smith, D., Device model investigation of single layer organic light emitting diodes. *Journal of applied physics* **1998**, *84* (2), 833-842.
 41. Malliaras, G.; Scott, J., Numerical simulations of the electrical characteristics and the efficiencies of single-layer organic light emitting diodes. *Journal of Applied Physics* **1999**, *85* (10), 7426-7432.
 42. Kotadiya, N. B.; Lu, H.; Mondal, A.; Ie, Y.; Andrienko, D.; Blom, P. W.; Wetzelaer, G.-J. A., Universal strategy for Ohmic hole injection into organic semiconductors with high ionization energies. *Nature materials* **2018**, *17* (4), 329.
 43. Joung, D.; Chunder, A.; Zhai, L.; Khondaker, S. I., Space charge limited conduction with exponential trap distribution in reduced graphene oxide sheets. *Applied Physics Letters* **2010**, *97* (9), 093105.
 44. Conwell, E. M., Impurity band conduction in germanium and silicon. *Physical Review* **1956**, *103* (1), 51.
 45. Mott, N., On the transition to metallic conduction in semiconductors. *Canadian journal of physics* **1956**, *34* (12A), 1356-1368.
 46. Miller, A.; Abrahams, E., Impurity conduction at low concentrations. *Physical Review* **1960**, *120* (3), 745.
 47. Van der Auweraer, M.; De Schryver, F. C.; Borsenberger, P. M.; Bäessler, H., Disorder in charge transport in doped polymers. *Advanced materials* **1994**, *6* (3), 199-213.
 48. Chen, B.; Lee, C.-s.; Lee, S.-t.; Webb, P.; Chan, Y.-c.; Gambling, W.; Tian, H.; Zhu, W., Improved time-of-flight technique for measuring carrier mobility in thin films of organic electroluminescent materials. *Japanese Journal of Applied Physics* **2000**, *39* (3R), 1190.
 49. Blom, P.; De Jong, M.; Van Munster, M., Electric-field and temperature dependence of the hole mobility in poly (p-phenylene vinylene). *Physical Review B* **1997**, *55* (2), R656.
 50. Frenkel, J., On pre-breakdown phenomena in insulators and electronic semi-conductors. *Physical Review* **1938**, *54* (8), 647.
 51. Bäessler, H., Charge transport in disordered organic photoconductors a Monte Carlo simulation study. *physica status solidi (b)* **1993**, *175* (1), 15-56.
 52. Gartstein, Y. N.; Conwell, E., High-field hopping mobility in molecular systems with spatially correlated energetic disorder. *Chemical Physics Letters* **1995**, *245* (4-5), 351-358.

-
53. Dunlap, D. H.; Parris, P. E.; Kenkre, V. M., Charge-dipole model for the universal field dependence of mobilities in molecularly doped polymers. *Physical review letters* **1996**, 77 (3), 542.
54. Novikov, S. V.; Dunlap, D. H.; Kenkre, V. M.; Parris, P. E.; Vannikov, A. V., Essential role of correlations in governing charge transport in disordered organic materials. *Physical review letters* **1998**, 81 (20), 4472.
55. Tanase, C.; Meijer, E.; Blom, P.; De Leeuw, D., Unification of the hole transport in polymeric field-effect transistors and light-emitting diodes. *Physical review letters* **2003**, 91 (21), 216601.
56. Tanase, C.; Meijer, E.; Blom, P.; De Leeuw, D., Local charge carrier mobility in disordered organic field-effect transistors. *Organic electronics* **2003**, 4 (1), 33-37.
57. Dimitrakopoulos, C.; Purushothaman, S.; Kymissis, J.; Callegari, A.; Shaw, J., Low-voltage organic transistors on plastic comprising high-dielectric constant gate insulators. *Science* **1999**, 283 (5403), 822-824.
58. Horowitz, G.; Hajlaoui, R.; Fichou, D.; El Kassmi, A., Gate voltage dependent mobility of oligothiophene field-effect transistors. *Journal of Applied Physics* **1999**, 85 (6), 3202-3206.
59. Horowitz, G.; Hajlaoui, M. E.; Hajlaoui, R., Temperature and gate voltage dependence of hole mobility in polycrystalline oligothiophene thin film transistors. *Journal of Applied Physics* **2000**, 87 (9), 4456-4463.
60. Tanase, C.; Blom, P.; De Leeuw, D., Origin of the enhanced space-charge-limited current in poly (p-phenylene vinylene). *Physical Review B* **2004**, 70 (19), 193202.
61. Vissenberg, M.; Matters, M., Theory of the field-effect mobility in amorphous organic transistors. *Physical Review B* **1998**, 57 (20), 12964.
62. Coehoorn, R.; Pasveer, W.; Bobbert, P.; Michels, M., Charge-carrier concentration dependence of the hopping mobility in organic materials with Gaussian disorder. *Physical Review B* **2005**, 72 (15), 155206.
63. Mahan, G., Excitons in degenerate semiconductors. *Physical Review* **1967**, 153 (3), 882.
64. Langevin, P., Recombinaison et mobilités des ions dans les gaz. *Ann. Chim. Phys* **1903**, 28 (433), 122.

-
65. Abbaszadeh, D.; Kunz, A.; Kotadiya, N. B.; Mondal, A.; Andrienko, D.; Michels, J. J.; Wetzelaer, G.-J. A.; Blom, P. W., Electron trapping in conjugated polymers. *Chemistry of Materials* **2019**, *31* (17), 6380-6386.
66. Abbaszadeh, D., *Reduction of Loss Processes in Polymer Light-emitting Diodes*. University of Groningen: 2016.
67. Graupner, W.; Leditzky, G.; Leising, G.; Scherf, U., Shallow and deep traps in conjugated polymers of high intrachain order. *Physical Review B* **1996**, *54* (11), 7610.
68. Meier, M.; Karg, S.; Zuleeg, K.; Brütting, W.; Schwoerer, M., Determination of trapping parameters in poly (p-phenylenevinylene) light-emitting devices using thermally stimulated currents. *Journal of applied physics* **1998**, *84* (1), 87-92.
69. Nicolai, H. T.; Kuik, M.; Wetzelaer, G.; De Boer, B.; Campbell, C.; Risko, C.; Brédas, J.; Blom, P., Unification of trap-limited electron transport in semiconducting polymers. *Nature materials* **2012**, *11* (10), 882.
70. Kotadiya, N. B.; Mondal, A.; Blom, P. W.; Andrienko, D.; Wetzelaer, G., A window to trap-free charge transport in organic semiconducting thin films. *Nature materials* **2019**.
71. Nicolai, H. T. Device physics of white polymer light-emitting diodes. University of Groningen, 2012.
72. Lampert, M. A., Simplified theory of space-charge-limited currents in an insulator with traps. *Physical Review* **1956**, *103* (6), 1648.
73. Mark, P.; Helfrich, W., Space-charge-limited currents in organic crystals. *Journal of Applied Physics* **1962**, *33* (1), 205-215.
74. Kuik, M.; Vandenbergh, J.; Goris, L.; Begemann, E. J.; Lutsen, L.; Vanderzande, D. J.; Manca, J. V.; Blom, P. W., Optical detection of deep electron traps in poly (p-phenylene vinylene) light-emitting diodes. *Applied Physics Letters* **2011**, *99* (18), 240.
75. Hwang, W.; Kao, K., Studies of the theory of single and double injections in solids with a Gaussian trap distribution. *Solid-State Electronics* **1976**, *19* (12), 1045-1047.
76. Wetzelaer, G.; Kuik, M.; Nicolai, H.; Blom, P., Trap-assisted and Langevin-type recombination in organic light-emitting diodes. *Physical Review B* **2011**, *83* (16), 165204.
77. Markov, D.; Hummelen, J.; Blom, P.; Sieval, A., Dynamics of exciton diffusion in poly (p-phenylene vinylene)/fullerene heterostructures. *Physical Review B* **2005**, *72* (4), 045216.

78. Kuik, M.; Koster, L.; Dijkstra, A.; Wetzelaer, G.; Blom, P., Non-radiative recombination losses in polymer light-emitting diodes. *Organic Electronics* **2012**, *13* (6), 969-974.
79. Abbaszadeh, D.; Kunz, A.; Wetzelaer, G.; Michels, J. J.; Crăciun, N.; Koynov, K.; Lieberwirth, I.; Blom, P. W., Elimination of charge carrier trapping in diluted semiconductors. *Nature materials* **2016**, *15* (6), 628.
80. Valeur, B., chapter 5, in" Molecular Fluorescence. WILEY-VCH Verlag GmbH, Weinheim: 2002.
81. Kasha, M., Characterization of electronic transitions in complex molecules. *Discussions of the Faraday society* **1950**, *9*, 14-19.
82. Menke, S.; Holmes, R., Energy & Environ. *Sci* **2014**, *7*, 499-512.
83. Dexter, D. L., A theory of sensitized luminescence in solids. *The Journal of Chemical Physics* **1953**, *21* (5), 836-850.
84. Park, J.; Shin, D.; Park, S., Large-area OLED lightings and their applications. *Semiconductor Science and Technology* **2011**, *26* (3), 034002.
85. Gaj, M. P. High-performance organic light-emitting diodes for flexible and wearable electronics. Georgia Institute of Technology, 2016.
86. Nelson, S.; Lin, Y.-Y.; Gundlach, D.; Jackson, T. N., Temperature-independent transport in high-mobility pentacene transistors. *Applied physics letters* **1998**, *72* (15), 1854-1856.
87. Shin, Y. H., OLED Encapsulation Technology. *Flat Panel Display Manufacturing* **2018**, 159-171.
88. CIE, C., Commission internationale de l'eclairage proceedings, 1931. *Cambridge University, Cambridge* **1932**.

Chapter 2

Visualization of trap dilution in polyfluorene based light-emitting diodes

The effects of electron trapping and resulting trap-assisted recombination can be strongly suppressed by diluting a semiconducting polymer with a large band gap polymer as polystyrene. Polyfluorene (PFO)-based light-emitting diodes (PLEDs) are an excellent model system to visualize this trap dilution effect. The blue emission from PFO is accompanied by a broad, featureless green emission band originating from ketone defects that act as an electron trap. In this chapter, we demonstrate that the visible green trap-assisted recombination from the ketone defect is nearly eliminated upon dilution, and the blue emission from PFO can be fully restored. The ratio between bimolecular blue emission and trap-assisted green emission as a function of dilution is in agreement with model predictions.

The results of this chapter are fully published in *Journal of Applied Physics* with <https://doi.org/10.1063/1.4995381> by E. Khodabakhshi et al. E. Khodabakhshi has performed the device fabrication, measurements, analyses and modeling.

2.1 Introduction

As discussed in Chapter 1, a fundamental problem for conducting polymers is that the transport of electrons is strongly reduced by the presence of electron traps. In a wide range of conjugated polymers it was found that the hole transport is trap-free, whereas the electron transport is governed by a defect with an energy level of 3.6 eV and a concentration of $3 - 5 \times 10^{23} \text{ m}^{-3}$.¹ Due to the unbalanced transport most of the recombination in a single layer PLEDs takes place near the metallic cathode, leading to losses due to quenching of excitons.² Furthermore, trapped electrons recombine with free holes via trap-assisted recombination, which is a non-radiative loss process. As a result the PLED performance is reduced by the presence of these electron traps, both via exciton quenching and trap-assisted recombination.

Recently, it has been demonstrated that the negative effects of electron trap states can be overcome by blending the emitting polymer with a miscible wide band gap inert polymer.^{3,4} The addition of a wide band gap inert polymer dilutes both the transport and trap states of the emissive polymer. Due to the statistics between free and trapped charge carriers, simultaneous dilution of both states leads to a strong enhancement of the trap-limited current. For poly[2-methoxy-5-(2-ethyl-hexyloxy)-1,4-phenylenevinylene] (MEH-PPV) as emitter, an up to 3 orders of magnitude increase of the electron current was observed by a ten times dilution. Furthermore, due to the reduced trap-assisted recombination the efficiency of the MEH-PPV PLED was doubled.

Another interesting class of conjugated polymers for PLEDs is that of the blue-emitting polyfluorenes, with poly (di-*n*-octylfluorene) (PFO) as its most widely used member. However, oxidation of monomers at the 9-position of the fluorene into fluorenone, either prior to or after

polymerization, is known to give rise to the appearance of a broad, featureless green emission band located around 530 nm.⁵⁻⁹

Charge transport measurements have revealed that the fluorenone acts as both an electron- and hole trap, since its HOMO and LUMO level are located in the bandgap of the pristine PFO.¹⁰ Furthermore, it was demonstrated that the fluorenone moieties act as recombination centers for a trap-assisted recombination mechanism. As a result, in a PFO-based PLED the blue emission arises from bimolecular Langevin recombination, whereas the green emission originates from trap-assisted Shockley-Read-Hall recombination. The presence of a light-emitting fluorenone trap makes a PFO-based PLED an ideal model system to study the effect of trap dilution, as now also the trap-assisted recombination can be followed optically using straightforward luminescence spectroscopy.

In this chapter we demonstrate that by diluting fluorenone-containing PFO, hereafter called PFO-F, with low molecular weight polystyrene the green trap-assisted fluorenone emission can be completely suppressed and the emission is tuned from green to blue with increasing degree of dilution. Quantitative analysis of the voltage-dependent electroluminescence spectra reveals that the ratio between blue Langevin emission and green trap-assisted recombination is in agreement with predictions obtained from a PLED device model based on drift-diffusion charge carrier dynamics.

2.2 Results and discussion

PFO-F was synthesized via the Suzuki method according to literature ($\bar{M}_w = 230$ kDa, PDI = 3.02).¹¹ We refrained from exhaustive monomer purification prior to polymerization to

deliberately incorporate a small amount of fluorenone defects. As large band gap material for the trap dilution polystyrene (PS) was used. The polystyrene (atactic, $\bar{M}_w = 1.1$ kDa, PDI = 1.15) was synthesized via anionic polymerization of styrene. PFO F: PS blend solutions were prepared by dissolving the polymers in chlorobenzene using weight ratios of 1:0, 1:1, 1:3 and 1:9. Films of the pristine conducting polymer and its blend with polystyrene were applied using standard spin-coating methods.

The electron current through the blends was measured on electron-only devices having a glass/Al (30 nm)/polymer/Ba (5 nm)/Al (100 nm) architecture. For hole-only and light emitting (dual carrier) devices, a 60 nm hole-injection layer of poly(3,4 ethylenedioxythiophene):poly(styrene sulfonic acid) (PEDOT:PSS) (Heraeus Clevios 4083) was spin-coated on ITO-patterned substrates and annealed at 140 °C. Subsequently, the PFO-F:PS blend was deposited by spin coating. As top contacts, for hole-only devices MoO₃ (10 nm)/Al (100 nm) and for PLEDs Ba (5 nm)/Al (100 nm) were thermally evaporated. After device preparation, steady-state current-voltage measurements were performed in inert (N₂) atmosphere using a Keithley 2400 source meter.

As a first step we study the effect of dilution with polystyrene on the electron- and hole transport in PFO-F. In Figure 2.1 the current density we obtain from single carrier devices for unblended PFO-F (Figure 2.1 a) and a PFO-F:PS blend with a 1:9 weight ratio (Figure 2.1 b) is plotted as a function of voltage. Since the active layer thickness of the hole-only devices (100 nm) was lower than for the electron-only devices (160 nm) we have also calculated the space-charge limited hole current densities for the thickness that corresponds with the electron-only device (dashed line). In this way a direct comparison between electron and hole current can be made. Figure 2.1 a) reveals that for the PFO-F device the hole- and electron current differ by

nearly 4 orders of magnitude. In contrast, for the 1:9 PFO-F:PS blend and in line with our previous observations on MEH-PPV:poly(vinyl carbazole) (PVK) blends,³ the electron current strongly *increases* by blending PFO-F with PS. As shown in Figure 2.1 b), the hole and electron current in the blend differs less than an order of magnitude due to the trap dilution. As a result in a PLED based on the PFO-F:PS (1:9) blend we will have a much more balanced transport and therefore a higher efficiency can be expected.

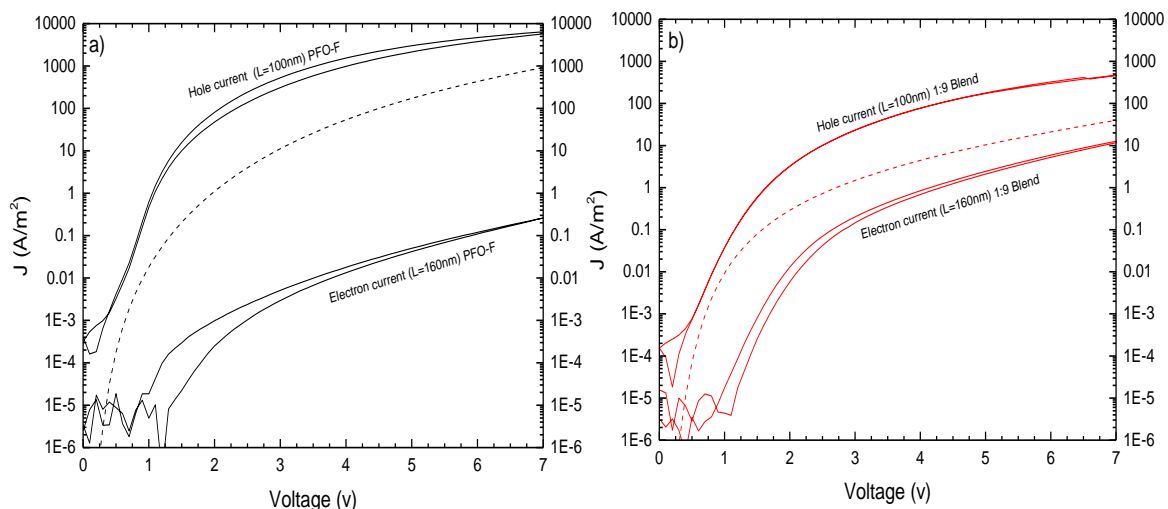


Figure 2.1 Hole and electron current density versus voltage for unblended PFO-F (a) and PFO-F:PS blend (1:9) (b). The thickness for the hole-only and electron-only devices amounts to 100 and 160 nm, respectively. The dashed lines are the calculated hole currents for the layer thickness that corresponds to the electron-only devices (160 nm).

As has been observed for many conducting polymers,¹ the electron transport in PFO-F is strongly hindered by traps. By adding PS both the trap- and transport sites are diluted, leading to a pronounced increase in the electron current. This effect of a simultaneous dilution of transport and trapping sites on charge transport can be easily explained by the Mark-Helfrich formalism for trap-limited currents. In their work, the effect of exponentially distributed trap states inside the band gap on the charge transport was studied.¹² For a trap distribution at a trap depth E_{tc}

below the conduction band/LUMO and a distribution width defined by the trap temperature T_t , the trap-limited current is given by

$$J = N_c q \mu_e \left(\frac{\epsilon_0 \epsilon_r}{q N_t e^{E_{tc}/kT_t}} \right)^r \left[\left(\frac{2r+1}{r+1} \right)^{r+1} \left(\frac{r}{r+1} \right)^r \right] \frac{V^{r+1}}{L^{2r+1}} \quad (1)$$

Where q is the elementary charge, μ_e the free electron mobility, $\epsilon_0 \epsilon_r$ the permittivity and $r = T_t/T$. V denotes the voltage and L the film thickness. Equation (1) reveals that the trap-limited current scales with N_c/N_t^r , with N_c the density of transport sites and N_t the density of trapping sites. We note that in the specific case of PFO-F, N_t represents the sum of the densities of the universal electron traps *and* fluorenone defects. The value of r can be directly derived from the slope of the experimental J - V measurements in log-log scale and amounts to $r = 4$ for PFO-F. As a result, a simultaneous lowering of N_c and N_t by one order of magnitude will lead to an enhancement of N_c/N_t^r , and thus the current, by three orders of magnitude. Experimentally, a strong increase of the electron current is observed and for the (1:9) PFO-F:PS blend the electron current is nearly equal to the trap-free space-charge limited hole current (see **Figure 2.1b**). This result unambiguously shows that the trap-dilution mechanism, as observed before in MEH-PPV:PVK,³ also applies to the PFO-F:PS blends.

As a next step we show the normalized electroluminescence (EL) spectra of the emitting dual carrier devices as a function of voltage in **Figure 2.2**. The additional green emission originating from the fluorenone moieties is clearly visible in the PFO-F spectrum. In agreement with earlier studies^{1,5,13} the green emission band is broad and featureless, having its maximum at approximately 530 nm. In order to confirm that this green peak originates from trap-assisted recombination, as would be expected from the fluorenone energy levels, we measured the voltage dependence of the EL spectrum and observe that with increasing voltage the green band

lowers in intensity relative to the blue signal. This can be explained by the fact that the blue light originates from bimolecular recombination of free electrons and holes, whereas the green light is generated by electrons that are trapped at fluorenone sites and subsequently recombine with a hole. Since the number of trapping sites is fixed the green trap-assisted recombination is linearly proportional to the hole density p in the PLED. In contrast, the bimolecular recombination is governed by the product of electron (n) and hole (p) concentration, and therefore depends quadratically on the charge carrier density. With increasing voltage, meaning an increased electron- and hole density, the bimolecular recombination grows faster, making the blue bimolecular emission dominant at higher voltages. This voltage dependence of the green emission relative to the blue bimolecular contribution hence demonstrates that it originates from trap-assisted recombination.

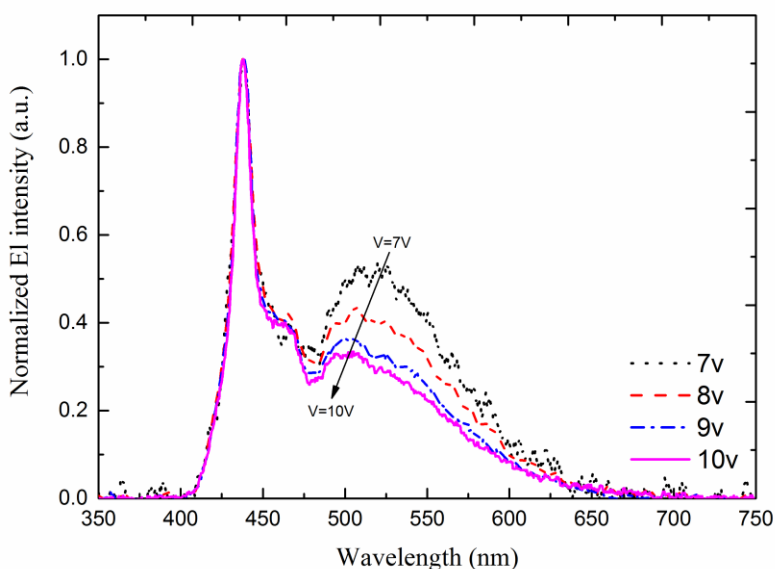


Figure 2.2 Electroluminescence spectra of a PLED based on a 100 nm active layer of unblended PFO-F, recorded at different voltages. The spectra have been normalized relative to the peak at 438 nm, corresponding to the 0-0 transition (color on-line).

We proceed with investigating the EL emission from PLEDs based on PFO-F:PS blends in various ratios. From **Figure 2.3** we observe that upon increasing the PS content a strong decline in the green emission occurs. For the PFO-F:PS blends with a 1:3 and 1:9 ratio the EL spectrum is nearly equal to the spectrum of pristine (defect free) PFO, the trap-assisted green recombination being almost completely suppressed.

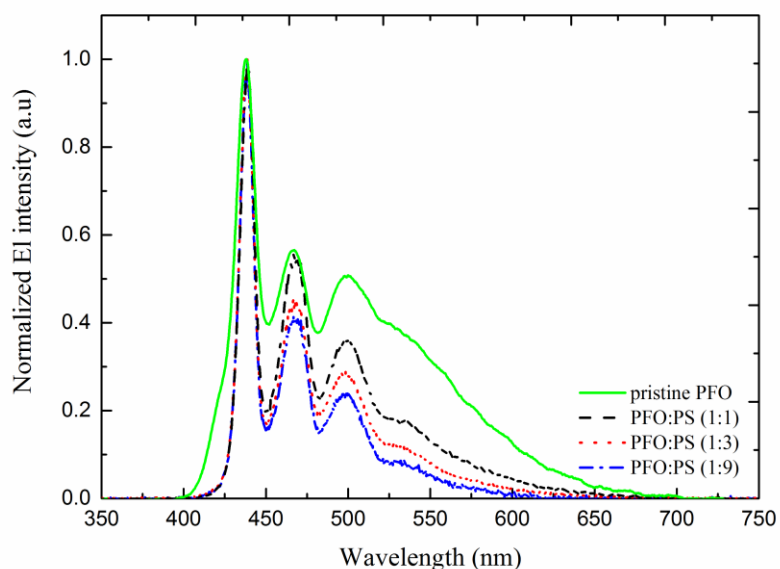


Figure 2.3 Electroluminescence spectra of PLEDs based on ~100 nm active layers of unblended PFO-F and PFO-F:PS blends with various blend ratios. All spectra have been recorded at 6V (color on-line).

To further verify that in case of a high PS content the EL spectrum of the blend is dominated by the contribution of the fluorenone-free PFO chain segments, we investigate its voltage dependence. As an example, in **Figure 2.4** the EL spectrum of the PFO-F:PS (1:3) blend PLED, which still shows some green emission, is shown for different voltages. As expected for an EL spectrum that is dominated by bimolecular recombination, the voltage dependence is indeed very low. The voltage dependence for the 1:9 blend is nearly absent.

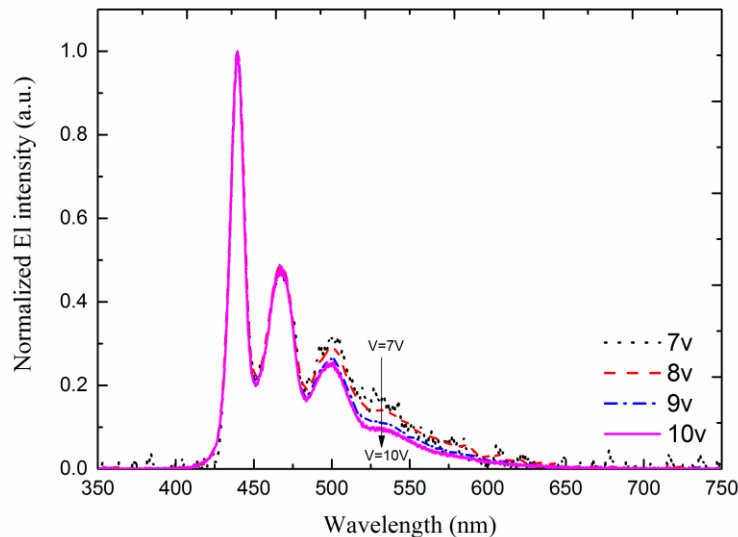


Figure 2.4 Electroluminescence spectrum of a PLED containing a 100nm active layer based on the 1:3 PFO-F:PS blend, recorded at different voltages. The spectra have been normalized relative to band corresponding to the 0-0 transition (438 nm).

To quantify the suppression of the trap-assisted green emission due to dilution of the fluorenone traps by blending, we compare the ratio of blue and green emission obtained from the EL spectra with calculations using a PLED device model. The model is based on a numerical drift-diffusion algorithm including both radiative Langevin recombination and non-radiative trap-assisted recombination, as well as exciton quenching at the electrodes.¹⁴ For the charge-carrier density dependent mobility, the extended Gaussian disorder model (EGDM) is used, that contains as relevant parameters μ_0 , a mobility prefactor containing the electronic overlap between transport sites, σ , representing the energetic disorder, and a , the average distance between two transport sites.¹⁵⁻¹⁶

If the blend components properly intermix, the site distance, a , and thus the density of transport sites, will naturally scale with the extent of dilution. The same holds for the trap density. In PFO-F, fluorenone defects act as deep electron traps and shallow hole traps.² The hole current can be described by a trap-limited current using an exponential trap distribution. By fitting the temperature dependence of the hole only J - V characteristics from 295K down to 215K the trap parameters $N_t(\text{eff}) = 5 \times 10^{23} \text{ m}^{-3}$ and $T_t = 1600 \text{ K}$ are obtained (**Figure 2.5**). As mentioned above for the electron-only characteristics, besides the universal electron traps that give rise to non-radiative recombination, an additional trap level originating from the fluorenone defect has to be considered. For these defects a density of $1 \times 10^{23} \text{ m}^{-3}$ with a trap depth E_{tc} of 0.46 eV consistently describes the experimental electron currents, in agreement with earlier reported values.¹⁷ With now the mobility and trapping parameters known the dual carrier PLED devices can be modeled.

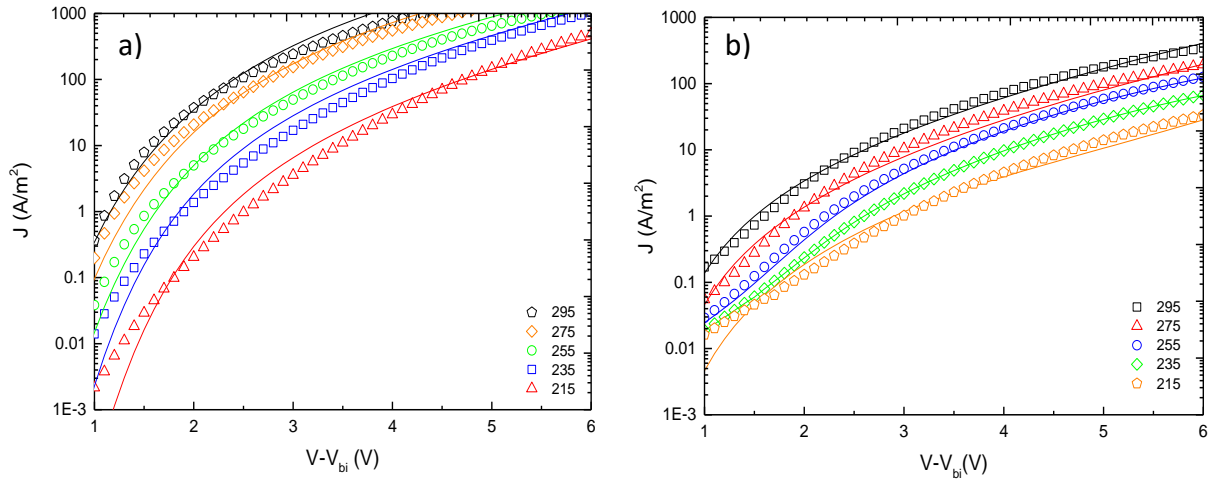


Figure 2.5 J - V characteristic of hole-only devices based on a 100nm film of a) unblended PFO-F and b) PFO-F:PS (1:9) blend for temperatures ranging from 295K to 215K.

By using the mobility and trapping parameters from single carrier devices, dual carrier devices (PLED) were consistently modeled. The numerical device model then provides the ratio

of Langevin recombination and Shokley-read-hall (SRH) recombination for various PFO-F:PS blend ratios, as shown in **Figure 2.6**. We predict this recombination ratio for the PFO-F:PS blend ratios used in this study by simply scaling both transport and trap densities proportional to the extent of dilution.

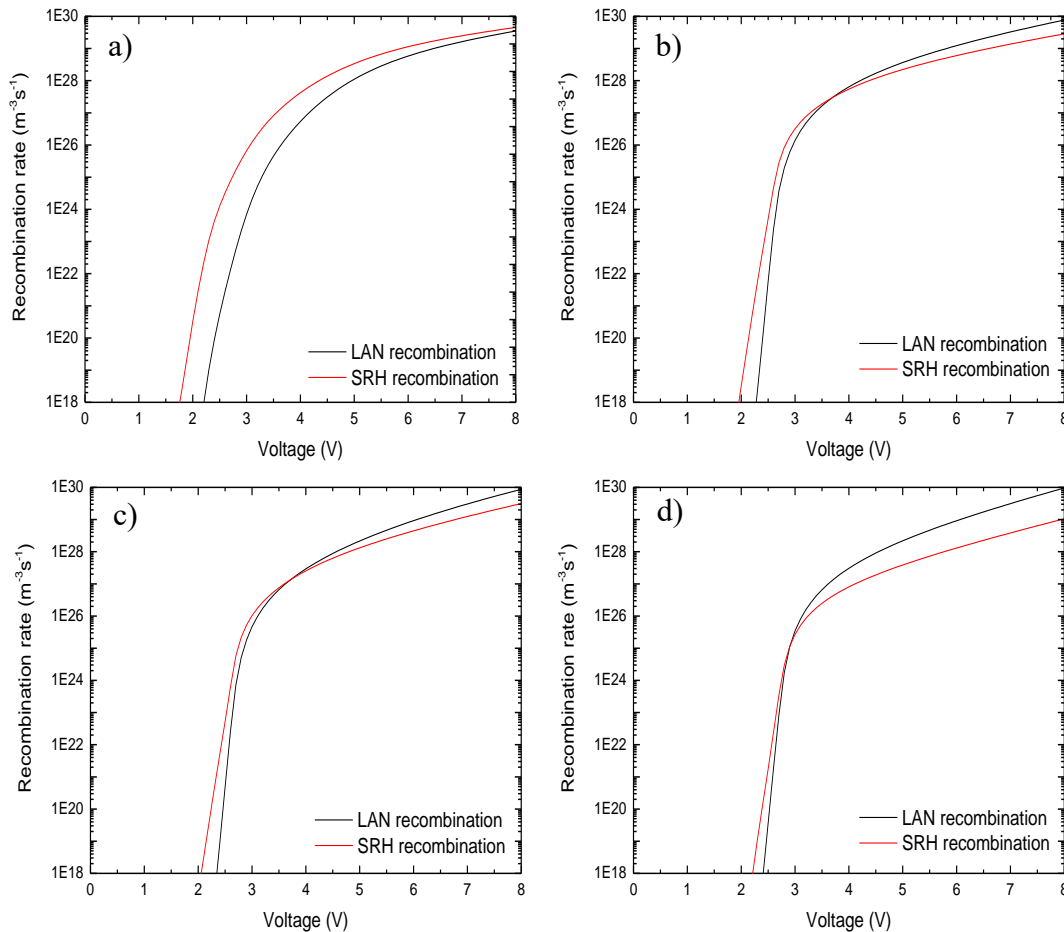


Figure 2.6 Ratio of bimolecular Langevin recombination and trap-assisted SRH recombination as a function of voltage for different blend ratios.

In order to experimentally validate the computationally predicted recombination ratios, we deconvoluted the EL spectra obtained for the different blend ratios (**Figure 2.3**), taking into account an extra green contribution to the total emission spectrum (**Figure 2.7**). Subsequent

integration of the green- and blue emission peaks gives an experimental measure for trap-assisted and bimolecular recombination.

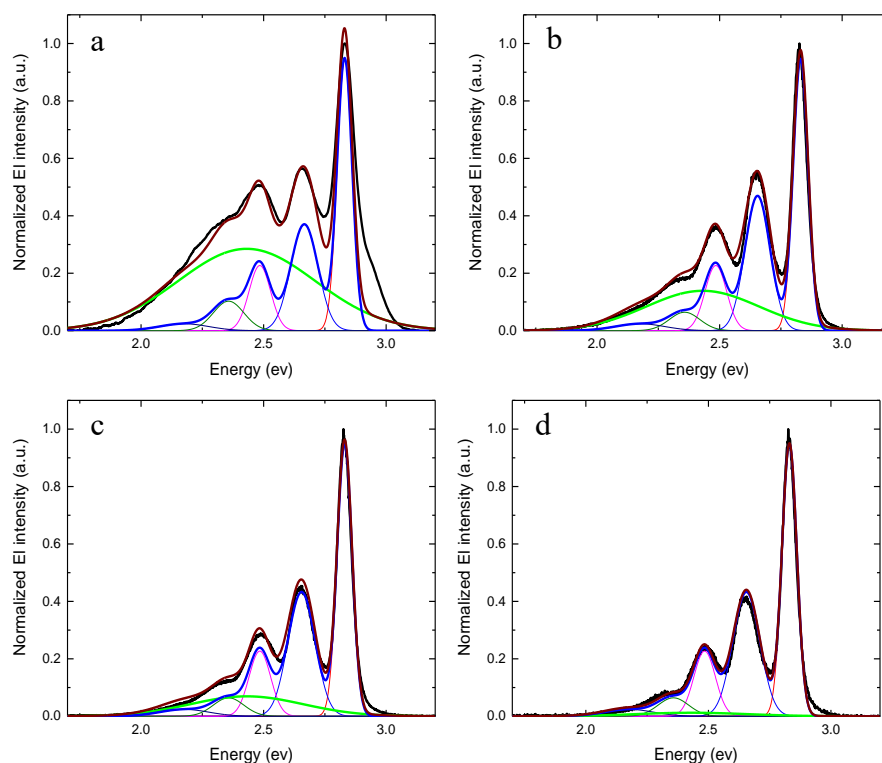


Figure 2.7 Deconvolution of Normalized electroluminescence intensity For a) Unblended PFO-F b) PFO-F:PS(1:1) c) PFO-F:PS(1:3) d) PFO-F:PS(1:9).

In **Figure 2.8**, the experimentally determined recombination ratio, measured at a bias of 6V, is compared with the predictions from the device model. We observe that the decrease of the green relative to the blue emission upon blending is consistently described by the numerical PLED model, taking into account a dilution of transport and trapping sites. The quantitative agreement shows that by a ten times dilution of the semiconductor with an insulator the trap-assisted (radiative) recombination can be almost completely suppressed.

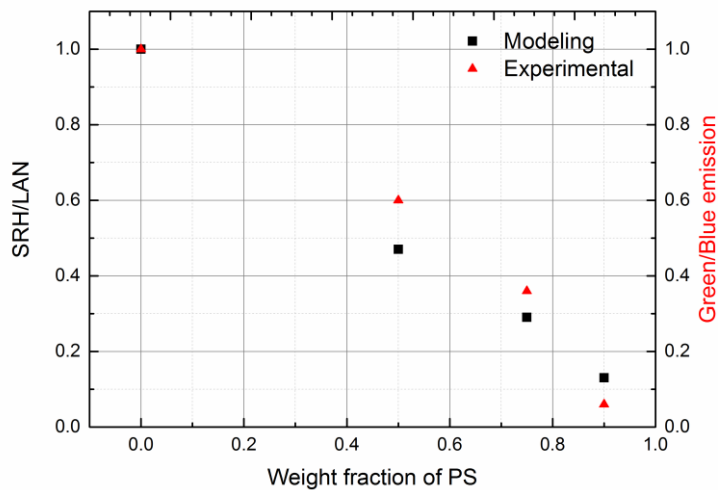


Figure 2.8 Comparison between calculated and experimentally determined ratios of green to blue emission, respectively stemming from trap-assisted and Langevin recombination in PFO-F:PS blends. The recombination ratio is plotted as a function of polystyrene weight fraction. The experimental and calculated data have respectively been obtained from EL-spectrum deconvolution and numerical drift-diffusion modeling and correspond to an operating voltage of 6V.

2.3 Conclusion

In conclusion, the charge transport and electroluminescence properties of PFO-F blended with polystyrene have been investigated. Due to the dilution of the trapping sites, the electron transport in the PFO-F:PS blends is strongly enhanced with increasing PS content. Furthermore, the green emission resulting from trap-assisted recombination at fluorenone defects in the PFO backbone can be completely suppressed by addition of sufficient polystyrene. The suppression of the green emission as a function of blending ratio is in agreement with the predictions of our numerical drift-diffusion-based device model.

References

1. Nicolai, H. T.; Kuik, M.; Wetzelaer, G. A. H. ; De Boer, B.; Campbell, C.; Risko, C.; Brédas, J.; Blom, P. W. M., Unification of trap-limited electron transport in semiconducting polymers. *Nature Materials* **2012**, 11 (10), 882-887.
2. Kuik, M.; Wetzelaer, G. J. A. H.; Nicolai, H. T.; Craciun, N. I.; De Leeuw, D. M.; Blom, P. W. M. , 25th Anniversary Article: Charge Transport and Recombination in Polymer Light-Emitting Diodes. *Advanced Materials* **2014**, 26 (4), 512-531.
3. Abbaszadeh, D.; Kunz, A.; Wetzelaer, G. A. H. ; Michels, J. J.; Craciun, N. I.; Koynov, K.; Lieberwirth, I.; Blom, P. W. M., Elimination of charge carrier trapping in diluted semiconductors. *Nature Materials* **2016**, 15 (6), 628-633.
4. Kunz, A., Blom, P. W. M., & Michels, J. J. Charge Carrier Trapping Controlled by Polymer Blend Phase Dynamics. *Journal of Materials Chemistry*, **2017**.
5. Gong, X.; Moses, D.; Heeger, A. J.; Xiao, S., Excitation energy transfer from polyfluorene to fluorenone defects. *Synthetic Metals* **2004**, 141 (1), 17-20.
6. Zojer, E.; Pogantsch, A.; Hennebicq, E.; Beljonne, D.; Brédas, J.-L.; Scandiucci de Freitas, P.; Scherf, U.; List, E. J., Green emission from poly (fluorene)s: The role of oxidation. *The Journal of Chemical Physics* **2002**, 117 (14), 6794-6802.
7. Lupton, J.; Craig, M.; Meijer, E., On-chain defect emission in electroluminescent polyfluorenes. *Applied Physics Letters* **2002**, 80 (24), 4489-4491.
8. Scherf, U.; List, E. J., Semiconducting polyfluorenes—towards reliable structure–property relationships. *Advanced Materials* **2002**, 14 (7), 477-487.
9. Gong, X.; Iyer, P. K.; Moses, D.; Bazan, G. C.; Heeger, A. J.; Xiao, S. S., Stabilized Blue Emission from Polyfluorene-Based Light-Emitting Diodes: Elimination of Fluorenone Defects. *Advanced Functional Materials* **2003**, 13 (4), 325-330.
10. Kadashchuk, A.; Schmechel, R.; Von Seggern, H.; Scherf, U.; Vakhnin, A., Charge-carrier trapping in polyfluorene-type conjugated polymers. *Journal of Applied Physics* **2005**, 98 (2), 024101.

11. Oh-e, T.; Miyaura, N.; Suzuki, A., Palladium-catalyzed cross-coupling reaction of organoboron compounds with organic triflates. *Journal of Organic Chemistry* **1993**, 58 (8), 2201-2208.
12. Mark, P.; Helfrich, W., Space-charge-limited currents in organic crystals. *Journal of Applied Physics* **1962**, 33 (1), 205-215.
13. List, E. J.; Gaal, M.; Guentner, R.; de Freitas, P. S.; Scherf, U., The role of keto defect sites for the emission properties of polyfluorene-type materials. *Synthetic Metals* **2003**, 139 (3), 759-763.
14. Koster, L. J. A.; Smits, E. C. P.; Mihailetschi, V. D. ; Blom, P. W. M., Device model for the operation of polymer/fullerene bulk heterojunction solar cells. *Physical Review B* **2005**, 72 (8), 085205.
15. Pasveer, W.; Cottaar, J.; Tanase, C.; Coehoorn, R.; Bobbert, P.; Blom, P. W. M.; De Leeuw, D. M.; Michels, M., Unified description of charge-carrier mobilities in disordered semiconducting polymers. *Physical Review Letters* **2005**, 94 (20), 206601.
16. Coehoorn, R.; Pasveer, W.; Bobbert, P.; Michels, M., Charge-carrier concentration dependence of the hopping mobility in organic materials with Gaussian disorder. *Physical Review B* **2005**, 72 (15), 155206.
17. Kuik, M.; Wetzelaer, G. J. A.H.; Laddé, J. G.; Nicolai, H. T.; Wildeman, J.; Sweelssen, J.; Blom, P. W. M., The effect of ketone defects on the charge transport and charge recombination in polyfluorenes. *Advanced Functional Materials* **2011**, 21 (23), 4502-4509.

Chapter 3

Efficiency enhancement of polyfluorene:polystyrene blend light-emitting diodes by simultaneous trap dilution and β -phase formation

As shown in the previous chapter, diluting poly(dioctylfluorene) (PFO) with low molecular weight polystyrene (PS), electron trapping and trap-assisted recombination can be strongly suppressed. For PLEDs based on a PFO:PS (1:3) blend a doubling of the efficiency is expected owing to trap dilution. Experimentally, we however observe a much larger efficiency increase of nearly an order of magnitude. The electroluminescence and photoluminescence spectra of the PFO:PS blend show a sharpening of the vibrational peaks in comparison to pristine PFO with the emission maximum at 436 nm. This spectral feature is characteristic for the formation of the β -phase in PFO, which, apparently, is enhanced by the addition of PS. From analysis of the absorption spectra the fraction of β -phase induced by blending typically amounts to 13%. The strong PLED efficiency enhancement therefore arises from the combined effect of β -phase formation (~ 4 times) and trap dilution (~ 2 times).

The results of this chapter are fully in *Applied Physics Letters* with <https://doi.org/10.1063/1.5058195> by E. Khodabakhshi et al. E. Khodabakhshi has performed the device fabrication, measurement and analysis.

3.1 Introduction

In order to realize full-color displays with high color purity, efficient and durable blue light emission is of essential importance.¹⁻³ Among the currently available blue light-emitting semiconducting polymers, poly(9,9-dioctylfluorene) (PFO) is one of the most widely studied, exhibiting good processability, high photoluminescence quantum efficiency and good thermal and electrochemical stability.⁴⁻⁶ In Chapter 2, the charge transport and electroluminescence in PFO blended with polystyrene have been investigated. We showed that the elimination of electron trapping by blending with PS^{7,8} in case of PFO can be achieved both for emissive and non-emissive traps.⁹ As described in Chapter 1, the PLED efficiency could be doubled by alleviating electron trapping via dilution of a semiconductor polymer with an inert polymer.^{7,8} In this chapter, we show that by diluting (ketone-free) PFO with a substantial fraction (75%) of low molecular weight PS, the OLED efficiency is not merely doubled, as is observed for poly(p-phenylene vinylene),^{7,8} but rather increased by an order of magnitude. We propose that this large increase in efficiency is due to a *dual effect* associated with blending the semiconductor with polystyrene. We show that blending not only leads to suppression of trap-assisted recombination, but also to the formation of a significant fraction of the strongly luminescent PFO β -phase.¹⁰

3.2 Experimental section

PFO ($\bar{M}_w = 230.000$ g/mol, $\bar{D} = 3.02$) was synthesized via the Yamamoto method according to known procedures.^{11,12} Polystyrene (PS) (atactic, $\bar{M}_w = 1.100$ g/mol, $\bar{D} = 1.15$) was synthesized via anionic polymerization of styrene and was used as inert material. The charge transport in PFO:PS blend films was studied using dual (PLED), as well as single carrier devices. The OLEDs had an architecture comprising: glass/ITO (100 nm)/PEDOT:PSS (60 nm)/PFO(:PS)/Ba

(5 nm)/Al (100). The electron- and hole-only devices (EO and HO) had a glass/Al (30 nm)/PFO(:PS)/Ba (5 nm)/Al (100 nm) and a glass/ITO (100 nm)/PEDOT:PSS (60 nm)/PFO(:PS)/MoO₃ (10 nm)/Al (100 nm) architecture, respectively.

The hole-injection layers of poly(3,4 ethylenedioxythiophene):poly(styrene sulfonic acid) (PEDOT:PSS) (Heraeus Clevis 4083) were spin-coated from a 1.3 wt % dispersion in water and dried at 140°C for 10 minutes. Thin films of PFO and its blends with PS were spin-coated from chlorobenzene to obtain films with a ~100 nm thickness. Top contacts of Ba (5 nm)/Al (100 nm) (OLED and EO) and MoO₃ (10 nm)/Al (HO) were thermally evaporated at 10⁻⁷ Torr. Electrical characterization was carried out in inert (N₂) atmosphere with a Keithley 2400 source meter. Light output was recorded with a calibrated Si photodiode, and electroluminescence (EL) spectra were recorded with a USB4000 UV-Vis-ES spectrometer. UV-Vis absorption spectra were recorded with a dual-beam Shimadzu UV-2600 spectrophotometer. Photoluminescence (PL) spectra were recorded using a TIDAS Mono RS232 spectrometer.

3.3 Results and discussion

We commence with studying how diluting PFO with PS affects the electron- and hole transport in single carrier devices. In **Figure 3.1** the current density measured as a function of voltage is plotted for devices comprising a PFO:PS blend (ratio 1:3 w/w) as active layer. The figure compares the results with those obtained for reference devices based on unblended PFO. As expected, for unblended PFO the electron current is three to four orders of magnitude lower than the hole current due to charge trapping. As we have shown before, by introducing PS in the system the electron current increases drastically owing to elimination of trapping and becomes as high as the hole current.⁹ Interestingly, the (non-trap-limited) hole current remains unaffected by

blending with PS, where we would have expected a decrease due to the spatial separation of transport sites, making charge carrier hopping more difficult. This may indicate that the presence of PS in the blend causes a morphological change in the semiconductor, upon which the hole mobility is enhanced.

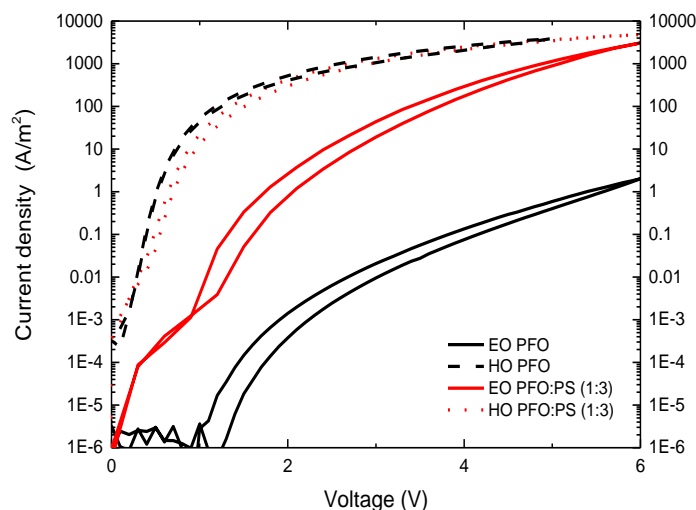


Figure 3.1 Hole and electron current density versus voltage for unblended PFO (dash black) and PFO:PS blend (1:3 w/w , solid red). The thickness for the hole-only (HO) and electron-only (EO) devices amounts to 100nm.

As a next step we study the effect of blending on the efficiency of the dual carrier device, *i.e.* the actual PLEDs. In earlier work it has been demonstrated that a doubling in efficiency is obtained upon full elimination of electron trapping.^{7,8} This effect is in agreement with theoretical predictions obtained by modeling of the PLED, taking all loss processes quantitatively into account. **Figure 3.2a** shows that the present PFO:PS blend behaves qualitatively similar: whereas the total current density, which is dominated by trap-free hole transport, remains unaffected by the blending, the light output of the device increases considerably as evidenced by the increase in photocurrent density. In other words, the luminous efficiency (LE) of the device,

expressed in Cd/A , increases upon blending with PS. However, in contrast to our earlier observations, **Figure 3.2b** shows that for PFO, blending with PS causes the LE not to increase by a mere factor two, but by a full order of magnitude: 1 Cd/A versus 0.1 Cd/A for unblended PFO,¹³ *i.e.* exceeding the theoretical prediction by a factor of five.

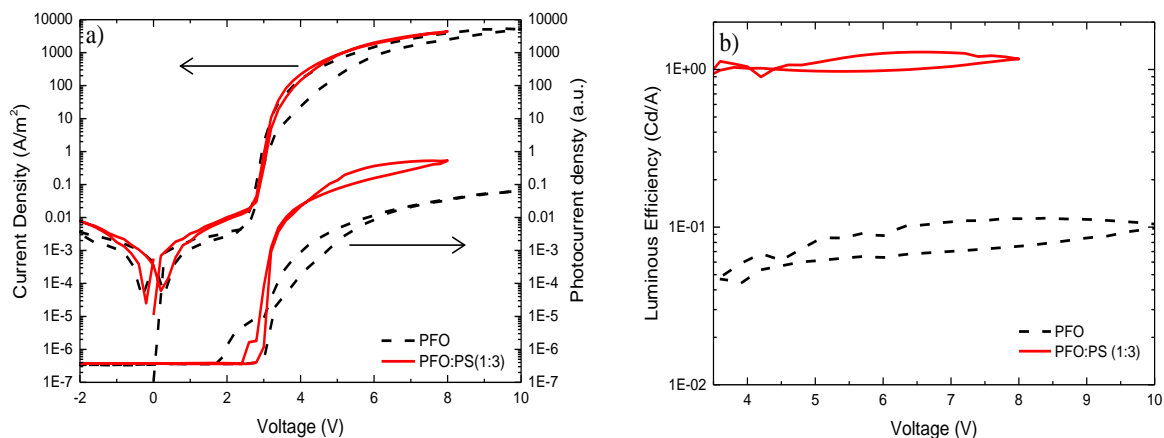


Figure 3.2 (a) Current density- and photocurrent density-voltage characteristics of PLEDs: unblended PFO (dash black) and blend with PS (1:3 w/w, solid red) (b) Luminous efficiency of the devices in part a.

In terms of absolute numbers, the efficiencies we measure are in good agreement with earlier studies on PFO-based OLEDs with similar device architecture,¹³⁻¹⁵ whereby we note that variations in material properties (such as PFO molecular weight¹⁵), processing intricacies²¹ and brightness dependence¹⁵ typically gives some spreading in the reported numbers. Other studies have specifically focused on maximizing OLED efficiency, with recent progress in emitters exhibiting thermally activated delayed fluorescence (TADF) showing good prospects.¹⁶ However, since in the present study we are primarily interested in understanding how structure-function relations affect photophysical behavior, efficiency maximization is out of the scope this

work. Instead, we are interested in the information obtained from *relative* comparison of the efficiencies of devices based on PS-blended and unblended PFO.

To investigate whether the order of magnitude increase in efficiency is accompanied by spectral changes induced by blending, we plot the *normalized* electroluminescence (EL), as well as the *absolute* photoluminescence (PL) spectra, respectively recorded on PLEDs and films of unblended (dash black) and PS-blended PFO (solid red) in **Figure 3.3**. Clearly, introducing PS into PFO leads to a drastic change in the spectral features. Unblended PFO exhibits a vibronic progression with peaks situated at $\lambda = 423, 448,$ and 476 nm, respectively associated with the 0-0, 0-1 and 0-2 transitions.¹⁷ In both the EL and PL spectrum of the PFO:PS blend, the peaks appear significantly red-shifted at $\lambda = 436, 465$ and 495 nm. These two spectral fingerprints evidence the presence of different morphological states in the PFO upon blending with PS. The spectra for the unblended PFO are representative for the amorphous (glassy) phase,^{17,18} whereas the ones for the PFO:PS blend are consistent with the presence of a significant fraction of the so-called β -phase.¹⁹

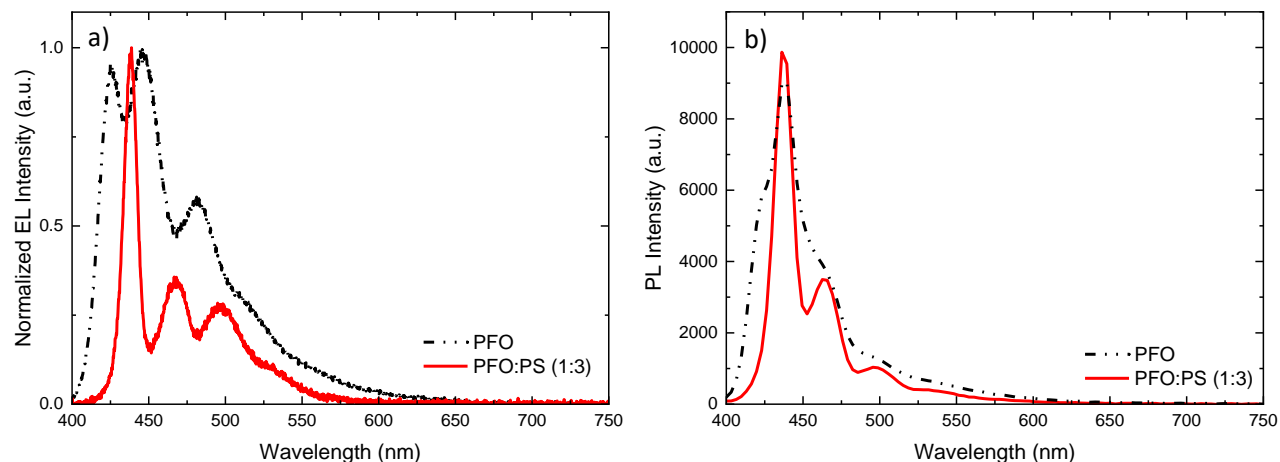


Figure 3.3 (a) Electroluminescence (EL) spectra of PLEDs based on unblended PFO (dash black) and PFO:PS (1:3 w/w, solid red) as emissive layer. The EL spectra have been normalized relative to band corresponding to the 0-1 transition (448 nm, unblended PFO) and 0-0 transition (PFO:PS blend) at 436 nm. (b) Photoluminescence (PL) spectra (in absolute counts) of PFO and PFO:PS (1:3) films ($d = 100$ nm) cast from chlorobenzene.

In the amorphous phase the PFO chains are disordered, featuring a broad distribution of inter-monomer torsion angles.²⁰⁻²² In contrast, in β -phase domains chains locally adopt a fully extended conformation in which the inter-monomer torsion angle²¹ of 160° but staggered orientation of the monomer units.^{17,20,23-25} Interestingly, our experiments demonstrate that the polystyrene induces this conformational change in the PFO. As seen in **Figure 3.3a** and **b**, the enhanced conformational order in the β -phase is expressed by well-resolved vibronic features, as well as a red-shifted emission owing to the increase in the conjugation length.²⁶ The enhanced electronic delocalization in β -phase PFO reduces the band gap by ~ 0.2 eV, as determined from the shift in the 0-1 transition. Owing to the excellent spectral overlap, energy transfer from the amorphous phase to the β -phase is highly efficient, typically occurring on a picosecond time

scale.²³ For this reason, already <2% of β -phase content in the amorphous matrix is known to fully dominate the emission spectrum of PFO.¹⁰

Since the above implies that quantification of the amount of β -phase in the sample based on the emission spectrum is difficult, we record UV-Vis absorption spectra of the films of PS-blended and unblended PFO (**Figure 3.4**). The unblended sample exhibits a featureless absorption band with $\lambda_{\text{max}} = 383$ nm, characteristic for fully amorphous PFO.¹⁷ In contrast, the spectrum of the PFO:PS blend appears as a linear superposition of this same band and a redshifted, more structured signal giving rise to a shoulder at ~435 nm. The latter feature results from absorption by a fraction of β -phase PFO embedded in the amorphous matrix.¹⁹ The fact that the unblended sample exclusively contains amorphous PFO allows us to estimate the β -phase content in the blend by subtracting the contribution of the amorphous component.^{14,27,28} This procedure involves normalizing the spectrum of the unblended PFO to that of the PFO:PS blend at $\lambda = 354$ nm, *i.e.* a wavelength where the β -phase does not absorb.¹⁴ Subtraction yields the percentage of β -phase in the blend film, tacitly assuming the effective extinction coefficient in both phases to be similar. For the 1:3 PFO:PS blend we calculate the amount of β -phase to be ~13% .

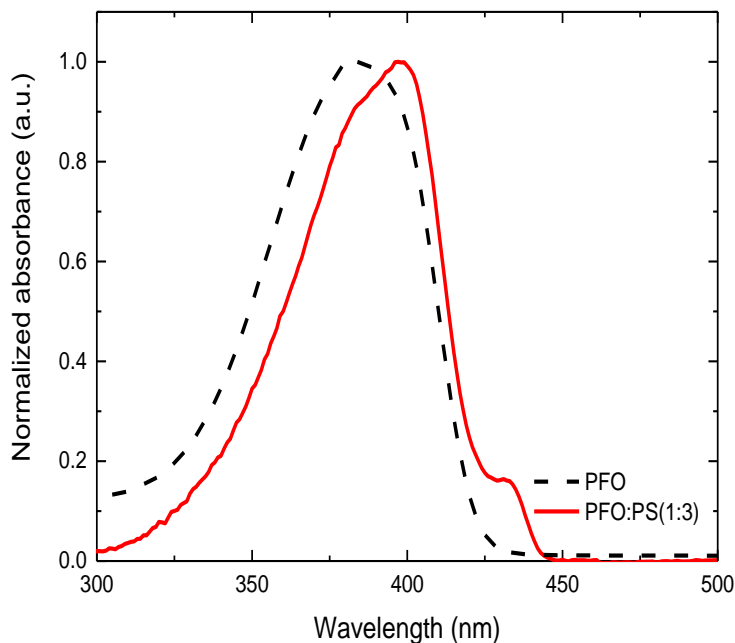


Figure 3.4 Peak-normalized absorption spectra of unblended PFO (dash black) and PFO:PS (1:3 w/w, solid red) films casted from chlorobenzene.

It has been acknowledged that the presence of β -phase in the light-emitting PFO layer has several notable advantages,¹⁰ such as reduced formation of (non-emissive) triplet excitons,²⁹ increased resilience against photobleaching³⁰ and, as we shall see below, a high luminescence quantum yield.²⁷ In the present work the enhanced luminescence quantum yield is directly expressed by the fact that films of pure PFO and PFO:PS (1:3) exhibit a similar PL intensity (**Figure 3.3b**), despite the fact that the latter only contains 25% of active material. This result is consistent with the order of magnitude increase in OLED efficiency upon blending: multiplication of the expected increase in efficiency owing to trap suppression^{7,8} (factor 2) by a factor ~ 4 lower exciton density due to dilution with 75% of insulator dilution, reproduces the observed $10\times$ increase in efficiency fairly well. The addition of polystyrene thus has a dual effect

in increasing the performance of PFO-based OLEDs: i) elimination of electron trapping and ii) increasing the luminescence quantum yield via inducing β -phase formation.

An interesting notion is that the apparent complete energy transfer from amorphous PFO to β -phase domains in principle makes light emission inhomogeneous at the nanoscale. However, on macroscopic lengthscales our PLEDs light in a fully homogeneous manner. The presence of a significant amount of β -phase PFO in the blended sample furthermore might explain the unaffected hole current (**Figure 3.1**), since it has been shown that the hole mobility is significantly higher for β -phase PFO than for the amorphous phase^{10,31}. We reason that this mobility-enhancing effect of the β -phase may compensate for the suppression of the current density due to spatial separation of transport sites.

A remaining question is why β -phase PFO is encountered in the PFO:PS blend and not in the unblended sample. Development of the β -phase has been associated with PFO residing in a poorly accommodating environment. For instance, processing PFO from a poor solvent, such as diiodooctane,¹⁴ cyclohexane,¹⁸ or methylcyclohexane,³² gives rise to β -phase formation, whereas in good solvents such as chloroform and THF¹⁸ the process is not observed. Hence, the absence of β -phase PFO in our unblended sample suggests that chlorobenzene is a good solvent.

Following the same reasoning, the actual formation of β -phase in the PFO:PS blend indicates that the polymers have limited compatibility and a thermodynamic driving force for phase separation exists, despite the fact that macro-phase separation is not observed (as it can be seen in **Figure 3.5**).²⁰ This may be a consequence of the phase diagram having a relatively small miscibility gap due to the low molecular weight of the polystyrene.³³ As a result, following the transition into the region of two-phase coexistence, the composition of the blend remains near

the critical point, which slows down mass transport over macroscopic distances. Hence, the rate of demixing is suppressed beyond that of film formation and vitrification. However, short-range processes such as stretching of PFO chain segments into the β -phase configuration, may well occur. For more details and context, we refer to our prior work on evaporation-driven quenches of binary polymer solutions.^{34,35}

In order to prove that there is no macro-phase separation in PFO blend with low molecular weight PS, we present the morphological characterization of the spin-coated Films. As indicated in AFM images in **Figure 3.5a**, for unblended PFO, there is no specific features as we expect for an unblended amorphous polymer film. In the next AFM image, we observed no phase separation for the PFO:PS (low molecular weight) (**Figure 3.5b**). However, the β -phase crystals are present on the film topology. For comparison we have also included the images for the PFO blend with higher molecular weight PS ($\bar{M}_w = 35,000$ g/mol) which reveals pronounced morphological differences with the low molecular weight PS blend. The drop-like features in this sample strongly suggest phase separation to occur via liquid–liquid demixing which is not the case in the blend with low molecular PS.

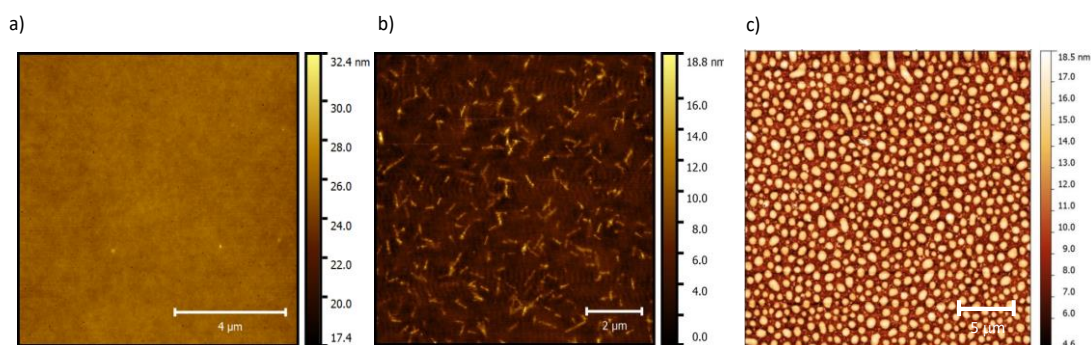


Figure 3.5 AFM surface topography a) Unblended PFO with scale bar 4 μm , b) PFO with low molecular weight PS with scale bar 2 μm and c) PFO with high molecular weight PS with scale bar 5 μm .

3.4 Conclusion

In summary, we have demonstrated how conformational changes in a luminescent conjugated polymer (polydioctylfluorene, PFO), brought about by blending with a flexible insulating polymer (polystyrene), drastically influences the optoelectronic behavior of the former. Blending induces the formation of PFO β -phase domains, consisting of fully extended chain segments with monomers oriented in a coplanar fashion. These ordered domains exhibit increased conjugation, a smaller optical bandgap, higher luminescence quantum yield and enhanced charge carrier conduction compared to the amorphous (disordered) bulk. We demonstrate that polymer light-emitting diodes based on PFO blended with 75% polystyrene exhibit a ten-fold increase in luminous efficiency compared to devices based on unblended amorphous PFO. We semi-quantitatively show that this substantial increase has two contributions: i) alleviation of electron trapping owing to a change in the statistics between free and trapped charges as a consequence of spatial separation of both transport and trap sites, and ii) formation of a substantial amount ($\sim 13\%$) of β -phase PFO embedded in the amorphous matrix. The presence of β -phase possibly counteracts a decrease in hole conduction due to the spatial separation of transport sites caused by dilution.

References

1. Kulkarni, A. P.; Jenekhe, S. A., Blue light-emitting diodes with good spectral stability based on blends of poly (9, 9-dioctylfluorene): interplay between morphology, photophysics, and device performance. *Macromolecules* **2003**, 36 (14), 5285-5296.
2. Kim, D.; Cho, H.; Kim, C., Blue light emitting polymers. *Progress in Polymer Science* **2000**, 25 (8), 1089-1139.
3. Abbaszadeh, D.; Blom, P. W. M., Efficient Blue Polymer Light-Emitting Diodes with Electron-Dominated Transport Due to Trap Dilution. *Advanced Electronic Materials* **2016**, 2 (7).
4. Tseng, S.-R.; Li, S.-Y.; Meng, H.-F.; Yu, Y.-H.; Yang, C.-M.; Liao, H.-H.; Horng, S.-F.; Hsu, C.-S., Deep blue light-emitting diode based on high molecular weight poly (9, 9-dioctylfluorene) with high efficiency and color stability. *Organic Electronics* **2008**, 9 (3), 279-284.
5. Lu, L. P.; Kabra, D.; Johnson, K.; Friend, R. H., Charge-Carrier Balance and Color Purity in Polyfluorene Polymer Blends for Blue Light-Emitting Diodes. *Advanced Functional Materials* **2012**, 22 (1), 144-150.
6. Scherf, U.; List, E. J., Semiconducting polyfluorenes—towards reliable structure—property relationships. *Advanced Materials* **2002**, 14 (7), 477-487.
7. Abbaszadeh, D.; Kunz, A.; Wetzelaer, G.; Michels, J. J.; Crăciun, N.; Koynov, K.; Lieberwirth, I.; Blom, P. W. M., Elimination of charge carrier trapping in diluted semiconductors. *Nature Materials* **2016**, 15 (6), 628.
8. Kunz, A.; Blom, P. W. M.; Michels, J. J., Charge carrier trapping controlled by polymer blend phase dynamics. *Journal of Materials Chemistry C* **2017**, 5 (12), 3042-3048.
9. Khodabakhshi, E.; Michels, J. J.; Blom, P. W. M., Visualization of trap dilution in polyfluorene based light-emitting diodes. *AIP Advances* **2017**, 7 (7), 075209.
10. Lu, H. H.; Liu, C. Y.; Chang, C. H.; Chen, S. A., Self-Dopant Formation in Poly (9, 9-di-n-octylfluorene) Via a Dipping Method for Efficient and Stable Pure-Blue Electroluminescence. *Advanced Materials* **2007**, 19 (18), 2574-2579.

11. Ohe, T.; Miyaura, N.; Suzuki, A., Palladium-catalyzed cross-coupling reaction of organoboron compounds with organic triflates. *The Journal of Organic Chemistry* **1993**, 58 (8), 2201-2208.
12. Li, W.-J.; Liu, B.; Qian, Y.; Xie, L.-H.; Wang, J.; Li, S.-B.; Huang, W., Synthesis and characterization of diazafluorene-based oligofluorenes and polyfluorene. *Polymer Chemistry* **2013**, 4 (6), 1796-1802.
13. Grice, A.; Bradley, D.D.C.; Bernius, M.; Inbasekaran, M.; Wu, W.; Woo, E., High brightness and efficiency blue light-emitting polymer diodes. *Applied Physics Letters* **1998**, 73 (5), 629-631.
14. Peet, J.; Brocker, E.; Xu, Y.; Bazan, G. C., Controlled β -Phase Formation in Poly (9, 9-di-n-octylfluorene) by Processing with Alkyl Additives. *Advanced Materials* **2008**, 20 (10), 1882-1885.
15. Weinfurter, K.-H.; Fujikawa, H.; Tokito, S.; Taga, Y., Highly efficient pure blue electroluminescence from polyfluorene: Influence of the molecular weight distribution on the aggregation tendency. *Applied Physics Letters* **2000**, 76 (18), 2502-2504.
16. Zeng, W.; Lai, H. Y.; Lee, W. K.; Jiao, M.; Shiu, Y. J.; Zhong, C.; Gong, S.; Zhou, T.; Xie, G.; Sarma, M., Achieving Nearly 30% External Quantum Efficiency for Orange-Red Organic Light Emitting Diodes by Employing Thermally Activated Delayed Fluorescence Emitters Composed of 1, 8-Naphthalimide-Acridine Hybrids. *Advanced Materials* **2018**, 30 (5), 1704961.
17. Bradley, D. D.C.; Grell, M.; Long, X.; Mellor, H.; Grice, A. W.; Inbasekaran, M.; Woo, E. P. In Influence of aggregation on the optical properties of a polyfluorene, Optical Probes of Conjugated Polymers, *International Society for Optics and Photonics*: **1997**; pp 254-260.
18. Grell, M.; Bradley, D.; Long, X.; Chamberlain, T.; Inbasekaran, M.; Woo, E.; Soliman, M., Chain geometry, solution aggregation and enhanced dichroism in the liquidcrystalline conjugated polymer poly (9, 9-dioctylfluorene). *Acta Polymerica* **1998**, 49 (8), 439-444.

19. Huber, D. L.; Avgin, I., Optical absorption of the β -phase of poly (9, 9-dioctylfluorene). *Journal of Polymer Science Part B: Polymer Physics* **2016**, 54 (12), 1109-1111.
20. Grell, M.; Bradley, D.; Ungar, G.; Hill, J.; Whitehead, K., Interplay of physical structure and photophysics for a liquid crystalline polyfluorene. *Macromolecules* **1999**, 32 (18), 5810-5817.
21. Chunwaschirasiri, W.; Tanto, B.; Huber, D.; Winokur, M., Chain conformations and photoluminescence of poly (di-n-octylfluorene). *Physical Review Letters* **2005**, 94 (10), 107402.
22. Knaapila, M.; Winokur, M. J., Structure and morphology of polyfluorenes in solutions and the solid state. In *Polyfluorenes*, Springer **2008**; pp 227-272.
23. Ariu, M.; Sims, M.; Rahn, M.; Hill, J.; Fox, A.; Lidzey, D.; Oda, M.; Cabanillas-Gonzalez, J.; Bradley, D., Exciton migration in β -phase poly (9, 9-dioctylfluorene). *Physical Review B* **2003**, 67 (19), 195333.
24. Ryu, G.; Stavrinou, P. N.; Bradley, D. D.C. , Spatial Patterning of the β -Phase in Poly (9, 9-dioctylfluorene): A Metamaterials-Inspired Molecular Conformation Approach to the Fabrication of Polymer Semiconductor Optical Structures. *Advanced Functional Materials* **2009**, 19 (20), 3237-3242.
25. Perevedentsev, A.; Aksel, S.; Feldman, K.; Smith, P.; Stavrinou, P. N.; Bradley, D. D.C., Interplay between solid state microstructure and photophysics for poly (9, 9-dioctylfluorene) within oriented polyethylene hosts. *Journal of Polymer Science Part B: Polymer Physics* **2015**, 53 (1), 22-38.
26. Coropceanu, V.; Cornil, J.; da Silva Filho, D. A.; Olivier, Y.; Silbey, R.; Brédas, J.-L., Charge transport in organic semiconductors. *Chemical reviews* **2007**, 107 (4), 926-952.
27. Perevedentsev, A.; Chander, N.; Kim, J. S.; Bradley, D. D.C., Spectroscopic properties of poly (9, 9-dioctylfluorene) thin films possessing varied fractions of β -phase chain segments: enhanced photoluminescence efficiency via conformation structuring. *Journal of Polymer Science Part B: Polymer Physics* **2016**, 54 (19), 1995-2006.

28. Ariu, M.; Lidzey, D.; Bradley, D. D. C., Influence of film morphology on the vibrational spectra of dioctyl substituted polyfluorene (PFO). *Synthetic metals* **2000**, 111, 607-610.
29. Hayer, A.; Khan, A. L.; Friend, R. H.; Köhler, A., Morphology dependence of the triplet excited state formation and absorption in polyfluorene. *Physical Review B* **2005**, 71 (24), 241302.
30. Becker, K.; Lupton, J. M., Dual species emission from single polyfluorene molecules: signatures of stress-induced planarization of single polymer chains. *Journal of the American Chemical Society* **2005**, 127 (20), 7306-7307.
31. Bai, Z.; Liu, Y.; Li, T.; Li, X.; Liu, B.; Liu, B.; Lu, D., Quantitative Study on β -Phase Heredity Based on Poly (9, 9-dioctylfluorene) from Solutions to Films and the Effect on Hole Mobility. *The Journal of Physical Chemistry C* **2016**, 120 (49), 27820-27828.
32. Bright, D. W.; Dias, F. B.; Galbrecht, F.; Scherf, U.; Monkman, A. P., The influence of alkyl-chain length on beta-phase formation in polyfluorenes. *Advanced Functional Materials* **2009**, 19 (1), 67-73.
33. Flory, P. J., Principles of polymer chemistry. Cornell University Press: **1953**.
34. Schaefer, C.; Michels, J. J.; van der Schoot, P., Structuring of thin-film polymer mixtures upon solvent evaporation. *Macromolecules* **2016**, 49 (18), 6858-6870.
35. Schaefer, C.; Michels, J. J.; van der Schoot, P., Dynamic surface enrichment in drying thin-film binary polymer solutions. *Macromolecules* **2017**, 50 (15), 5914-5919.

Chapter 4

Suppression of electron trapping by quantum dot emitters using a grafted polystyrene shell

A fundamental problem of adding chromophores to an organic host is that their smaller band gap leads to severe trapping of either electrons or holes, resulting in strongly unbalanced transport. We demonstrate that electron trapping by an inorganic quantum dot (QD) in a conjugated polymer host can be suppressed by functionalizing its shell with a thin insulating polystyrene layer. The polystyrene shell not only reduces trapping, but also suppresses detrapping of captured electrons, resulting in increased charging of the QDs with subsequent voltage scans. After initial charging, a red-emitting hybrid polymer:QD light-emitting diode is obtained with voltage independent electroluminescence spectrum and equal efficiency as the blue polymer host.

The results of this chapter are fully published in *Materials Horizons* with DOI: 10.1039/C9MH00551J by E. Khodabakhshi et al. E. Khodabakhshi has performed the device fabrication, measurements, analyses and modeling. The QDs with polymer shell in this chapter were provided by Dr. Benjamin Klöckner in group of Prof. Rudolf Zentel at Johannes Gutenberg university of Mainz.

4.1 Introduction

As described in the introduction of chapter 1, organic light-emitting diodes are a promising option for large-area lighting panels,^{1,2} eventually produced by roll-to-roll processes. A disadvantage of using organic semiconductors for displays and lighting is their relatively broad emission spectrum due to inhomogeneous broadening. The emission spectrum can be considerably narrowed by blending a blue-emitting organic host with a green or red-emitting (phosphorescent) dye with narrow linewidth.³ In polymer based LEDs it has been demonstrated that due to efficient energy transfer from the host to the dye already for 1% dye concentration 95% of the blue excitons are transferred to the dye.⁴ For display fabrication using ink-jet printing this is convenient since such a small dye concentration does not affect the rheology of the solution, allowing all colors to be printed using the same host and identical conditions.⁵ A reduction of the dye concentration towards 0.1% or less, giving rise to a partial energy transfer, can be used for the generation of white light.⁶⁻⁸ This allows for the fabrication of lighting devices consisting of only one solution-processed layer. However, for efficient energy transfer the absorption spectrum of the dye has to overlap with the emission spectrum of the host, such that by definition dyes have a smaller bandgap as compared to the host. This will inevitably lead to severe trapping of charge carriers, as indicated in **Figure 4. 1a**. For a white-emitting polymer with only 0.02% red dye incorporated in the blue-emitting main chain it has been demonstrated that the electron transport was reduced by several orders of magnitude.⁹ The resulting strongly imbalanced transport leads to a strong reduction of the efficiency of the corresponding PLED containing dyes. Another unwanted side-effect of the strong electron trapping by the dyes is that the electroluminescence spectrum becomes voltage dependent. The blue emission of the host is governed by bimolecular Langevin recombination, with a rate given by

$$R_L = B_L np \quad (1)$$

with $p(x)$ and $n(x)$ the density of mobile holes and electrons, and B_L the Langevin recombination constant that is proportional to the sum of the electron and hole mobilities. In contrast, the recombination via the red dye is trap-assisted (Shockley-Read-Hall, SRH) and for recombination of trapped electrons with free holes can be approximated by

$$R_{SRH} = B_{SRH} n_t p \quad (2)$$

with B_{SRH} proportional to the hole mobility μ_p and $n_t(x)$ the amount of trapped electrons. In case that the trap-assisted recombination originates from a region where all traps are filled this changes into

$$R_{SRH} = B_{SRH} N_t p \quad (3)$$

with N_t the total amount of traps. For the case of a blue host and low concentration of red-emitting dye, such that complete trap-filling occurs, the trap-assisted red emission from the dye has a linear dependence on carrier density (Eq. 3), whereas the blue bimolecular Langevin recombination varies quadratically with density (Eq. 1). As a result, the PLED exhibits a bias voltage dependent electroluminescence spectrum with the blue emission more dominant at higher voltages, as schematically indicated in **Figure 4. 1a**.⁹ Finally, the resulting narrowing of the emission zone due to the enhanced trapping in the PLED is detrimental for their lifetime.

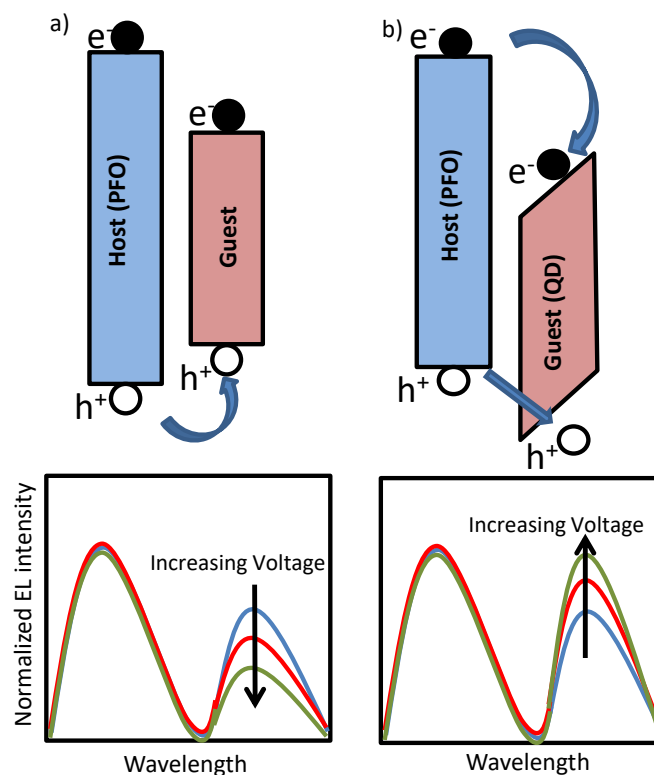


Figure 4. 1 Schematic energy diagram and electroluminescence spectrum of a) Blend of large band gap organic host and an organic dye resulting in severe electron trapping. b) Blend of large band gap organic host and an inorganic QD, leading to electron trapping and charging effects that enhance hole capture.

An interesting alternative for organic dyes are inorganic quantum dots (QDs). High quality colloidal core/shell semiconductor quantum dots (QDs) offer stable, tunable narrow and intense photoemission as function of size in the visible range.¹⁰⁻¹⁵ These properties can be exploited in solution-processed hybrid QD/organic polymer light-emitting diodes, which combine the emitting properties of QDs with the flexibility in device construction of the polymeric materials.¹⁶⁻¹⁹ However, the conduction and valence band of inorganic semiconductors as CdSe and ZnS are deeper in energy as compared to the corresponding molecular orbitals of most organic hosts, as schematically indicated in **Figure 4. 1b**, resulting in strong electron trapping. Furthermore, the

holes have to surmount an energy barrier before they can recombine with the trapped electron on the QD. As a result the QD emission can be a combination of Förster energy transfer and trap-assisted recombination.¹⁷ In multilayer organic LEDs based on evaporated small molecules, one or a few monolayers of QDs are sandwiched between electron and hole transporting organic layers.^{11,12} The trapped electrons are then confined in a narrow QD region, enabling the trapped electrons to build up a large electric field that enhances the hole injection into the deep QD valance band. With increasing voltage this charging effect becomes more dominant such that the QD emission grows relative to the host emission (**Figure 4. 1b**), which is the opposite spectral dependence as compared to the typical trap-assisted recombination occurring with organic dyes (**Figure 4. 1a**). However, at high voltages the high carrier concentration and electric field in the confined QD layers leads to efficiency losses due to Auger recombination and field-induced spatial separation of the electron and hole wave function.²⁰ For solution processed devices such a multilayer approach combined with a few monolayers of QDs is not feasible. Realization of balanced charge transport remains a fundamental problem due to the severe electron trapping of the QDs.^{21,22} Next to the mismatch in energy levels between organic semiconductors and inorganic QDs for hybrid polymer:QD blends also the blend morphology plays a crucial role.²³ For the incorporation of a larger amount of QDs within a polymer matrix the physical blending of the two components is usually insufficient to obtain a homogeneous distribution of QDs and phase separation typically occurs. By hybridizing QDs with conducting polymer brushes a more homogeneous distribution of QDs in the polymer matrix was obtained,²⁴ leading to a better distribution of charges and excitons across the active layer with a reduced efficiency roll-off.^{23,25}

Ideally, a solution would be preferred where the negative contribution of severe electron trapping by the QDs is reduced. Furthermore, a homogeneous distribution of the QDs in the

polymer host matrix is required, which can be achieved by coating them with a suitable polymer.²⁴ Charge transport and electron trapping in conjugated polymers has been extensively studied.²⁶ The hopping distance for charge carriers is determined by the wave function overlap of the localized sites and typically amounts to 1.5-2 nm.²⁶ This distance also governs the charge transfer process from a host polymer into a trap. In contrast, fluorescence resonance energy transfer (FRET) is driven by dipole–dipole interaction between an excited donor molecule and an acceptor molecule, with a Förster radius of 5-8 nm.²⁷ Grafting of a thin insulating shell with thickness 3-5 nm on the QD is therefore expected to have a stronger effect on trapping as compared to energy transfer. In the present study we demonstrate that electron trapping by CdSe/Cd_xZn_{1-x}S core/shell red QDs in a blue-emitting poly (dioctylfluorene) (PFO) host can be suppressed by functionalizing them with a thin insulating shell of polystyrene. The strong reduction of trapping is confirmed by charge transport measurements. Upon charging of the QDs a voltage independent electroluminescence spectrum, dominated by QD emission, is obtained for the hybrid polymer:QD blend LEDs.

4.2 Experimental section

Materials: Styrene (Acros) was distilled before use, 2-(Dodecylthiocarbonothioylthio)-2-methylpropionic acid (CTA) was used as purchased (Sigma-Aldrich). 2,2-Azobis(2-methylpropionitrile) (AIBN) was purchased from Acros and recrystallized from diethyl ether prior to use. Cysteaminemethyldisulfide, pentafluorophenyl acrylate (PFPA) and quantum dots with CdSe core, Cd_xZn_{1-x}S shell (core diameter 4 nm, total diameter 16 nm with oleic acid surface ligands) were synthesized according to literature²⁸⁻³⁰ PFO was synthesized via the Yamamoto method according to literature ($M_w = 230.000$ g/mol, $M_w/M_n = 3.02$).³¹ THF was dried over sodium and distilled prior to use and all other solvents were used without further purification.

Materials characterization: For all polymers, size exclusion chromatography (SEC) was performed in THF with polystyrene as external and toluene as an internal standard to calculate the molecular weights. Both a refractive index detector (G 1362A RID, Jasco) and a UV/vis detector (UV-2075 Plus, Jasco) were used to detect the polymer. TGA measurements were performed at a Perkin Elmer Pyris 6 TGA under nitrogen flow. Heating rate was $10\text{ }^{\circ}\text{C}\cdot\text{min}^{-1}$ from 50 to $700\text{ }^{\circ}\text{C}$. Infrared spectroscopy was performed on a Jasco FT/IR-4100 with an ATR sampling accessory (MIRacle, Pike Technologies) using 16 scans per measurement. IR spectra were analyzed using Spectra Manager 2.0 (Jasco).

Synthesis of poly(styrene-block-cysteamine methyl disulfide) (P(S-b-SSMe): At first, the macro chain transfer agent (macro-CTA) was synthesized: Styrene (60 eq.), 2-cyano-2-propyl dodecyl trithiocarbonate (CTA) (1 eq.) and 2,2'-azobis(2-methylpropionitrile) (AIBN) (0.1 eq.) were dissolved in dry THF. After three freeze-pump-thaw cycles the flask was filled with nitrogen and the solution was heated to $70\text{ }^{\circ}\text{C}$ for 24 hours. The macro-CTA was purified by dissolution in THF and precipitation from methanol three times and dried under vacuum for 24 h. SEC: $M_n = 2000\text{ g}\cdot\text{mol}^{-1}$, $M_w/M_n = 1.17$. Second, the reactive diblock copolymer was synthesized: the macro-CTA (1 eq.), pentafluorophenyl acrylate (PFPA) (30 eq.) and AIBN (0.1 eq.) were dissolved in dry THF. After three freeze-pump-thaw cycles the flask was filled with nitrogen and the solution was heated to $70\text{ }^{\circ}\text{C}$ for 48 hours. The diblock copolymer was purified by dissolution in THF and precipitation from hexane three times. Then, the CTA end group was removed directly. The diblock copolymer (1 eq.) was dissolved in dry THF. AIBN (70 eq.) was added and the mixture was stirred at $70\text{ }^{\circ}\text{C}$ for 24 hours. The reaction solution was cooled down and precipitated into hexane three times. The polymer appeared as white powder. M_n , SEC: $3300\text{ g}\cdot\text{mol}^{-1}$, $M_w/M_n = 1.19$. Third, the diblock copolymer (1 eq.), cysteaminemethyldisulfide (30 eq.) and triethylamine

(60 eq.) were dissolved in dry THF and heated to 40 °C for 24 hours under an argon atmosphere. The solution was purified by precipitation from hexane three times. The desired diblock copolymer P(S-b-SSMe) was dried under vacuum for 24 h. M_n , SEC: $M_n = 2600 \text{ g} \cdot \text{mol}^{-1}$, $M_w/M_n = 1.18$.

Quantum dot/ polymer hybridization: The QD/PS-hybrids were prepared using CdSe/Cd_xZn_{1-x}S core/shell Type-I hetero-structured QDs with a core diameter of 4 nm and a total diameter of 16 nm and the corresponding diblock copolymer. This specific type of QDs has extensively been used in our previous works in the field of QLED and QD-semiconducting polymer hybrid studies.³² The QD/PS-hybrids were surface functionalized with polymer chains by the ligand exchange procedure^{33,34}: diblock copolymer P(S-b-SSMe) and quantum dots (QD, red, CdSe core, core diameter 4 nm, Cd_xZn_{1-x}S shell, total diameter 16 nm, oleic acid ligands) were separately dispersed in chlorobenzene (each 100 μL) and subsequently combined (weight ratio polymer to QD 1:1). The reaction mixture was sonicated for one hour and ethanol (1.5 mL) was added to precipitate the functionalized QDs. The precipitate was dispersed in chlorobenzene (250 μL), sonicated for one additional hour and left at room temperature overnight. Ethanol (1.5 mL) was added to precipitate the functionalized QDs. The precipitate was dispersed in chlorobenzene (250 μL) and sonicated for one additional hour at room temperature. Hexane (1.5 mL) was added to remove the remaining QDs which were not coated with the diblock copolymer and to precipitate the functionalized QDs. Finally, the precipitate was dispersed in chlorobenzene to obtain the desired QD-/polymer hybrid solution.

Device fabrication: PFO and QD/PS-hybrid solutions were prepared by dissolving PFO and QD/PS-hybrids in chlorobenzene and consequently blending the solutions using different weight ratios. Films of the pristine conducting polymer and also the hybrid solution were applied using standard spin-coating methods.

The electron current through the blends was measured using electron-only devices having a glass/Al (30 nm)/polymer-QD/Ba (5 nm)/Al (100 nm) architecture. For hole-only and light emitting (dual carrier) devices, a 60 nm hole-injection layer of poly(3,4 ethylenedioxythiophene):poly(styrene sulfonic acid) (PEDOT:PSS) (Heraeus Clevios 4083) was spin-coated on ITO-patterned substrates and annealed at 140 °C. Subsequently, the hybrid solution was deposited by spin coating. As top contacts, for hole-only devices MoO₃ (10 nm)/Al (100 nm) and for PLEDs Ba (5 nm)/Al (100 nm) were thermally evaporated. After device preparation, steady-state current-voltage measurements were performed in inert (N₂) atmosphere using a Keithley 2400 source meter.

4.3 Results and discussion

We designed a novel QD/polymer hybrid material in which the surface of QDs is covered with a thin shell of insulating polystyrene. In addition, the polymer coverage of the QD allows us to tune the miscibility with the host polymer matrix to obtain a homogenous distribution of the QDs. The ligand exchange procedure enables the synthesis of various QD/PS hybrids by replacing the initial stabilizing oleic acid ligands coordinated onto the QDs surface with new polymeric ligands containing anchor units.³² Reversible addition-fragmentation chain transfer (RAFT) radical polymerization and post-polymerization modification techniques were employed for the synthesis of the diblock copolymer poly(styrene-block-cysteaminemethyldisulfide) (P(S-b-SSMe) containing a chemical and electrochemical robust polystyrene block and cysteaminemethyldisulfide anchoring block, as shown in **Figure 4.2a**. First, the polystyrene block was synthesized and used as a macro-initiator in a second RAFT polymerization for the polymerization of the reactive ester monomer pentafluorophenyl acrylate (PFPA) leading to

diblock copolymer. After polymerization, the reactive CTA group was replaced with an inert 2-cyanoisopropyl group by reaction with excess of AIBN to obtain defined end-groups on both sides of the polymer. For the anchor block, cysteaminemethyldisulfide was chosen since due to its high affinity to unsaturated Zn-centres it enables the replacement of pristine oleic acid ligands that are initially grafted on the QDs for stabilization.^{28,35} The ligand exchange (**Figure 4.2b**) was further monitored with the solubility change of the QDs, IR spectroscopy and thermogravimetric analysis (**Figure 4.3-5**) as well as NMR spectroscopy and size-exclusion chromatography (**Figure 4. 6-8**). The obtained molecular weight of the diblock copolymer P(S-b-SSMe) amounts to 2600 g/mol.

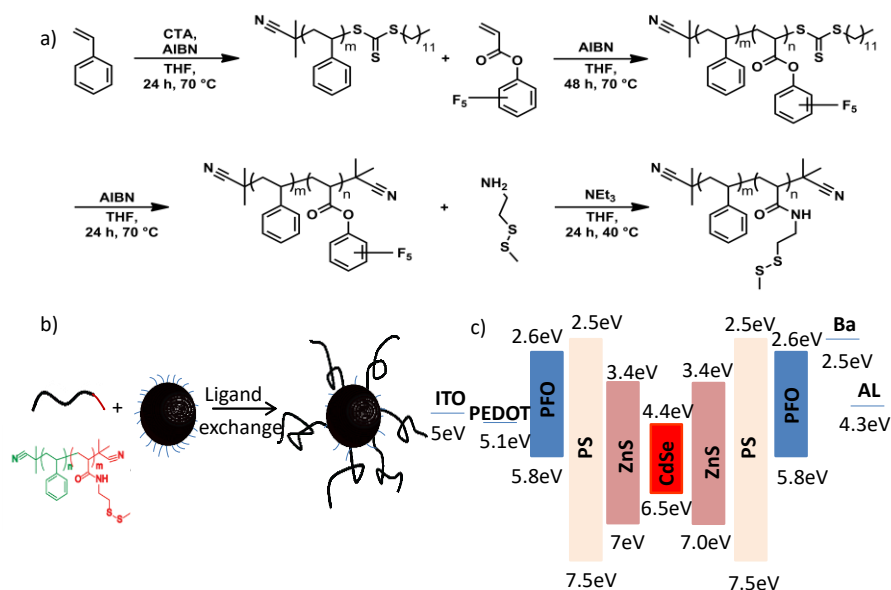


Figure 4.2 a) Synthesis of diblock copolymer poly(styrene-block-cysteaminemethyldisulfide) (P(S-b-SSMe)), b) The ligand exchange procedure and c) Energy-band diagram of PFO:QD system

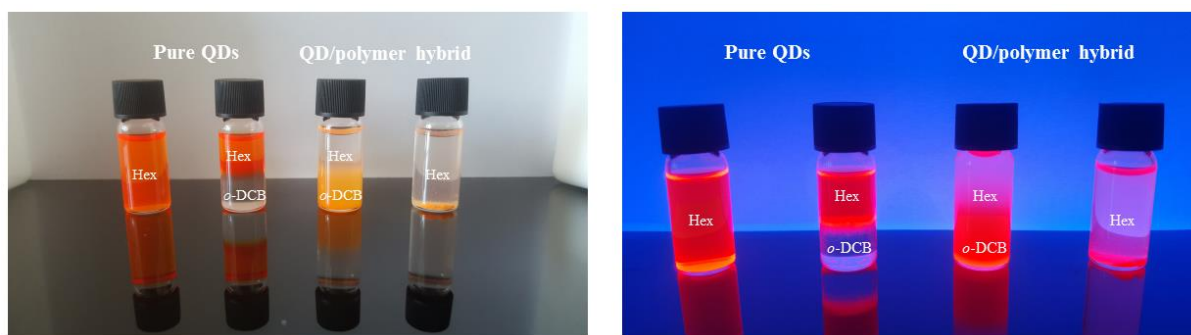


Figure 4.3 Solubility change from pure QDs to QD/PS-hybrids, normal (left) and UV light (right). Pure QDs, coated by oleic acid, are soluble in hexanes. QD/PS-hybrids, coated by polymer, are insoluble in hexanes, resulting in precipitation. In a biphasic system of hexanes (upper phase) and *ortho*-dichlorobenzene (lower phase), pure QDs are soluble in upper hexanes phase, QD/PS-hybrids are soluble in lower *ortho*-dichlorobenzene phase.

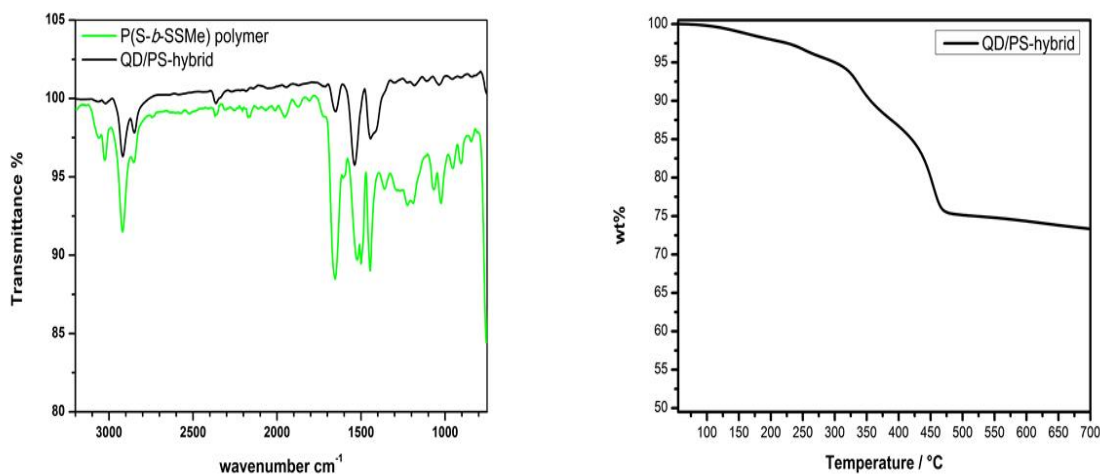


Figure 4.4 IR spectra of QD/PS-hybrids and polymer and TGA spectra of pure QDs and QD/PS-hybrids. (left) IR spectra of QD/PS-hybrids and polymer, signals at 3000 cm^{-1} attributed to $-\text{CH}-$ vibrations and signals at 1650 cm^{-1} and 1520 cm^{-1} attributed to the disulfide anchor group are observed in the IR spectra of QD/PS-hybrid, (right) TGA spectra of QD/PS-hybrids, coated with polymer, weight loss 25 wt%.

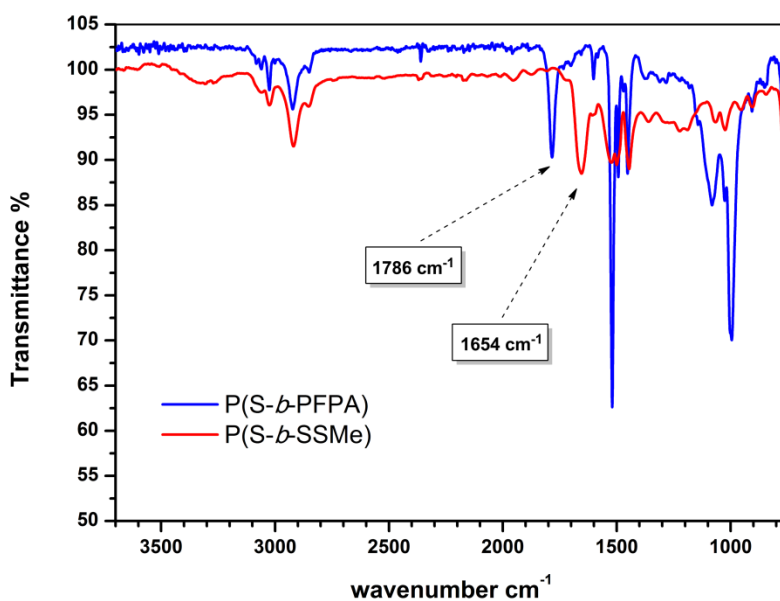


Figure 4.5 IR spectra of P(S-*b*-PFPA) and after post-polymerization modification of P(S-*b*-SSMe). IR spectra of P(S-*b*-PFPA) shows characteristic signal at 1786 cm⁻¹ attributed to reactive ester block before post-polymerization modification and IR spectra of P(S-*b*-SSMe) shows characteristic signal at 1654 cm⁻¹ attributed to the amide group of the disulfide anchor block, the signal at 1786 cm⁻¹ vanished after post-polymerization modification.

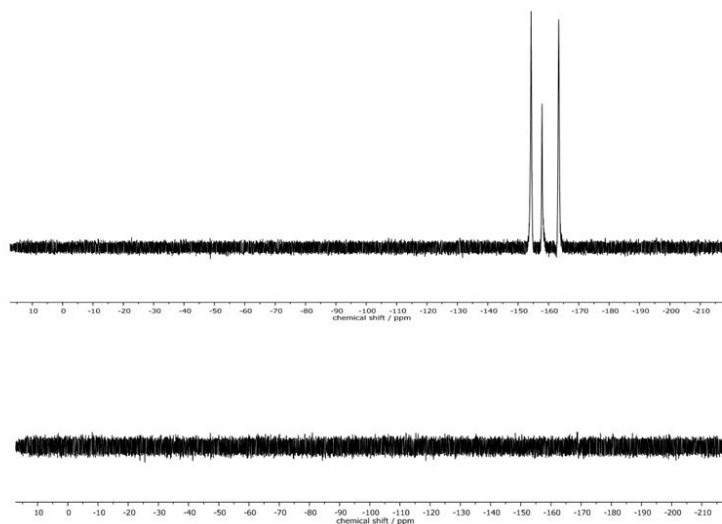


Figure 4.6 ¹⁹F-NMR spectra of P(S-*b*-PFPA) (top) and after post-polymerization modification of P(S-*b*-SSMe) (bottom). ¹⁹F-NMR spectra of P(S-*b*-PFPA) shows characteristic signal of reactive ester block

before post-polymerization modification and after post-polymerization modification the signals of the reactive pentafluorophenyl ester vanished.

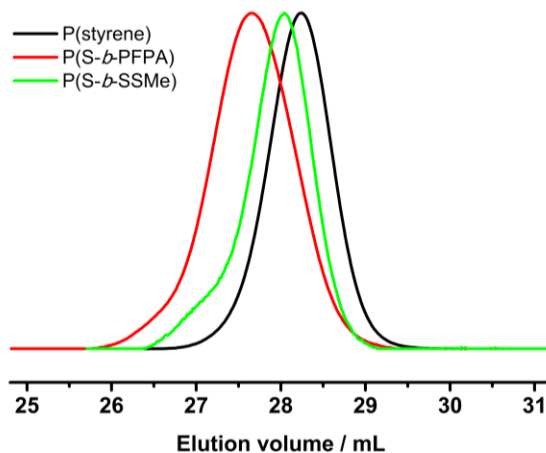


Figure 4.7 SEC curves of all reaction steps. Measured in THF, polystyrene standards (UV-vis detector).

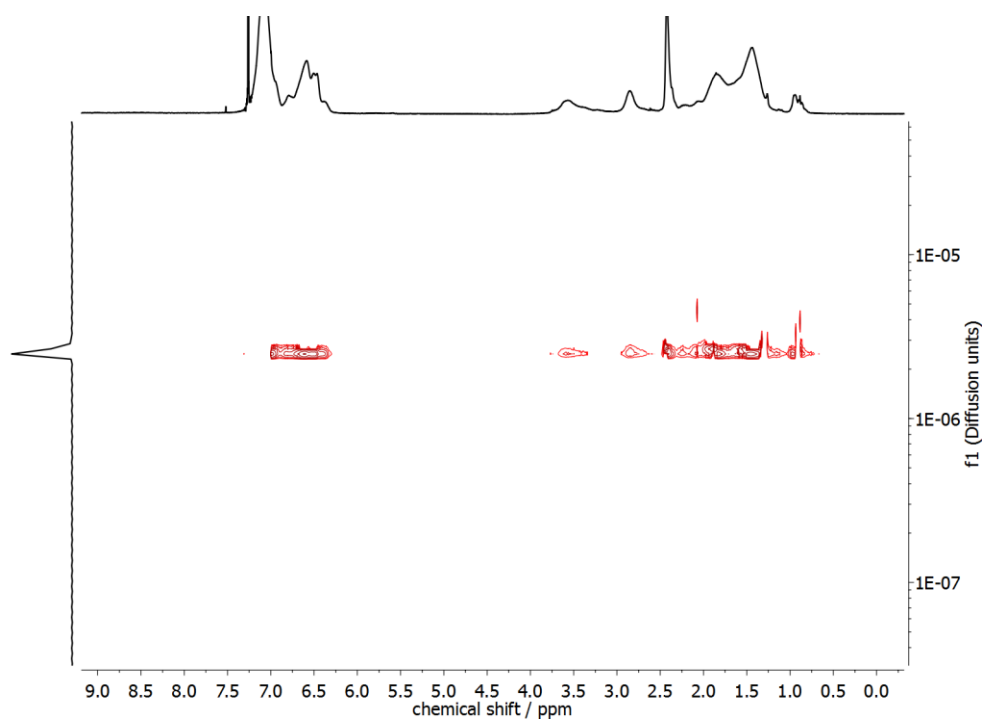


Figure 4.8 DOSY 2 D NMR spectrum of P(S-*b*-SSMe). Only one diffusing species demonstrates the successful post-polymerization modification step.

The thickness of the grafted polystyrene shell can be estimated from the dimensions of the polymer chain. The persistence length of polystyrene amounts to $l_p \sim 1$ nm. Our polystyrene blocks consist of about 20 repeat units. We hence estimate the contour length of the polymer to be $R_{\max} \approx 5$ nm, based on an inter-monomer spacing of ~ 2.5 Å. For the determination of the shell thickness the root-mean-square end-to-end distance of the chain is needed, which according to the worm-like chain model³⁶ can be written as a function of l_p and R_{\max} :

$$\sqrt{\langle R^2 \rangle} = \left[2l_p R_{\max} - 2l_p^2 \left(1 - \exp(-R_{\max}/l_p) \right) \right]^{1/2} \quad (4)$$

Plugging in the above given estimates for l_p and R_{\max} gives $\sqrt{\langle R^2 \rangle} \approx 3$ nm, which should be sufficient to suppress charge transfer to the QDs.

To investigate the effect of the PS shell on performance of PFO:QDs hybrid LEDs we first compare the electroluminescence spectra of blends of PFO with the unmodified QDs, containing oleic acid ligands (oa-QDs), and with the QD/PS-hybrids, respectively. As is evident from the energy diagram, (**Figure 4. 2c**) QDs with a ZnS shell are expected to act as an electron trapping center in PFO. To investigate the mechanism of the QD emission we chose a QD concentration of 3 wt%, in which part of the blue emission from the host can still be observed.

The voltage-dependence of the normalized (to the blue emission) EL spectra of the PLEDs with 3% QD are shown in **Figure 4. 9a-b**) (unmodified oa-QD) and 4.9c-f) (QD/PS-hybrid), respectively. As expected, the FWHM linewidth of the red QD emission is significantly smaller as compared to the blue PFO emission (0.1 eV vs. 0.5 eV, **Figure 4. 10**). For PLEDs based on the PFO:oa-QD blend the contribution of the red QD emission reduces at higher voltages, both in the up-scan (**Figure 4. 9a**) and down-scan (**Figure 4. 9b**), which is a fingerprint for trap-assisted

recombination. For every subsequent voltage scan the magnitude and voltage dependence of the EL spectrum remains identical (not shown). The spectra are not dependent on the bias history of the device, indicating that the QDs charge and discharge with every up- and down scan, respectively. Furthermore, we observe that for the unmodified oa-QD a significant blue emission remains. In contrast, for the QD/PS-hybrid blends in the first up-scan the contribution from the QD is very small and voltage independent, whereas during the down-scan the relative contribution from the red QD emission strongly grows. This behaviour, a voltage independent EL spectrum in the up-scan and larger but voltage dependent QD emission in the down-scan repeats in subsequent scans (**Figure 4.11**). Also, with every new scan the overall QD contribution to the EL spectrum is becoming slightly larger. After five scans (**Figure 4.9e** and **9f**) the contribution from the QD emission is comparable to the spectra from the PFO:oa-QD blend (**Figure 4.9a** and **9b**), but now the spectrum is nearly voltage independent. These EL spectra and corresponding voltage independence are maintained in subsequent scans, even when taken after ten days.

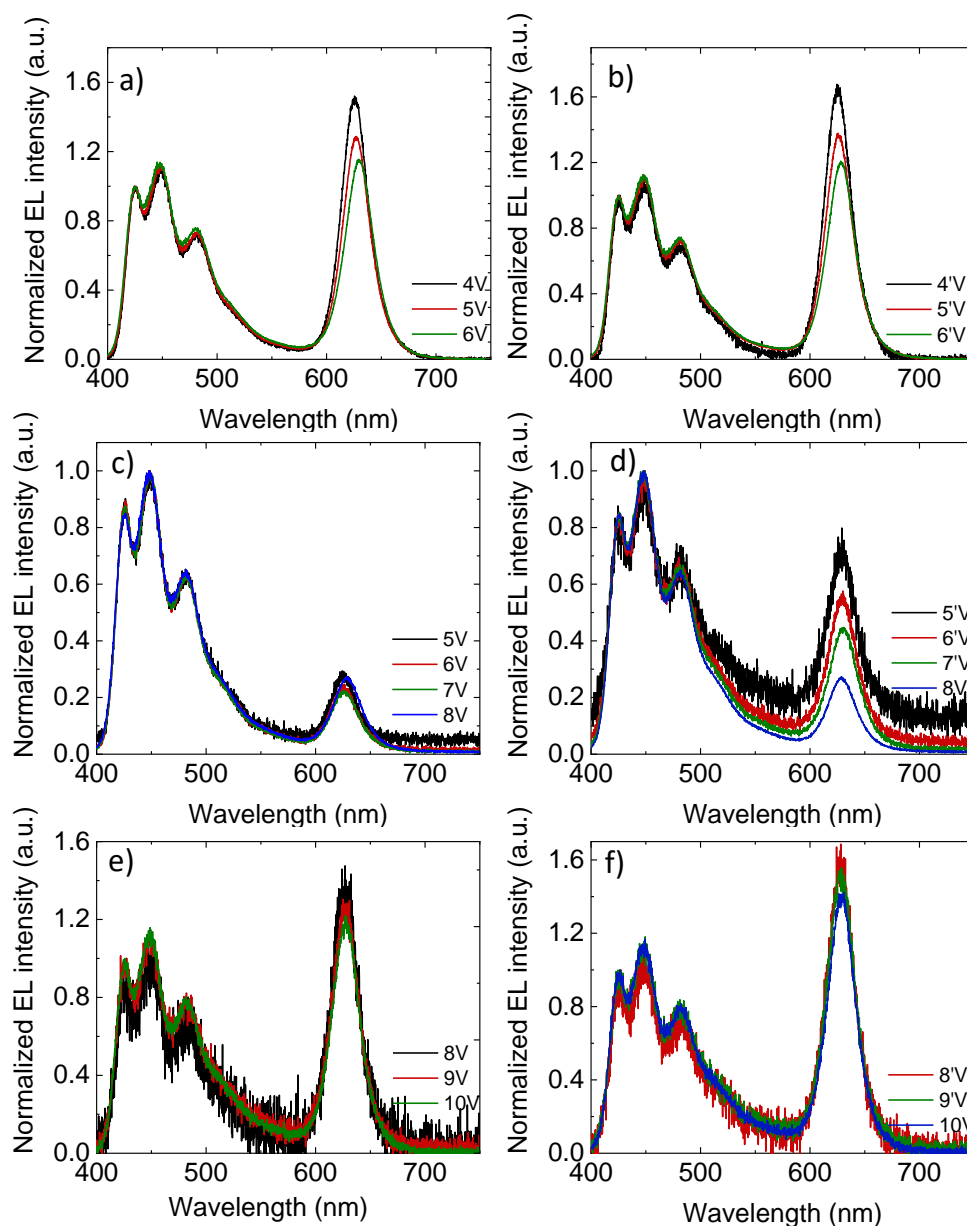


Figure 4.9 Voltage dependence of normalized EL spectra for PLED with 100 nm PFO:3% oa-QD/PS blend active layer a) first up-scan and b) consecutive down-scan. Voltage dependence of normalized EL spectra for PLED with 100 nm PFO:3% QD/PS-hybrid blend active layer c) first up-scan) and d) consecutive down-scan, e) fifth up-scan and f) corresponding down-scan.

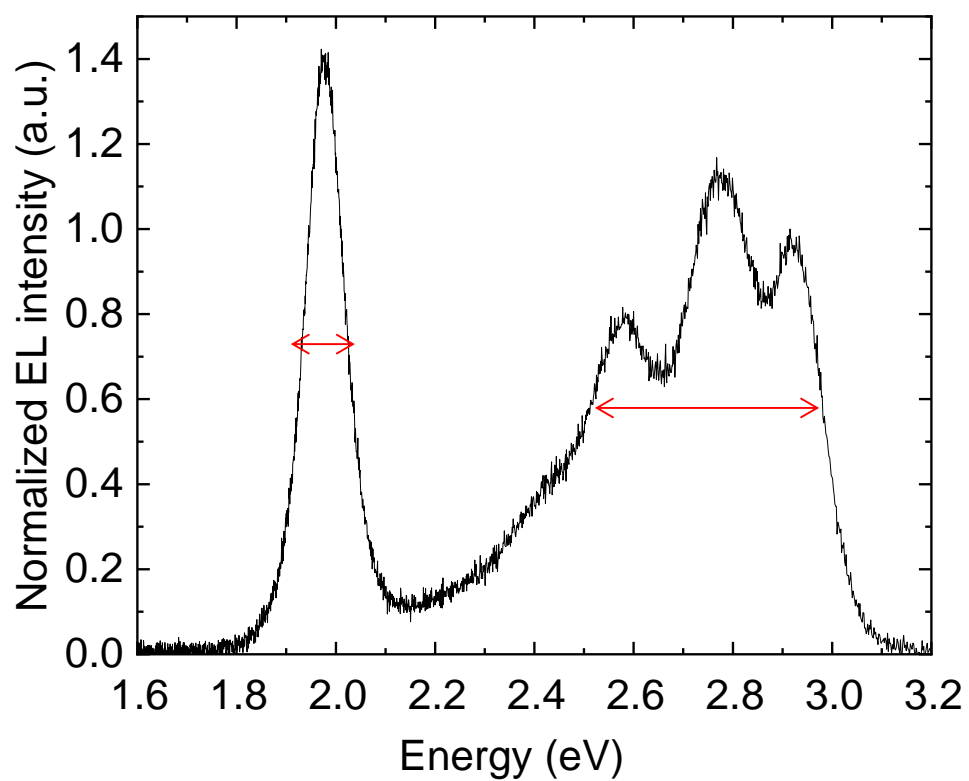


Figure 4.10 EL spectrum of a device based on PFO with 3% QD-Hybrid versus energy. the FWHM linewidth of the red QD emission is significantly smaller as compared to the blue PFO emission

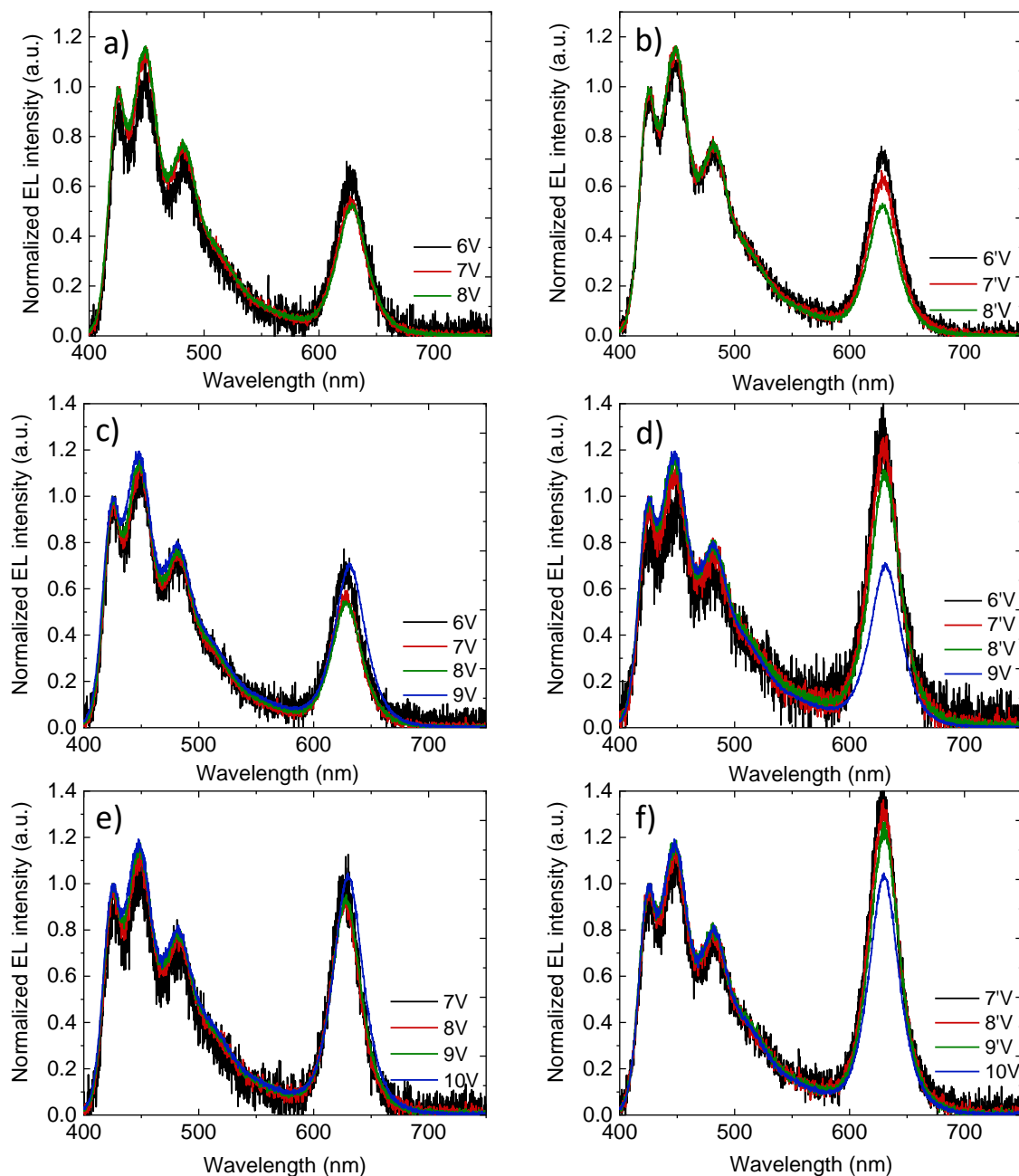


Figure 4.11 Voltage dependence of normalized EL spectra for PLED with 100 nm PFO:5% QD/PS-hybrid blend active layer a) second up-scan), b) consecutive down-scan, c) third up-scan and d) corresponding down-scan, e) fourth up-scan and f) corresponding down-scan.

The voltage dependence of the EL spectra of the PFO:oa-QD blend already indicates that the red QD emission is dominated by trap-assisted recombination. Clearly, coverage of the QD with an oleic-acid ligand, which is representative for an insulating shell of only ~ 1.5 nm, does not suppress electron trapping. The near absence of energy transfer is further confirmed by photoluminescence measurements, where the contribution of the QD is hardly visible (**Figure 4.12**).

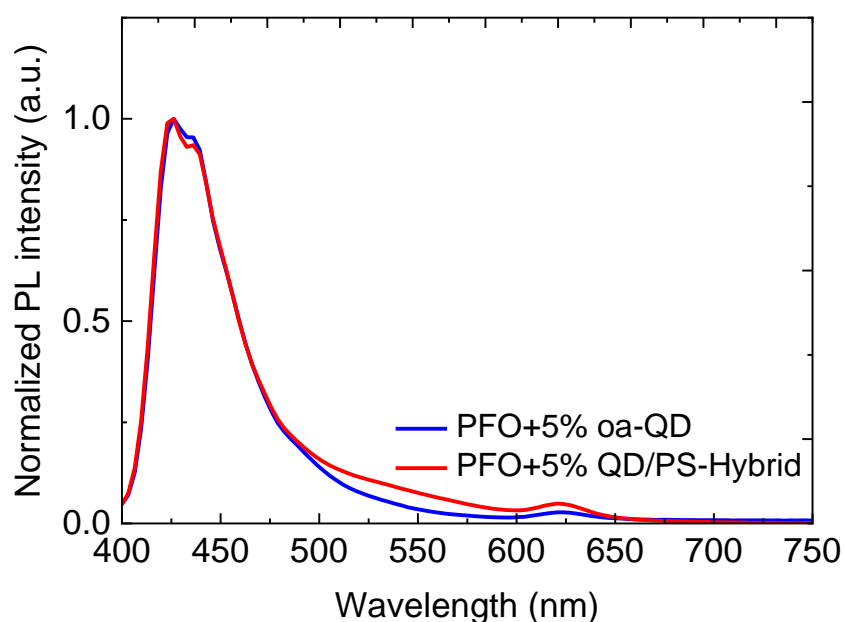


Figure 4.12 Photoluminescence spectra of PFO: oa-QD blend and QD/PS-hybrid blend for 5% QD concentrations. An excitation wavelength of 390 nm was used.

The very small contribution of red QD emission during the first voltage up-scan of the QD/PS-hybrid blend indicates that now the trap-assisted recombination of the QDs is strongly suppressed due to reduced electron trapping. By varying the molecular weight of the PS from 2600 g/mol to

9800 g/mol, corresponding to a variation in PS shell thickness from 3 nm to 6 nm, we demonstrate that the contribution of red QD emission to the EL spectra strongly decreases with increasing PS layer thickness (**Figure 4.13**). This strong dependence is the result of the exponential dependence of charge transfer on distance.

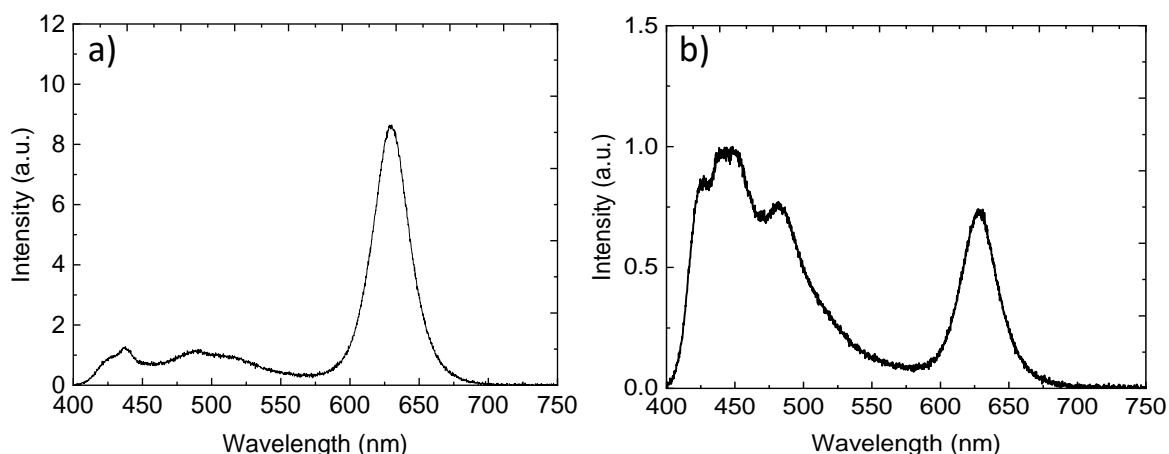


Figure 4.13 Normalized electroluminescence spectra of PFO with 5% QD/PS hybrids with shell thickness of a) 3 nm b) 6 nm. The relative contribution of red QD emission to blue PFO emission strongly decreases with increasing PS shell thickness.

One could argue that the relative large blue contribution to the electroluminescence of the PFO:oa-QD and QD/PS-hybrid blends could also have a morphological origin. Strong phase separation leading to pure PFO regions would also enhance the blue emission. However, as shown in the Scanning Electron Microscopy (SEM) images of **Figure 4.14a** and **14b** for both types of QD with 5 wt% there is no significant macroscopic phase separation observed. In case of films with 5 wt% QD/PS-hybrid, the QDs are well dispersed even in the bulk of the film (**Figure 4.15**). By

further increasing the QD content we found that for the QD/PS-hybrid phase separation starts to occur for loadings of about 7% as shown in **Figure 4.16**.

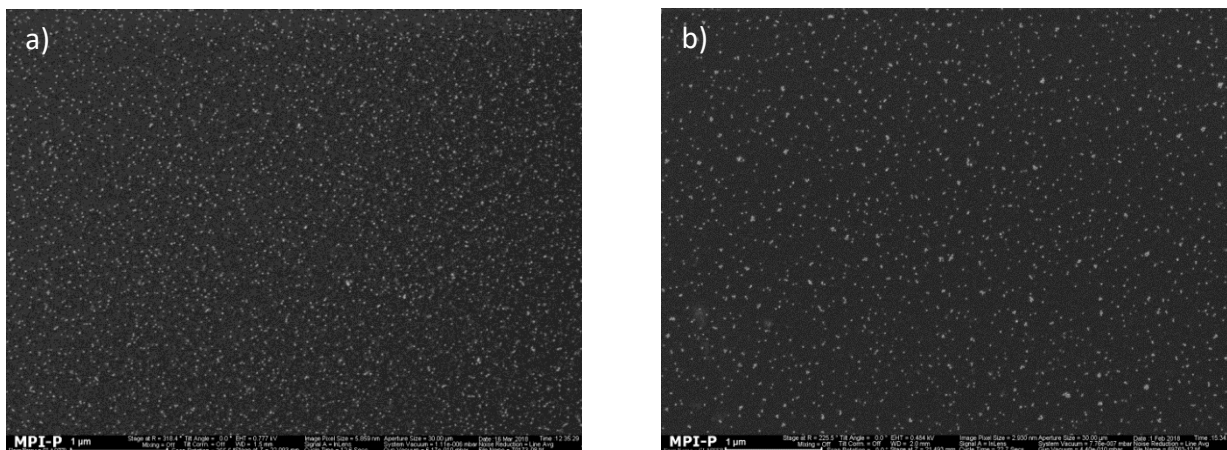


Figure 4.14 SEM image of PLED active layer with PFO:5% oa-QDs. b) SEM image of PLED active layer with PFO:5% QD/PS-hybrids.

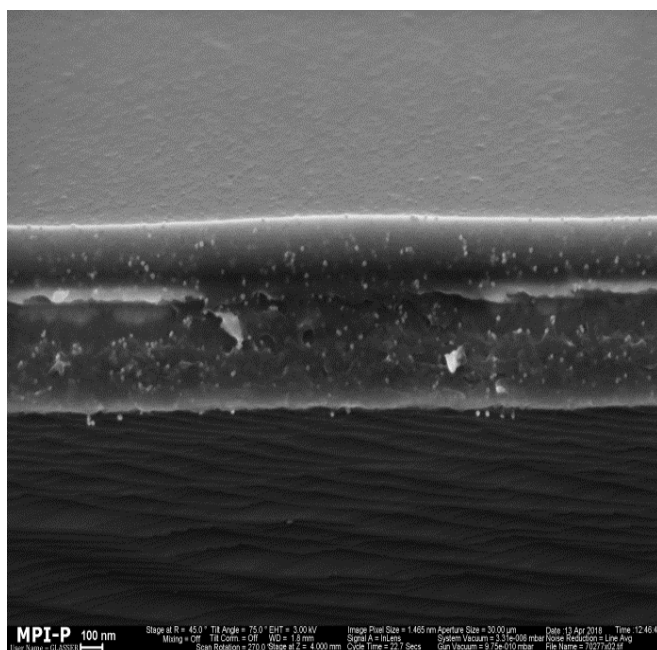


Figure 4. 15 Cross-sectional SEM image of PLED active layer with PFO:5% QD/PS-hybrids.

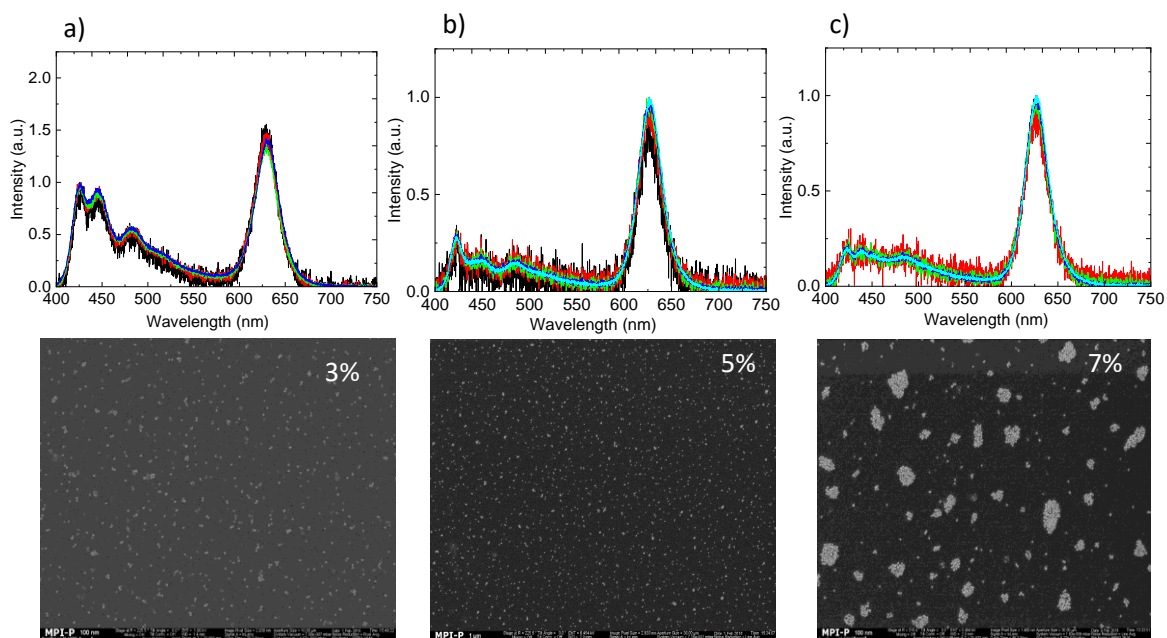


Figure 4. 16 Voltage dependence of normalized EL spectra and SEM images for PLED with 100 nm. a) PFO:3% QD/PS-hybrid b) PFO:5% QD/PS-hybrid c) PFO:7% QD/PS-hybrid blend active layer.

To verify the reduced electron trapping in the QD/PS-hybrid blends further we have carried out charge transport measurements on pristine PFO and PFO blended with oa-QDs and QD/PS-hybrids, respectively. In **Figure 4. 17a** the electron current is shown using Al/blend/Ba/Al electron-only devices. It is observed that the incorporation of 5% of QD/PS-hybrids leads to a reduction of the electron current of only one order of magnitude. In contrast, the incorporation of 5% of unmodified oa-QDs reduces the electron current nearly by 3 orders of magnitude and clearly shows strong trapping behaviour. The trap-limited electron current of pristine PFO can be described using a Gaussian trap distribution²⁶ and a universal trap density of $2 \times 10^{17} \text{ cm}^{-3}$. Estimating the effect of electron trapping by the QDs is difficult since it is not known how many electrons are trapped by a single QD. However, we can make a relative estimation by calculating the amount of traps that would be required to explain the observed J - V characteristics under the assumption that each trap captures one electron. From numerical device modelling we then obtain

that a reduction by one order of magnitude of the electron current of pristine PFO corresponds to $4 \times 10^{16} \text{ cm}^{-3}$ additional single level traps with trap depth of 0.8 eV (**Figure 4.2c**). For the oa-QDs $2 \times 10^{17} \text{ cm}^{-3}$ additional traps are required to describe the electron current. From this relative comparison we obtain that the PS shell suppresses the trapping efficiency by approximately a factor of 5.

We furthermore verified that the incorporation of the QD/PS-hybrids does not significantly affect the hole transport (**Figure 4.17b**).

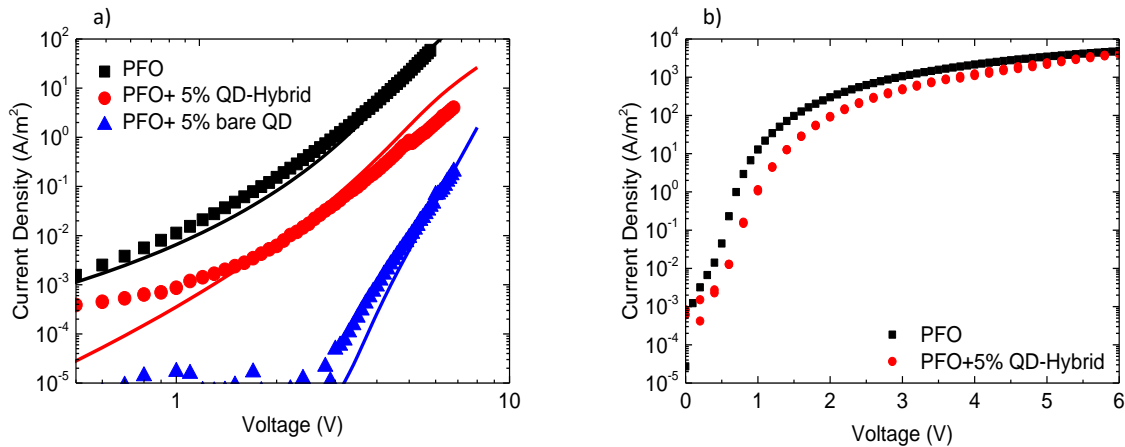


Figure 4. 17 a) Experimental electron-only currents (symbols) and modelled currents using additional single-level traps (lines) as function of voltage for pristine PFO and blends of PFO with 5% oa-QD and QD/PS-hybrid with 110 nm active layer, b) Hole current density of devices with 110 nm active layer for unblended PFO and blend of PFO with 5% QD/PS-hybrid.

As mentioned above, the voltage dependence of the EL spectra for PFO:oa-QD blend PLEDs is characteristic for trap-assisted recombination. Due to the severe trapping the trap-assisted recombination mainly takes place close to the cathode where most of the traps are filled, such that Equation 3 applies, giving rise to a linear dependence on carrier density. However, due to the strongly reduced electron trapping in the PFO:QD/PS-hybrid blends the traps are only partially

filled, such that Eq. 2 applies. Since QDs have a well-defined conduction band level, the QDs can be considered as single level traps. For a single level trap n_t is proportional to n , such that Eq. 1 and 2 exhibit an identical voltage dependence. This is the reason why during the up-scan the EL spectrum is voltage independent. However, next to the reduced trapping the PS shell also inhibits escape from electrons that are trapped in a QD. As a result, during the back scan the electrons that were being trapped at 8V remain in the QDs, such that the trap-assisted recombination can be approximated by $R_{SRH} = B_{SRH} \times n_t(@8V) \times p$, leading again to a linear dependence on carrier density. This not only leads to a voltage dependence in the EL spectrum, but also to a stronger contribution of the QD emission at lower voltages as compared to the up-scan, due to the larger amount of trapped electrons. This process repeats in subsequent scans. Since in the subsequent up-scans the amount of trapped electrons is further increased the red emission of the QDs gets more pronounced after each scan.

We note that due to the ‘permanently’ trapped electrons the system is out of thermal equilibrium. The increased amount of trapped electrons also enhances the injection of holes into the QDs due to the build-up of an electric field in the QDs. This charging effect typically leads to an enhanced contribution of QD emission. After about five scans a steady-state is reached, where the effect of trap-assisted recombination and charging on the EL spectra cancel each other, leading to nearly voltage independent EL spectra for both up and down scan.

Finally, PLEDs with 5% QD/PS-hybrids were fabricated and after initial charging (five J - V scans) compared with pristine PFO PLEDs. As can be seen in **Figure 4.18a** the current and light-output measured by the photocurrent density of a Si photodiode remain almost unchanged. We note that the measured photocurrent density is corrected for the difference in sensitivity for blue (PFO) and red (QD) emission of the Si-photodiode. As a result (**Figure 4.18b**) we were able to

obtain enhanced voltage independent red QD emission without losing efficiency, as is typical for standard polymer:QD blends due to imbalanced transport as result of severe electron trapping.

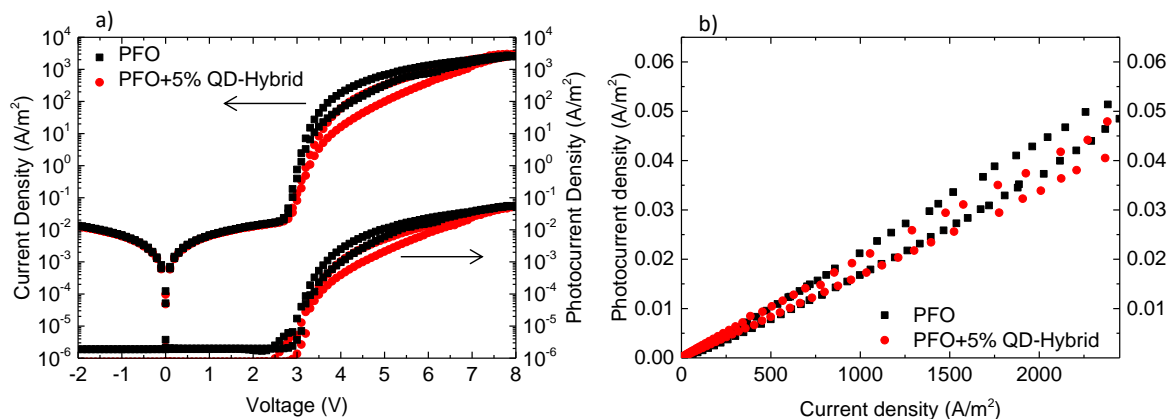


Figure 4.18 a) Current density and photocurrent density vs voltage after initial charging, b) Photocurrent efficiency vs current density of PLED.

We verified that the concept of electron trapping suppression also applies to other blue-emitting polymers as polyspirobifluorene (PSF), copolymerized with N,N,N',N'- tetraaryldiamino biphenyl (TAD), as shown in **Figure 4.19**. However, we note that in this PSF-TAD polymer the hole transporting TAD units lift the HOMO level up to 5.2 eV, thereby increasing the energy barrier for hole transfer to the QD. As a result, the contribution of the red QD decreases when blended with PSF-TAD as compared to PFO, which has a deeper HOMO of 5.8 eV (**Figure 4.2c**).

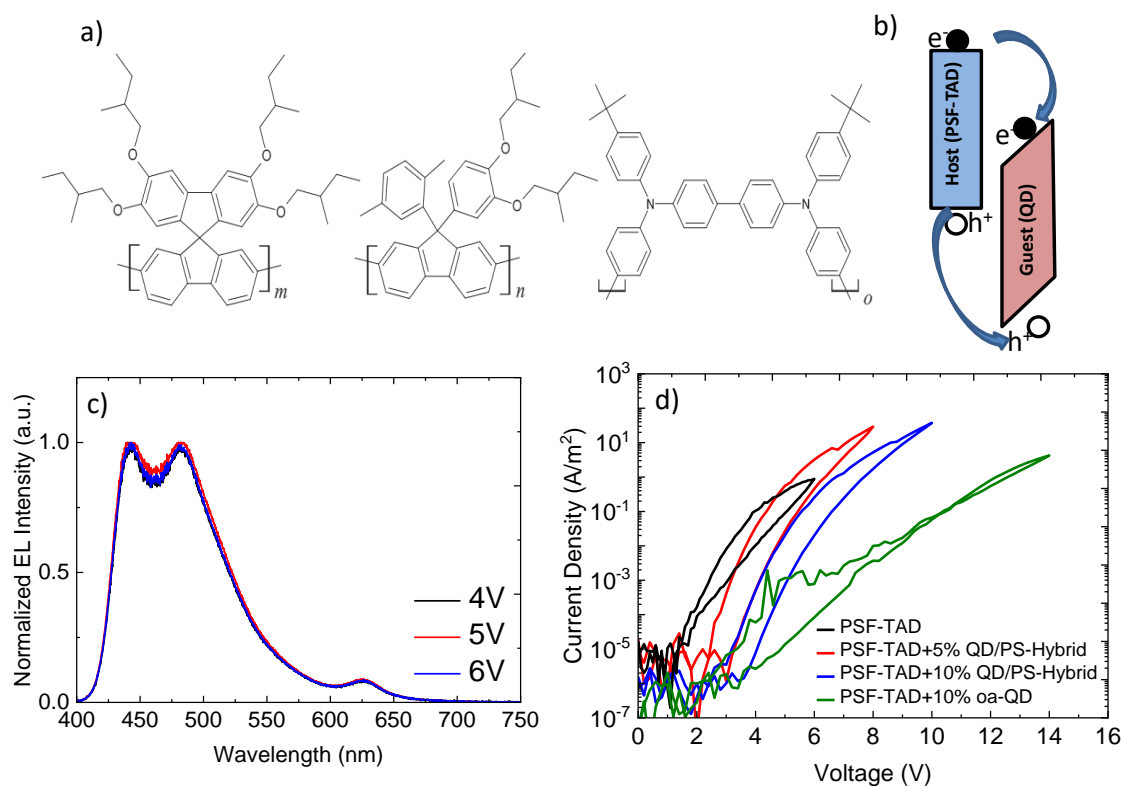


Figure 4.19 a) Chemical structure of the PSF-TAD polymer. The composition copolymers are $m = 50\%$ and $n = 37.5\%$ (PSF) and $o = 12.5\%$ (TAD) b) schematic energy diagram of blend of PSF-TAD with QD with high injection barrier for holes from host to guest. c) Electroluminescence spectra of PSF-TAD with 5% QD/PS-Hybrid d) electron current density of devices with 110nm active layer for unblended PSF-TAD and blend of PSF-TAD with 5% and 10% QD/PS-hybrid and 10% of oa-QD.

Furthermore, initial lifetime experiments show that the decrease of light-output under current stress is reduced for the QD/PS-hybrid blends as compared to pristine PFO PLEDs (**Figure 4. 20**), which is a subject of further study.

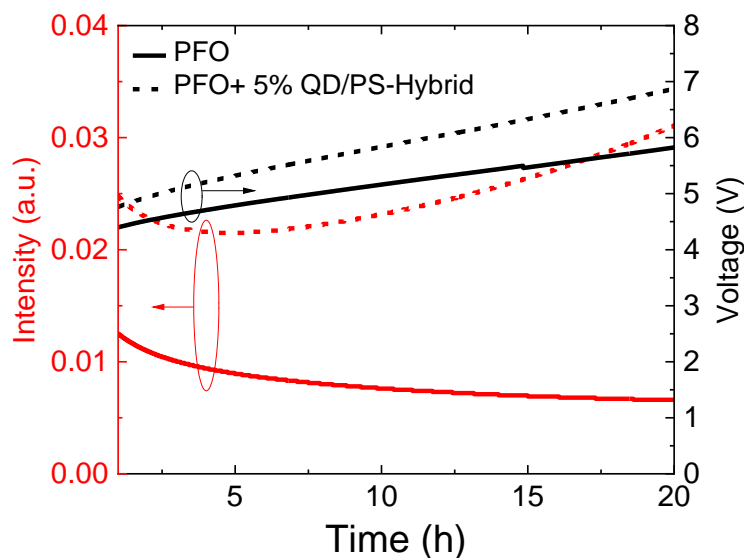


Figure 4.20 Lifetimes of devices with 110nm active layer for unblended PFO and blend of PFO with 5% QD/PS-hybrid under constant-current over time.

4.4 Conclusion

In conclusion, we have demonstrated how to incorporate highly fluorescent quantum dots into a conjugated polymer matrix without inducing severe electron trapping. Trapping of electrons is prevented by shielding the quantum dot by an insulating shell with optimized thickness. The reduced trapping is demonstrated by the realization of a red-emitting hybrid polymer:QD light-emitting diode exhibiting a voltage independent electroluminescence spectrum and no efficiency loss compared to a device based on the unblended host polymer.

References

1. Tang, C. W.; VanSlyke, S. A., Organic electroluminescent diodes. *Applied Physics Letters* **1987**, *51* (12), 913-915.
2. Reineke, S.; Lindner, F.; Schwartz, G.; Seidler, N.; Walzer, K.; Lüssem, B.; Leo, K., White organic light-emitting diodes with fluorescent tube efficiency. *Nature* **2009**, *459* (7244), 234.
3. Forrest, S. R., The path to ubiquitous and low-cost organic electronic appliances on plastic. *Nature* **2004**, *428* (6986), 911.
4. Virgili, T.; Lidzey, D. G.; Bradley, D. D., Efficient energy transfer from blue to red in tetraphenylporphyrin-doped poly (9, 9-dioctylfluorene) light-emitting diodes. *Advanced Materials* **2000**, *12* (1), 58-62.
5. Chang, S.-C.; Bharathan, J.; Yang, Y.; Helgeson, R.; Wudl, F.; Ramey, M. B.; Reynolds, J. R., Dual-color polymer light-emitting pixels processed by hybrid inkjet printing. *Applied Physics Letters* **1998**, *73* (18), 2561-2563.
6. Berggren, M.; Inganäs, O.; Gustafsson, G.; Rasmusson, J.; Andersson, M. R.; Hjertberg, T.; Wennerström, O., Light-emitting diodes with variable colours from polymer blends. *Nature* **1994**, *372* (6505), 444.
7. Kido, J.; Shionoya, H.; Nagai, K., Single-layer white light-emitting organic electroluminescent devices based on dye-dispersed poly (N-vinylcarbazole). *Applied Physics Letters* **1995**, *67* (16), 2281-2283.
8. Ego, C.; Marsitzky, D.; Becker, S.; Zhang, J.; Grimsdale, A. C.; Müllen, K.; MacKenzie, J. D.; Silva, C.; Friend, R. H., Attaching perylene dyes to polyfluorene: three simple, efficient methods for facile color tuning of light-emitting polymers. *Journal of the American Chemical Society* **2003**, *125* (2), 437-443.
9. Nicolai, H. T.; Hof, A.; Blom, P. W. M., Device Physics of White Polymer Light-Emitting Diodes. *Advanced Functional Materials* **2012**, *22* (10), 2040-2047.

10. Dai, X.; Zhang, Z.; Jin, Y.; Niu, Y.; Cao, H.; Liang, X.; Chen, L.; Wang, J.; Peng, X., Solution-processed, high-performance light-emitting diodes based on quantum dots. *Nature* **2014**, *515* (7525), 96.
11. Yang, Y.; Zheng, Y.; Cao, W.; Titov, A.; Hyvonen, J.; Manders, J. R.; Xue, J.; Holloway, P. H.; Qian, L., High-efficiency light-emitting devices based on quantum dots with tailored nanostructures. *Nature Photonics* **2015**, *9* (4), 259.
12. Mashford, B. S.; Stevenson, M.; Popovic, Z.; Hamilton, C.; Zhou, Z.; Breen, C.; Steckel, J.; Bulovic, V.; Bawendi, M.; Coe-Sullivan, S., High-efficiency quantum-dot light-emitting devices with enhanced charge injection. *Nature Photonics* **2013**, *7* (5), 407.
13. Shirasaki, Y.; Supran, G. J.; Tisdale, W. A.; Bulović, V., Origin of efficiency roll-off in colloidal quantum-dot light-emitting diodes. *Physical Review Letters* **2013**, *110* (21), 217403.
14. Shirasaki, Y.; Supran, G. J.; Bawendi, M. G.; Bulović, V., Emergence of colloidal quantum-dot light-emitting technologies. *Nature Photonics* **2013**, *7* (1), 13.
15. Lee, K.-H.; Lee, J.-H.; Kang, H.-D.; Park, B.; Kwon, Y.; Ko, H.; Lee, C.; Lee, J.; Yang, H., Over 40 cd/A efficient green quantum dot electroluminescent device comprising uniquely large-sized quantum dots. *ACS nano* **2014**, *8* (5), 4893-4901.
16. Sun, Q.; Wang, Y. A.; Li, L. S.; Wang, D.; Zhu, T.; Xu, J.; Yang, C.; Li, Y., Bright, multicoloured light-emitting diodes based on quantum dots. *Nature Photonics* **2007**, *1* (12), 717.
17. Chin, P. T.; Hikmet, R. A.; Janssen, R. A., Energy transfer in hybrid quantum dot light-emitting diodes. *Journal of Applied Physics* **2008**, *104* (1), 013108.
18. Tu, M.-L.; Su, Y.-K.; Chen, R.-T., Hybrid light-emitting diodes from anthracene-contained polymer and CdSe/ZnS core/shell quantum dots. *Nanoscale Research Letters* **2014**, *9* (1), 611.
19. Liu, Y.; Li, F.; Xu, Z.; Zheng, C.; Guo, T.; Xie, X.; Qian, L.; Fu, D.; Yan, X., Efficient all-solution processed quantum dot light emitting diodes based on inkjet printing technique. *ACS applied materials & interfaces* **2017**, *9* (30), 25506-25512.
20. Bozyigit, D.; Wood, V., Challenges and solutions for high-efficiency quantum dot-based LEDs. *MRS bulletin* **2013**, *38* (9), 731-736.

21. Park, Y. R.; Jeong, H. Y.; Seo, Y. S.; Choi, W. K.; Hong, Y. J., Quantum-dot light-emitting diodes with nitrogen-doped carbon nanodot hole transport and electronic energy transfer layer. *Scientific Reports* **2017**, *7*, 46422.
22. Park, Y. R.; Doh, J. H.; Shin, K.; Seo, Y. S.; Kim, Y. S.; Kim, S. Y.; Choi, W. K.; Hong, Y. J., Solution-processed quantum dot light-emitting diodes with PANI: PSS hole-transport interlayers. *Organic Electronics* **2015**, *19*, 131-139.
23. Bae, W. K.; Lim, J.; Zorn, M.; Kwak, J.; Park, Y.-S.; Lee, D.; Lee, S.; Char, K.; Zentel, R.; Lee, C., Reduced efficiency roll-off in light-emitting diodes enabled by quantum dot–conducting polymer nanohybrids. *Journal of Materials Chemistry C* **2014**, *2* (25), 4974-4979.
24. Kwak, J.; Bae, W. K.; Zorn, M.; Woo, H.; Yoon, H.; Lim, J.; Kang, S. W.; Weber, S.; Butt, H. J.; Zentel, R., Characterization of quantum dot/conducting polymer hybrid films and their application to light-emitting diodes. *Advanced Materials* **2009**, *21* (48), 5022-5026.
25. Fokina, A.; Lee, Y.; Chang, J. H.; Park, M.; Sung, Y.; Bae, W. K.; Char, K.; Lee, C.; Zentel, R., The Role of Emission Layer Morphology on the Enhanced Performance of Light-Emitting Diodes Based on Quantum Dot-Semiconducting Polymer Hybrids. *Advanced Materials Interfaces* **2016**, *3* (18), 1600279.
26. Kuik, M.; Wetzelaer, G. J. A.; Nicolai, H. T.; Craciun, N. I.; De Leeuw, D. M.; Blom, P. W. M., 25th Anniversary Article: Charge Transport and Recombination in Polymer Light-Emitting Diodes. *Advanced Materials* **2014**, *26* (4), 512-531.
27. Anni, M.; Manna, L.; Cingolani, R.; Valerini, D.; Creti, A.; Lomascolo, M., Förster energy transfer from blue-emitting polymers to colloidal CdSe/ ZnS core shell quantum dots. *Applied Physics Letters* **2004**, *85* (18), 4169-4171.
28. zur Borg, L.; Lee, D.; Lim, J.; Bae, W. K.; Park, M.; Lee, S.; Lee, C.; Char, K.; Zentel, R., The effect of band gap alignment on the hole transport from semiconducting block copolymers to quantum dots. *Journal of Materials Chemistry C* **2013**, *1* (9), 1722-1726.
29. Choi, J.; Schattling, P.; Jochum, F. D.; Pyun, J.; Char, K.; Theato, P., Functionalization and patterning of reactive polymer brushes based on surface reversible addition and fragmentation

chain transfer polymerization. *Journal of Polymer Science Part A: Polymer Chemistry* **2012**, 50 (19), 4010-4018.

30. Lim, J.; Jeong, B. G.; Park, M.; Kim, J. K.; Pietryga, J. M.; Park, Y. S.; Klimov, V. I.; Lee, C.; Lee, D. C.; Bae, W. K., Influence of Shell Thickness on the Performance of Light-Emitting Devices Based on CdSe/Zn1-XCdXS Core/Shell Heterostructured Quantum Dots. *Advanced Materials* **2014**, 26 (47), 8034-8040.

31. Li, W.-J.; Liu, B.; Qian, Y.; Xie, L.-H.; Wang, J.; Li, S.-B.; Huang, W., Synthesis and characterization of diazafluorene-based oligofluorenes and polyfluorene. *Polymer Chemistry* **2013**, 4 (6), 1796-1802.

32. Mathias, F.; Fokina, A.; Landfester, K.; Tremel, W.; Schmid, F.; Char, K.; Zentel, R., Morphology control in biphasic hybrid systems of semiconducting materials. *Macromolecular Rapid Communications* **2015**, 36 (11), 959-983.

33. Klöckner, B.; Daniel, P.; Brehmer, M.; Tremel, W.; Zentel, R., Liquid crystalline phases from polymer functionalized ferri-magnetic Fe₃O₄ nanorods. *Journal of Materials Chemistry C* **2017**, 5 (27), 6688-6696.

34. Fokina, A.; Lee, Y.; Chang, J. H.; Braun, L.; Bae, W. K.; Char, K.; Lee, C.; Zentel, R., Side-chain conjugated polymers for use in the active layers of hybrid semiconducting polymer/quantum dot light emitting diodes. *Polymer Chemistry* **2016**, 7 (1), 101-112.

35. Klöckner, B.; Niederer, K.; Fokina, A.; Frey, H.; Zentel, R., Conducting polymer with orthogonal catechol and disulfide anchor groups for the assembly of inorganic nanostructures. *Macromolecules* **2017**, 50 (10), 3779-3788.

36. Rubinstein, M.; Colby, R., Oxford University Press; New York: **2003**. *Polymer Physics*.

Chapter 5

Trap-Assisted Triplet Emission in Ladder Polymer-based Light Emitting Diodes

The charge transport and recombination in light-emitting diodes (LEDs) based on a methyl-substituted poly(p-phenylene) ladder polymer (Me-LPPP) are investigated. The transport is characterized by a high room temperature hole mobility of $2 \times 10^{-8} \text{ m}^2/\text{Vs}$, combined with anomalously strong electron trapping. The electroluminescence (EL) spectrum is characterized by blue singlet emission, a broad green featureless peak and yellow-orange triplet emission. The voltage dependence of the EL spectrum and negative contribution to the capacitance indicate that the triplet-emission is of trap-assisted nature, consistent with the strong electron trapping. Consequently, the color purity of the blue emissive Me-LPPP polymer LEDs can be strongly improved using trap dilution.

The results of this chapter are ready to submit in 2019 by E. Khodabakhshi et al. E. Khodabakhshi has performed the device fabrication, measurement, analysis and modeling. Me-LPPP used in this chapter was provided by group of Dr. Ullrich Scherf at Wuppertal university.

5.1 Introduction

Conjugated polymers are of considerable interest as potential active materials in organic electronic applications such as polymeric light-emitting diodes (PLEDs), plastic lasers, photovoltaic devices (solar cells), and field-effect transistors.¹⁻⁵ One of the main goals of materials development for OLEDs is obtaining stable pure blue emission, which is required for full-color displays, combined with good charge transporting properties.⁶⁻¹⁰ However, charge transport in organic semiconductors is typically reduced by energetic disorder and trapping sites due to defects.¹¹ Ladder-type poly(para-phenylene) polymers (LPPP) are an interesting class of conjugated polymers due to their purity and low degree of structural and energetic disorder.¹² The reduced disorder is reflected in the sharp spectral features of the absorption and fluorescence spectra as well as a low amount of aggregate formation that could lead to trapping.¹³ Time-of-flight measurements revealed that the hole transport in ladder-type methyl-substituted poly(p-phenylene) (Me-LPPP) is non-dispersive, combined with a hole mobility in the 10^{-7} - 10^{-6} m²/Vs range, which is much larger as compared to other poly(p-phenylene vinylene) (PPV) derivatives.¹⁴ The very small dependence of the mobility on temperature furthermore reflects the small inhomogeneous width of the density of states (DOS) as a result of reduced disorder.

Next to blue singlet emission this class of materials also exhibits some additional spectral features at higher wavelengths. At low temperatures triplet emission has been observed using gated detection.¹⁵ The observed phosphorescence spectrum was shifted with respect to the fluorescence spectrum by ~0.6 eV and exhibited similar vibronic replica. Furthermore, a featureless broad excimer-like band was observed at an intermediate energy with respect to the fluorescent and phosphorescent spectra. In a later study, electrically induced phosphorescence even at room temperature was found in a diaryl (diphenyl)-substituted LPPP derivative.¹⁶ It was proposed that

the room temperature phosphorescence was the result of triplet diffusion towards sites where residual traces of palladium are covalently bound to the polymer. Probing the sensitivity of the spectra to oxygen confirmed that the phosphorescent features were quenched by oxygen, whereas the broad featureless peak got stronger.¹⁶ The latter indicates that this broad peak is the result of oxidative defects similar to fluorenone in polyfluorenes (PFO), as also reported in later studies on LPPP polymers.¹⁷⁻¹⁹

In spite of extensive optical characterization the device operation of LPPP-based polymer light-emitting diodes has not been addressed so far. In this study, we address the electron- and hole transport of Me-LPPP as well the voltage dependence of the electroluminescence spectra of Me-LPPP based PLEDs. We observe that the electron current is severely limited by trapping, which leads to highly unbalanced charge transport. Similar to Lupton et al.¹⁶ we also observe room temperature electro-phosphorescence for Me-LPPP. The electroluminescence spectra are strongly dependent on the bias voltage, with the relative contribution of the phosphorescent triplet emission being weakened at higher bias. Such behavior is characteristic for trap-assisted recombination. The presence of trap-assisted triplet emission is further manifested by a negative contribution to the PLED capacitance. The trap-assisted character of the triplet-emission allows us to completely suppress the phosphorescence using trap dilution by blending Me-LPPP with low molecular weight polystyrene (PS), resulting in pure blue emission. Me-LPPP used in this chapter was synthesized via the Suzuki method according to literature ($\bar{M}_w = 51$ kDa, PDI = 1.96) by group of Dr. Ullrich Scherf at Wuppertal university.

5.2 Results and discussion

Single carrier devices. Understanding the operation of PLEDs requires a thorough characterization of charge transport, charge injection, and recombination mechanisms. Single-

carrier devices are excellently suited for exploring the hole and electron transport independently. Hence, as first step we study the electron and hole current in Me-LPPP-based single carrier devices, of which the device architecture is given in the Experimental section.

In **Figure 5. 1**, the measured hole and electron current densities of Me-LPPP are plotted (symbols) as a function of voltage ($\log J$ - $\log V$). The observed slope of two in the $\log J$ - $\log V$ plot for $V \geq 1$ V shows that, as has been observed for many semiconducting polymers,²⁰ the hole current is space-charge limited (quadratic dependence of current on voltage) and trap-free. Applying Childs law $J = \frac{9}{8} \varepsilon \mu \frac{V^2}{L^3}$, with ε the permittivity and μ the mobility, leads to an estimated room temperature hole mobility for Me-LPPP of $3 \times 10^{-8} \text{ m}^2/\text{Vs}$ (**Figure 5. 1**, solid black line). In order to gain more quantitative information on the hole transport in Me-LPPP, the hole-only devices were also measured at different temperature (**Figure 5. 2a**), symbols). To model the trap-free hole current the extended Gaussian disorder model (EGDM) was used, that contains as relevant parameters μ_0 , a mobility prefactor containing the electronic overlap between transport sites, the energetic disorder σ and a , the average distance between two transport sites.^{21,22} These parameters then define the dependence of the mobility on temperature, charge carrier density and electric field. From the modeling (**Figure 5. 2a**), solid lines) we found $\mu_0 = 120 \text{ m}^2/\text{Vs}$, $\sigma = 0.06 \text{ eV}$ and $a = 2.5 \times 10^{-9} \text{ m}$. At room temperature and zero electric field these parameters result in a hole mobility of $2 \times 10^{-8} \text{ m}^2/\text{Vs}$, which is one order of magnitude lower as compared to earlier time-of-flight data.¹⁴ The weak temperature dependence, as also reported in literature,¹⁴ originates from a low value for the energetic disorder of $\sigma = 0.06 \text{ eV}$, which is significantly lower than values found for other PPV derivatives, typically ranging from $\sigma = 0.12$ to 0.15 eV .

In contrast, the electron transport in Me-LPPP is strongly suppressed and exhibits a steeper voltage dependence, which is characteristic for trap-limited currents. **Figure 1** reveals that for the Me-LPPP device the hole- and electron current differ by nearly 5 orders of magnitude. Such a large difference is ten to hundred times larger than observed for other poly[p-phenylene-vinylene] (PPV) derivatives,^{23,24} or PFO-based¹⁰ semiconductors. In an earlier study it has been reported that the electron current in conjugated polymers is mediated by universal electron traps, with a typical density of $\sim 5 \times 10^{23} \text{ m}^{-3}$.²⁰ The extraordinary low electron current observed in Me-LPPP could point to the fact that next to these universal traps additional trap centers are present in the band gap of MeLPPP.

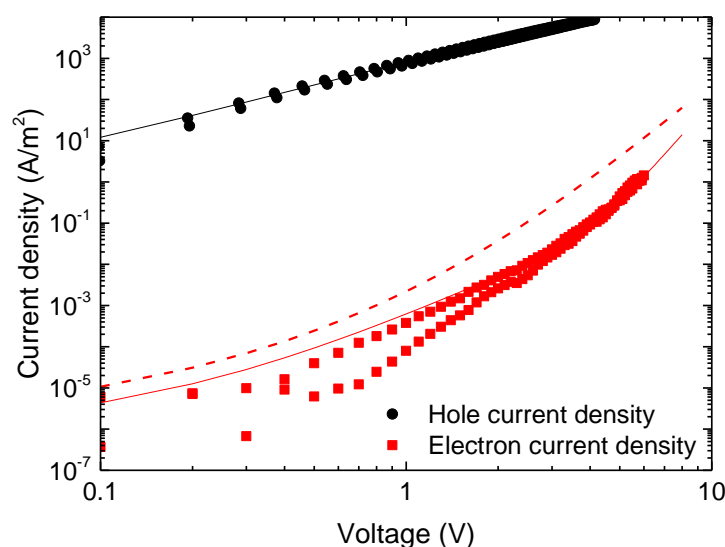


Figure 5. 1 Hole and electron current density versus voltage for Me-LPPP hole- and electron-only devices. Symbols are experimental results, the solid lines are fits using EGDM (free electrons and holes) and electron traps consisting of universal electron traps (dashed line) and an additional single-level trap (solid line).

In order to model the electron current assuming similar free electron mobility as measured for the holes, two trap distributions had to be considered to provide for a proper description of the measured data. As first step, the electron current is modeled using the “universal trap level”²⁰ with a depth of $E_{tc} = 0.6$ eV and a density of $5 \times 10^{23} \text{ m}^{-3}$. As shown in **Figure 5. 1** (dashed line) the calculated electron current is almost an order of magnitude larger than the experimental one. Using an additional trap level with a trap depth of $E_{tc} = 0.53$ eV and a density of $6 \times 10^{22} \text{ m}^{-3}$ provides a consistent description of the electron current and its temperature dependence (**Figure 5. 2b**).

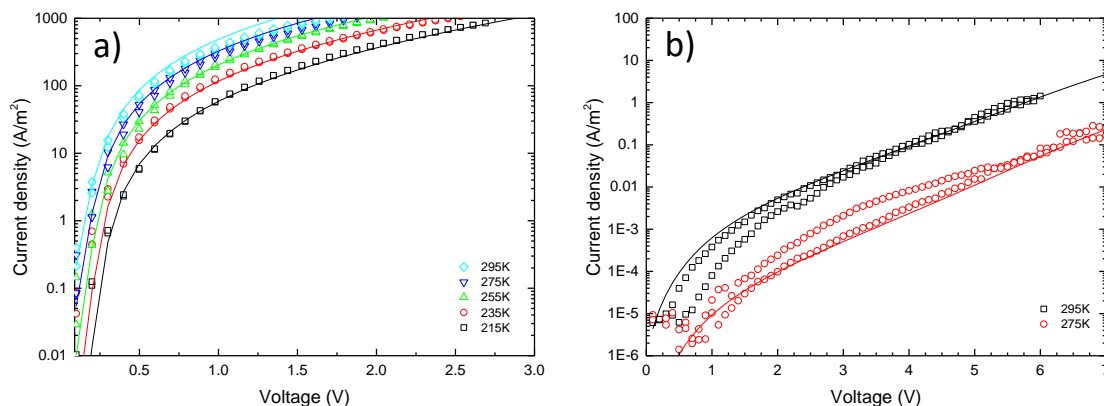


Figure 5. 2 J - V characteristic of a) hole-only devices based on a 115 nm film of Me-LPPP for temperatures ranging from 295 K to 215 K. b) electron-only devices based on a 115 nm film of Me-LPPP for temperatures ranging from 295 K to 275 K. (symbols: experimental results, solid lines: modeling results)

Steady state electro- and photoluminescence. As next step, dual carrier devices were fabricated to investigate the recombination properties of the Me-LPPP-based PLEDs. **Figure 5. 3a** shows the current and photocurrent density of the PLED and **Figure 5. 3b** shows the electroluminescence and photoluminescence spectra of Me-LPPP devices, normalized to the 0-1 peak. Both spectra exhibit the typical spectral PL characteristic of LPPPs: The S0-S1 (0-0) transition band of the PL spectrum peaks at 460 nm and is followed by a vibronic fine structure.²⁵ However, in the EL spectrum, the intensity of the 0-0 peak is much lower than the one in PL, which might originate

from self-absorption. Besides the vibronic peaks of the singlet to ground state transition, the EL spectrum reveals two additional features observed at higher wavelength: i) a broad green emission band more or less centered around 560nm and ii) a vibronically structured feature with a peak maximum at 590 nm. Strikingly, both features are absent in PL. As discussed in the introduction, the broad green emission at 560 nm may be due to the presence of a small amount of ketone defects, similar to polyfluorenes,¹⁰ or an excimer.^{15, 26}

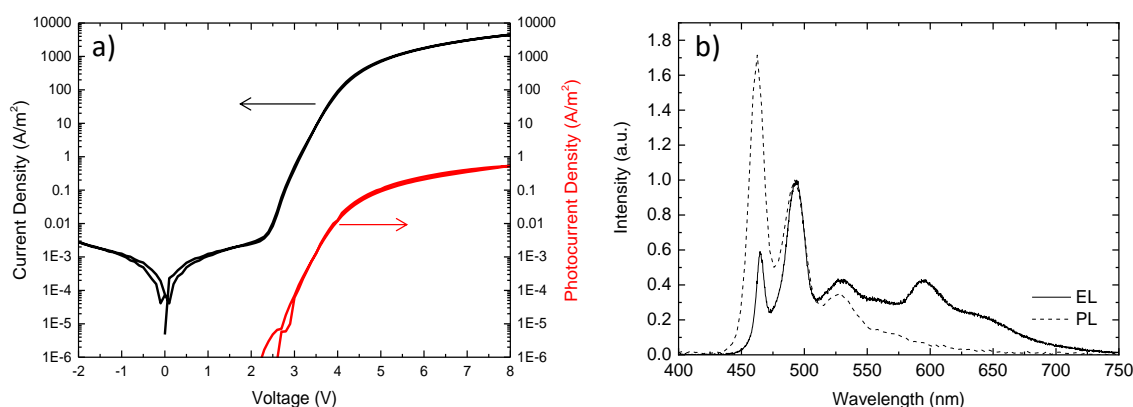


Figure 5. 3 a) Current and photocurrent density of PLED based on a 120nm active layer of Me-LPPP, b) Electroluminescence spectrum (solid line) and Photoluminescence spectrum (dash line) of the same device.

The second additional feature at 590 nm bears strong resemblance with the structured long wavelength emission observed in the EL spectrum measured for PhLPPP, which was ascribed to electrophosphorescence due to triplet diffusion towards covalently attached palladium centers, remaining in the material after the Suzuki polycondensation.¹⁶ The lower emission intensity observed for the long wavelength feature for MeLPPP compared to PhLPPP is consistent with the lower Pd content in our sample of ~2 ppm, compared to 80 ppm for PhLPPP.¹⁶ A question that arises is whether these Pd centers that give rise to triplet emission are also responsible for the anomalously low electron current in Me-LPPP. In that case the triplet emission is expected to be of trap-assisted nature.

A typical fingerprint of trap-assisted recombination is that the EL spectrum is voltage dependent. In **Figure 5. 4** the EL spectrum is shown as a function of voltage. When normalized to the blue (singlet) bimolecular recombination we observe that the triplet emission at higher wavelength is relatively weakened. There are two possible explanations for this negative voltage dependence: i) enhanced annihilation of triplets upon increasing the operating voltage as a result of an increase in excitation density,^{16, 27, 28} and ii) emissive recombination of trapped electrons with free holes. In case of the latter, since the number of trapping sites is fixed, the rate of trap-assisted recombination is only dependent on the hole density in the PLED, *i.e.* linearly dependent on the charge carrier density. In contrast, the recombination rate of free electrons and holes leading to the blue singlet emission is bimolecular as it is a function of both the electron and holes density and hence quadratically dependent on the charge carrier density, making the blue bimolecular emission dominant at higher voltages. As a result of this difference in scaling of the trap-assisted and bimolecular (Langevin) recombination rates on the charge carrier density, the light emission resulting for these processes scales with the current density as $\sim J^{1/2}$ and $\sim J$.²⁹

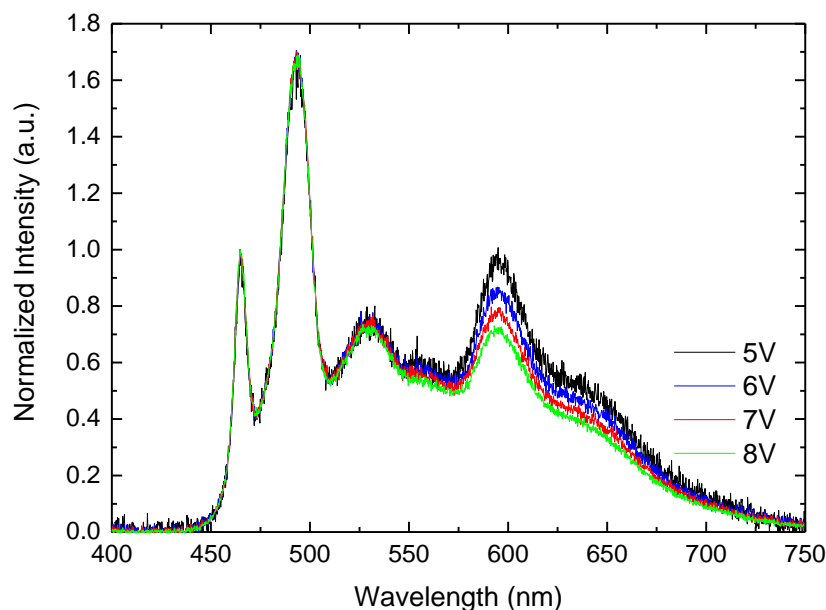


Figure 5. 4 Voltage sweep of normalized electroluminescence spectra for PLED with Me-LPPP as emissive layer.

To evaluate this further, we deconvoluted the EL spectra recorded at different voltages (**Figure 5. 5**). The total emission was reconstructed by using three Gaussian peaks to describe the singlet spectrum: an additional one for the broad green emission band (green line), centered at ~ 2.2 eV, and two more (vibronic) peaks to account for the structured red emitting feature (red and blue lines). We note that the energy splitting between the latter is almost identical to the splitting of the zeroth and first vibronic transition in the singlet spectrum (*i.e.* ~ 0.15 eV), which supports the triplet-nature of the long wavelength feature.¹⁶

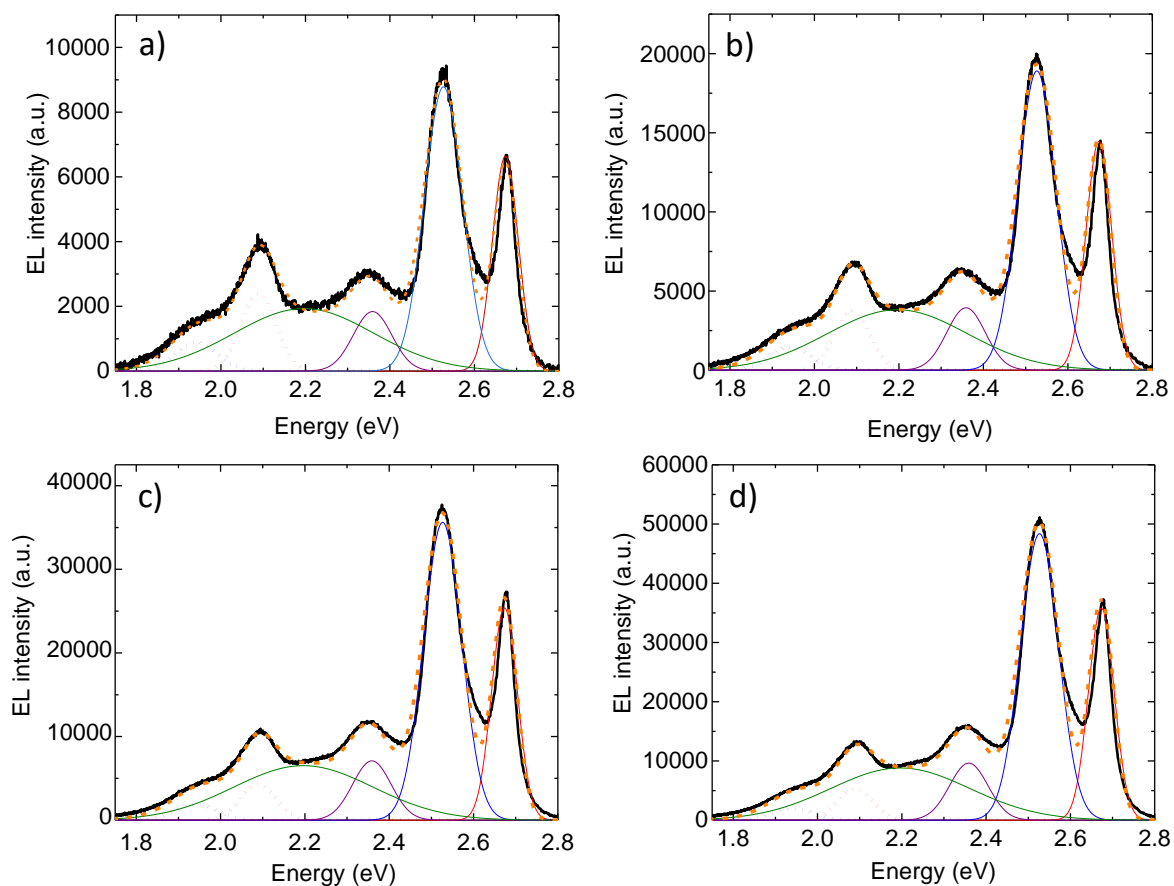


Figure 5. 5 Deconvolution of EL Spectra recorded at different voltage a) 5V b) 6V c) 7V d) 8V

Plotting the peak area as a function of the current density for the red and blue region of the emission spectrum on a double logarithmic scale produces lines with slopes of, respectively, $\frac{1}{2}$ and 1, demonstrating the trap-assisted origin of the long wavelength emission feature (see **Figure 5. 6**).

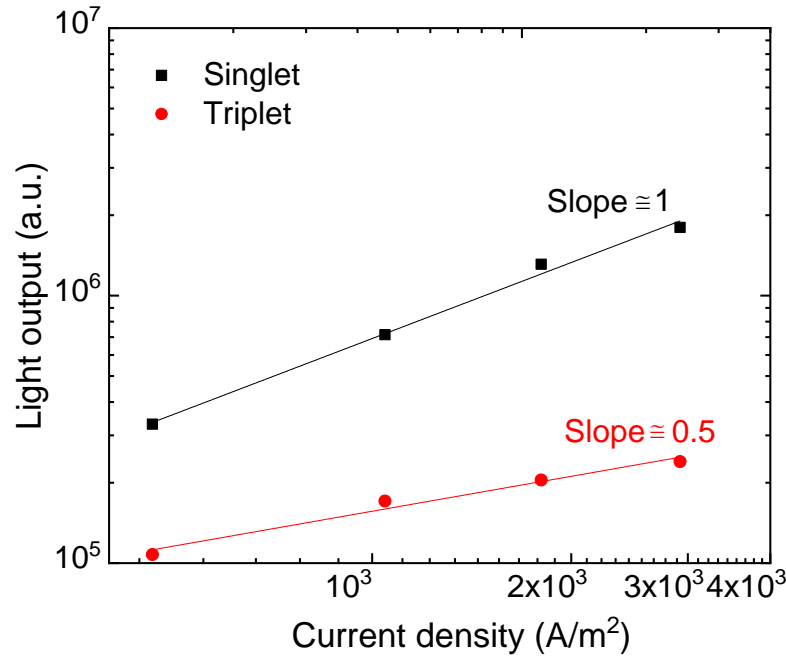


Figure 5. 6 The light output of the singlet and triplet peaks as function of PLED current density.

Impedance Spectroscopy. In order to further investigate the recombination mechanism in Me-LPPP based PLEDs, we performed Impedance spectroscopy (IS) measurements. IS is powerful technique to study charge transport and recombination in semiconductors at different time scale.³⁰ In a recent study, it has been demonstrated that trap-assisted recombination gives rise to a negative contribution in the PLED capacitance.³¹ For a single exponential transient recombination current, $J_r(t) = -J_0 \exp(-t/\tau_r)$ with J_0 the prefactor and τ_r the relaxation time, the capacitance is given by:

$$C(\omega) = C_0 - \frac{\alpha\tau_r}{1+\omega^2\tau_r^2} \quad (3)$$

with C_0 the geometrical capacitance $\epsilon_0\epsilon_r A/d$, ω the angular frequency and α a proportionality factor that scales with the PLED current density. The relaxation time τ_r observed in the IS spectra is a measure for the inverse rate for trap-assisted recombination. When only bimolecular

recombination is present, by suppressing trap-assisted recombination using trap-dilution, the negative capacitance effect disappears.³¹ As it can be observed in **Figure 5. 7** the capacitance of PLEDs based on MeLPPP exhibits a very strong negative contribution compared to, for instance, typical poly[p-phenylene-vinylene] (PPV)-based LEDs. This strong negative contribution is qualitatively consistent with the severe electron trapping observed in Me-LPPP (**Figure 5. 1**). In PPV-based PLEDs it was shown that the relaxation time τ_r is given by $\tau_r = \frac{2}{N_t C_p}$, with C_p representing the hole capture coefficient given by $(q/\epsilon_0 \epsilon_r) \mu_p$, with μ_p the hole mobility and N_t the total amount of electron traps. By applying Eq. (3) to the experimental data with τ_r and α as fitting parameters, the frequency dependence of the capacitance at various voltages (**Figure 5. 8a**) is fitted. We obtain a voltage-independent relaxation time τ_r of 20 ms for the Me-LPPP-based PLED. This time constant is orders of magnitude larger than the typical expected time constant for non-radiative trap-assisted recombination using the hole capture coefficient. The high hole mobility of Me-LPPP results in a large capture coefficient C_p of typically $\sim 1 \times 10^{-16} \text{ m}^3 \text{ s}^{-1}$. Combined with a universal trap density of $\sim 5 \times 10^{23} \text{ m}^{-3}$ this would result in a relaxation time τ_r of only $\sim 30 \text{ ns}$. It should be noted that the use of a hole capture coefficient $C_p = (q/\epsilon_0 \epsilon_r) \mu_p$ implicitly assumes that the slowest step in the trap-assisted recombination is the time that the hole needs to find the trapped electron. If, however, the recombination process itself is much slower than this time this relation is not valid. In that case it is also not possible to derive a trap concentration from the observed relaxation time. The observed relaxation time of 20 ms is therefore characteristic for a very slow trap-assisted recombination process. The fact that this observed relaxation time is in very good agreement with the life time reported for triplet emission in ladder-type polymers³² is a further proof that the recombination observed at longer wavelength originates from trap-assisted triplet recombination.

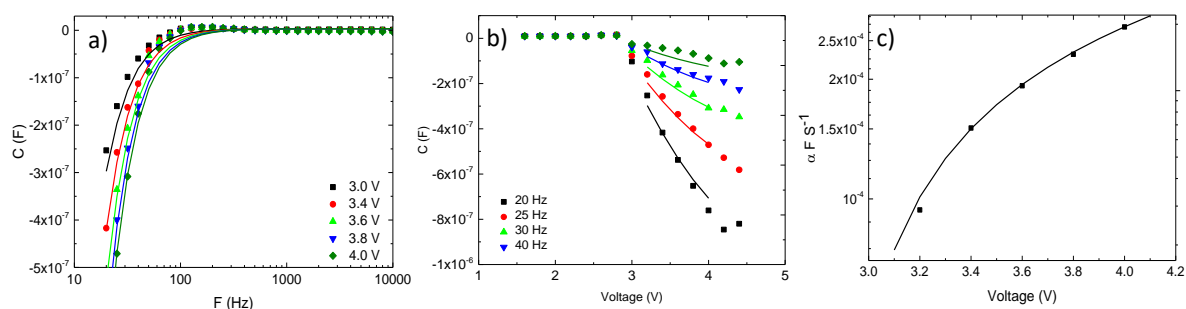


Figure 5. 7 a) Differential capacitance C versus frequency at various bias voltages. The symbols represent the experimental data, while the solid lines are a fit to Eq. (3) using τ_r 20 ms and b) C - V characteristics of a Me-LPPP PLED at different frequencies c) $\alpha(V)$ values obtained from Eq. (3) as a function of voltage.

Trap-dilution. In PFO-based PLEDs the singlet blue emission is accompanied by a broad green emission band, originating from emissive ketone defects. The voltage dependence of the EL spectra demonstrated that the green emission has a trap-assisted origin.¹⁰ A direct consequence of the trap-assisted nature of the green emission is that it is clearly visible in EL spectra, but far less pronounced in photoluminescence. It has recently been shown that trapping effects can be strongly suppressed by blending the semiconductor with a large band gap host.²⁴ This trap dilution nearly eliminates the contribution of emissive green trap-assisted recombination in the EL spectra of PFO.¹⁰ As final step, we therefore proceed with investigating the trap dilution effect using polystyrene (PS) on the EL spectra of Me-LPPP based PLEDs. **Figure 5. 8** shows that upon increasing the PS content in the blend, a strong decline in the yellow-orange triplet emission occurs. For the Me-LPPP: PS blends with a 1:6 ratio the EL spectrum is nearly equal to the PL spectrum of Me-LPPP in which the trap-assisted emission is absent. The suppression of the triplet emission as compared to the singlet emission by trap dilution is also consistent with the trap-assisted nature of the triplet emission in ME-LPPP. The fact that the triplet emission is trap-assisted also explains why in electroluminescence the triplet emission is far more pronounced as compared

to photoluminescence and can even occur at room temperature.¹⁶ As a result, trap dilution can be used to eliminate the negative effect of the triplet emission on the color purity of the EL spectra for blue Me-LPPP PLEDs.

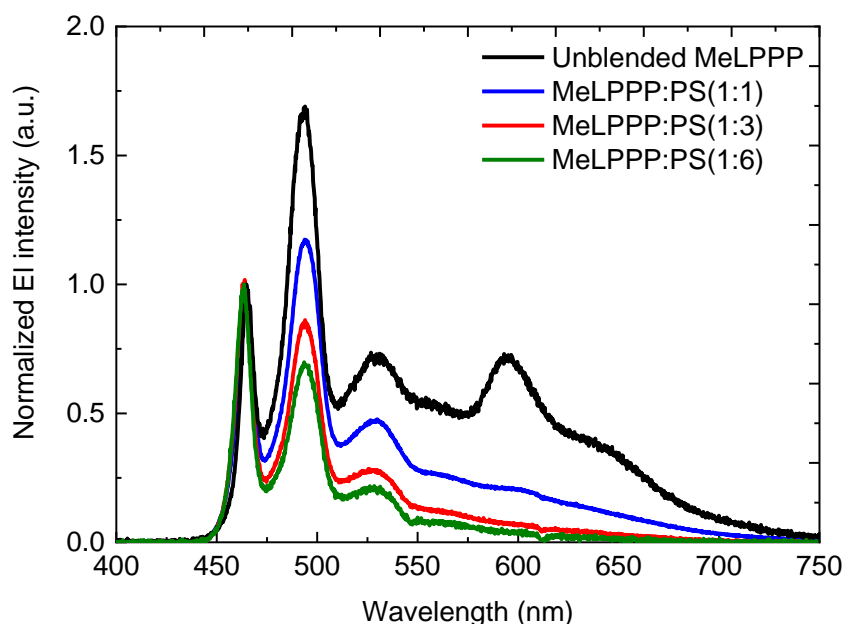


Figure 5. 8 Electroluminescence spectra of PLEDs based on ~120 nm active layers of unblended Me-LPPP and Me-LPPP:PS blends with various blend ratios. All spectra have been recorded at 8V.

5.3 Conclusion

In conclusion, the hole transport in Me-LPPP is characterized by a trap-free space-charge limited with a high mobility of $2 \times 10^{-8} \text{ m}^2/\text{Vs}$ due to reduced energetic disorder. The electron transport is strongly trap-limited, additional traps are required on top of the universal trapping sites in order to explain the large difference between electron and hole currents. The EL spectrum shows next to the blue singlet peaks additional features at longer wavelengths, including yellow-orange triplet emission. The triplet emission shows a weaker dependence on voltage as compared to the

singlet emission and Me-LPPP PLEDs show a strongly pronounced negative capacitance governed by a long time constant of 20 ms. Both features indicate show that the triplet emission is of trap-assisted nature, which is further confirmed by trap-dilution experiments.

References

1. Friend, R.; Gymer, R.; Holmes, A.; Burroughes, J.; Marks, R.; Taliani, C.; Bradley, D.; Dos Santos, D.; Bredas, J.; Lögdlund, M., Electroluminescence in conjugated polymers. *Nature* **1999**, *397* (6715), 121.
2. Bernius, M. T.; Inbasekaran, M.; O'Brien, J.; Wu, W., Progress with light-emitting polymers. *Advanced Materials* **2000**, *12* (23), 1737-1750.
3. Heeger, A. J., Light emission from semiconducting polymers: light-emitting diodes, light-emitting electrochemical cells, lasers and white light for the future. *Solid State Communications* **1998**, *107* (11), 673-679.
4. Kraft, A.; Grimsdale, A. C.; Holmes, A. B., Electroluminescent conjugated polymers—seeing polymers in a new light. *Angew. Chem. Int. End Engl* **1998**, *37*, 402-428.
5. Zhang, X.; Jenekhe, S. A., Electroluminescence of multicomponent conjugated polymers.
1. Roles of polymer/polymer interfaces in emission enhancement and voltage-tunable multicolor emission in semiconducting polymer/polymer heterojunctions. *Macromolecules* **2000**, *33* (6), 2069-2082.
6. Kulkarni, A. P.; Jenekhe, S. A., Blue light-emitting diodes with good spectral stability based on blends of poly (9, 9-dioctylfluorene): interplay between morphology, photophysics, and device performance. *Macromolecules* **2003**, *36* (14), 5285-5296.
7. Kim, D.; Cho, H.; Kim, C., Blue light emitting polymers. *Progress in Polymer Science* **2000**, *25* (8), 1089-1139.

8. Abbaszadeh, D.; Blom, P. W.M., Efficient Blue Polymer Light-Emitting Diodes with Electron-Dominated Transport Due to Trap Dilution. *Advanced Electronic Materials* **2016**, 2 (7).
9. Khodabakhshi, E., Blom, P.W.M. and Michels, J.J., Efficiency enhancement of polyfluorene: Polystyrene blend light-emitting diodes by simultaneous trap dilution and β -phase formation. *Applied Physics Letter* **2019**, 114(9), 093301.
10. Khodabakhshi, E., Michels, J.J. and Blom, P.W.M., 2017. Visualization of trap dilution in polyfluorene based light-emitting diodes. *AIP Advances* **2017**, 7(7), 075209
11. Bässler, H., Charge transport in disordered organic photoconductors a Monte Carlo simulation study. *physica status solidi (b)* **1993**, 175 (1), 15-56.
12. Scherf, U.; Müllen, K., Polyarylenes and poly (arylenevinylens), 7. A soluble ladder polymer via bridging of functionalized poly (p-phenylene)-precursors. *Die Makromolekulare Chemie, Rapid Communications* 1991, 12 (8), 489-497.
13. Lemmer, U.; Heun, S.; Mahrt, R.; Scherf, U.; Hopmeier, M.; Siegner, U.; Go, E.; Mu, K.; Ba, H. aggregate fluorescence in conjugated polymers. *Chemical physics letters* 1995, 240 (4), 373-378.
14. Hertel, D.; Scherf, U.; Bässler, H., Charge carrier mobility in a ladder-type conjugated polymer. *Advanced Materials* **1998**, 10 (14), 1119-1122.
15. Romanovskii, Y. V.; Gerhard, A.; Schweitzer, B.; Scherf, U.; Personov, R.; Bässler, H., Phosphorescence of π -conjugated oligomers and polymers. *Physical review letters* **2000**, 84 (5), 1027.
16. Lupton, J.; Pogantsch, A.; Piok, T.; List, E.; Patil, S.; Scherf, U., Intrinsic room-temperature electrophosphorescence from a π -conjugated polymer. *Physical review letters* **2002**, 89 (16), 167401.

17. Romaner, L.; Heimel, G.; Wiesenhofer, H.; Scandiucci de Freitas, P.; Scherf, U.; Brédas, J.-L.; Zojer, E.; List, E. J., Ketonic defects in ladder-type poly (p-phenylene) s. *Chemistry of materials* **2004**, 16 (23), 4667-4674.
18. Liu, L.; Qiu, S.; Wang, B.; Zhang, W.; Lu, P.; Xie, Z.; Hanif, M.; Ma, Y.; Shen, J., Study on the formation of the ketonic defects in the thermal degradation of ladder-type poly (p-phenylenes) by vibrational spectroscopy. *The Journal of Physical Chemistry B* **2005**, 109 (49), 23366-23370.
19. Kobin, B.; Bianchi, F.; Halm, S.; Leistner, J.; Blumstengel, S.; Henneberger, F.; Hecht, S., Green Emission in Ladder-Type Quarterphenyl: Beyond the Fluorenone-Defect. *Advanced Functional Materials* **2014**, 24 (48), 7717-7727.
20. Nicolai, H. T.; Kuik, M.; Wetzelaer, G.A.H.; De Boer, B.; Campbell, C.; Risko, C.; Brédas, J.; Blom, P.W.M., Unification of trap-limited electron transport in semiconducting polymers. *Nature materials* **2012**, 11 (10), 882.
21. Pasveer, W.; Cottaar, J.; Tanase, C.; Coehoorn, R.; Bobbert, P.; Blom, P.W.M.; De Leeuw, D.M.; Michels, M., Unified description of charge-carrier mobilities in disordered semiconducting polymers. *Physical review letters* **2005**, 94 (20), 206601.
22. Coehoorn, R.; Pasveer, W.; Bobbert, P.; Michels, M., Charge-carrier concentration dependence of the hopping mobility in organic materials with Gaussian disorder. *Physical Review B* **2005**, 72 (15), 155206.
23. Blom, P. W.M. ; De Jong, M.; Vleggaar, J., Electron and hole transport in poly (p-phenylene vinylene) devices. *Applied Physics Letters* **1996**, 68 (23), 3308-3310.
24. Abbaszadeh, D.; Kunz, A.; Wetzelaer, G.; Michels, J. J.; Craciun, N. I.; Koynov, K.; Lieberwirth, I.; Blom, P. W.M., Elimination of charge carrier trapping in diluted semiconductors. *Nature materials* **2016**, 15 (6), 628-633.
25. Snedden, E.; Thompson, R.; Hintshich, S.; Monkman, A., Fluorescence vibronic analysis in a ladder-type conjugated polymer. *Chemical Physics Letters* **2009**, 472 (1-3), 80-84.

26. Wyman, M., Kinetics of charge recombination in a ladder phenylene polymer. **2016**.
27. Partee, J.; Frankevich, E.; Uhlhorn, B.; Shinar, J.; Ding, Y.; Barton, T., Delayed fluorescence and triplet-triplet annihilation in π -conjugated polymers. *Physical review letters* **1999**, 82 (18), 3673.
28. Baldo, M. A.; O'brien, D.; You, Y.; Shoustikov, A.; Sibley, S.; Thompson, M.; Forrest, S. R., Highly efficient phosphorescent emission from organic electroluminescent devices. *Nature* **1998**, 395 (6698), 151.
29. Wetzelaer, G.A.H.; Kuik, M.; Nicolai, H.T.; Blom, P.W.M., Trap-assisted and Langevin-type recombination in organic light-emitting diodes. *Physical Review B* **2011**, 83 (16), 165204.
30. Macdonald, J., DR Franceschetti in JR Macdonald. Impedance Spectroscopy, Wiley, New York **1987**, 90.
31. Niu, Q.; Crăciun, N. I.; Wetzelaer, G.-J. A.H.; Blom, P. W.M., Origin of negative capacitance in bipolar organic diodes. *Physical review letters* **2018**, 120 (11), 116602.
32. Bagnich, S. A.; Bässler, H.; Neher, D., Sensitized phosphorescence of benzil-doped ladder-type methyl-poly (para-phenylene). *The Journal of chemical physics* **2004**, 121 (18), 9178-9183.

Chapter 6

Summary and conclusion

Semiconducting polymers are a very attractive class of materials for a new generation of electronic devices owing to the potential of cheap fabrication using solution processing. In addition, there are an almost infinite number of possibilities for tuning the chemical structure of the organic compounds to easily obtain different optoelectronic properties. After 30 years of development, organic light emitting diodes have been widely used in recent display industry and are believed to be the most promising candidate for the next generation planer and flexible lighting. However, despite this potential, there are still some issues with organic-semiconductors (especially polymeric ones) that have to be solved for devices to compete with commercialized technology. To make that happen, one of the ideal solutions would be focusing on eliminating the negative effect of loss processes in OLEDs in order to improve the device performance. One of the main loss processes is the charge trapping occurs in the active layer of the OLEDs which can adversely affect the device performance, specially the efficiency. Mostly when a charge trapped in the trap centers, it would decay by a non-radiative process. However, there are some trap-assisted recombination originating either from the defects exist on some conjugated polymers or extra component like an added chromophore into the system. In this cases, the trap-assisted recombination and therefore eliminating their negative effect would be feasible to be tracked visually. As a result, in this thesis we focused mostly on the system with radiative trap-assisted recombination and eliminating their negative effect on the device performance.

After a brief history and introduction in Chapter 1, the charge transport and electroluminescence in/of a blue emitting conjugated polymer, poly(dioctylfluorene) (PFO), containing a low density of fluorenone defects (PFO-F), blended with the insulating polymer polystyrene (PS) have been investigated in Chapter 2. Due to the dilution of the trap sites, the electron transport in the PFO-F:PS blends is strongly enhanced with increasing PS content.

Furthermore, the green emission resulting from trap-assisted recombination at fluorenone defects in the PFO backbone can be completely suppressed by addition of polystyrene. The suppression of the green emission as a function of blending ratio is in agreement with the predictions by our numerical drift-diffusion-based device model.

In Chapter 3, we have demonstrated how a conformational change in PFO, brought about by blending with polystyrene, drastically influences the optoelectronic behavior of the former. Blending induces the formation of PFO β -phase domains, consisting of fully extended chain segments with monomers oriented in a coplanar fashion. These ordered domains exhibit increased conjugation, a smaller optical bandgap, higher luminescence quantum yield and enhanced charge carrier transport rates compared to the amorphous (disordered) bulk. We demonstrated that PLEDs based on PFO blended with 75% PS exhibit a ten-fold increase in luminous efficiency compared to devices based on unblended amorphous PFO. We semi-quantitatively showed that this substantial increase has two contributions: i) alleviation of electron trapping owing to a change in the statistics between free and trapped charges as a consequence of spatial separation of both transport and trap sites, and ii) formation of a substantial amount ($\sim 13\%$) of β -phase PFO embedded in the amorphous matrix. The presence of β -phase domains possibly counteracts a decrease in hole conduction due to the spatial separation of transport sites caused by dilution.

In Chapter 4, one of the main issues of adding a chromophore into an organic host which leads to severe charge trapping has been addressed. We have presented a new concept how to incorporate highly fluorescent red-emitting quantum dots (QDs) into a blue-emitting conjugated polymer matrix without inducing severe electron trapping. Trapping of electrons is prevented by shielding of the quantum dot by a thin insulating polymeric shell. The reduced trapping is demonstrated by

the realization of a red-emitting hybrid polymer:QD light-emitting diode with voltage-independent electroluminescence spectrum and no efficiency loss as compared to the pristine host.

In Chapter 5, the charge transport characteristics of the blue emitting ladder polymer methyl-substituted poly(p-phenylene) ladder polymer (Me-LPPP) are studied. We showed that the hole transport in Me-LPPP is characterized by a trap-free space-charge limited with a high mobility of $2 \times 10^{-8} \text{ m}^2/\text{Vs}$ due to reduced energetic disorder. The electron transport is strongly trap-limited. Only by assuming the presence of additional electron traps on top of the universal trapping sites explains the large difference between the electron and hole currents. The EL spectrum shows next to the blue singlet peaks additional features at longer wavelengths, including yellow-orange triplet emission. The triplet emission shows a weaker voltage-dependent emission compared to the singlets. This finding is also in agreement with impedance measurements for Me-LPPP PLEDs which shows negative capacitance. Both features showed that the triplet emission is of trap-assisted nature, which was further confirmed by trap-dilution experiments.

Appendix

Declaration

I hereby declare that I wrote the dissertation submitted without any unauthorized external assistance and used only sources acknowledged in this work. All textual passages which are appropriate verbatim or paraphrased from published and unpublished texts, as well as all information obtained from oral sources, are duly indicated and listed in accordance with bibliographical rules. In carrying out this research, I complied with the rules of standard scientific practice as formulated in the statutes of Johannes Gutenberg-University Mainz to insure standard scientific practice.

.....
(Elham Khodabakhshi Shalamzari)

List of publications

1. **Elham Khodabakhshi**, B Klöckner, JJ Michels, R Zentel, PWM Blom. Suppression of electron trapping by quantum dot emitters using a grafted polystyrene shell. *Materials Horizons*, 2019.
2. **Elham Khodabakhshi**, D Hertel , JJ Michels, K Meerholz, U Scherf, PWM Blom, Charge transport properties in ladder-type polymer MeLPPP: Origin of higher energy emission, *Ready to submit*, 2019
3. **Elham Khodabakhshi**, JJ Michels, PWM Blom. Efficiency enhancement of polyfluorene:polystyrene blend light emitting diodes by simultaneous trap dilution and β -phase formation, *Applied physics letter*, 2019, 093301.
4. **Elham Khodabakhshi**, JJ Michels, PWM Blom. Visualization of trap dilution in polyfluorene based light-emitting diodes, *Journal of Applied Physics*, 2017, 075209.

List of conferences

1. **Elham Khodabakhshi**, B Klöckner, JJ Michels, R Zentel, PWM Blom. Suppression of electron trapping by shielding quantum dot using a grafted polystyrene shell. *INFORM, 2019, Spain*
2. **Elham Khodabakhshi**, JJ Michels, PWM Blom. Controlling charge transport and recombination in polymer/QD based LED. *Advanced Materials workshop, 2018, Bulgaria*
3. **Elham Khodabakhshi**, JJ Michels, PWM Blom. Spectroscopic identification of reduced charge trapping in blue-emitting OLED by blending, *SPIE Organic Photonics+Electronics, 2017, San Diego, United States.*
4. **Elham Khodabakhshi**, G.A.H. Wetzelaer, JJ Michels, PWM Blom. Visualization of trap dilution in polyfluorene based light-emitting OLED, *14th European Conference on Molecular Electronics, 2017, Dresden, Germany.*
5. **Elham Khodabakhshi**, JJ Michels, PWM Blom. Boosting OLED efficiency by blending: spectroscopic identification of reduced charge trapping. *13th International Conference on Organic Electronics(ICOE), 2017, St. Petersburg, Russia.*
6. **Elham Khodabakhshi**, JJ Michels, PWM Blom. Suppression of green emission in polyfluorene light-emitting diodes by Polymer Blending, *Macromolecular Colloquium 2016, Freiburg, Germany.*

Curriculum Vitae

Elham Khodabakhshi Shalamzari
 Date of Birth: 22/09/1990
 Place of Birth: Shahrekord, Iran
 Nationality: Persian

UNIVERSITY EDUCATION

- 03/2016-07/2019 PhD student at the Max-Planck Institute for Polymer Research, Mainz
 Group of Prof. Dr. Paul Blom: Molecular Electronics
 PhD Thesis: *Optimization of polymeric light emitting diodes by organic/organic or organic/inorganic blending*
- 05/2012 - 11/2014 M.Sc., Polymer Engineering, University of Amirkabir (Tehran, Iran)
 Master Thesis: *Modification of conjugated polymer/graphene nanocomposite thin film as transparent conductive electrode for organic opto-electronics (OLED, OPV and Gas sensors, grade: 1.0)*
- 10/2008 □ 05/2012 B.Sc., Polymer Engineering, University of Amirkabir (Tehran, Iran).
 Bachelor Thesis: „ *Investigating contribution of chromophores in conjugated polymer MEH-PPV, with different numbers of repeating units to overall emission, grade: 1.0)*

PROFESSIONAL CAREER

Tutoring:

Supervision of laboratory at the University of Mainz,
 Supervision of Girls' Day 2017 at the Max-Planck Institute, Mainz
 Supervision of experiments at the Science Market 2016, Mainz,

Internship:

Property improvement of polyurethane and epoxy based floor coating, Basa
 Polymer company, 2012, Tehran, Iran

ADVANCED TRAINING

- 04/2018 - 06/2018 Online course of Six Sigma principles by University of Georgia
- 10/2017 - 04/2018 Online courses of Foundation of Management Specialization by IESE Business school
- 11/2017 Time management and Decision Making by Dr. M. Meyer at MPIP

Mainz, November 27, 2019